INTERMOLECULAR FORCES FROM THE SPEED OF SOUND IN GASES

A thesis submitted to the University of London for
the degree of Doctor of Philosophy
by

Maria Prodromou ZARARI

Department of Chemical Engineering and Chemical Technology
Imperial College of Science and Technology
LONDON SW7

December 1993

ABSTRACT

Extremely accurate speed of sound measurements have been performed on gaseous methane, propane and a methane-propane mixture, using a spherical resonator. The data have been analysed in order to obtain perfect gas heat capacities and second and third acoustic virial coefficients.

A new integration technique has been developed by which the speed of sound data obtained for methane have been integrated to yield the compression factor. The propagation of error in the integration has been studied both numerically and analytically. It has been found that the integration is of increasing accuracy as the temperature increases.

A new method has been also developed which allows second and third volumetric virial coefficients to be calculated by simultaneously fitting second and third acoustic virial coefficient data to a spherical intermolecular pair potential. The method is found to be accurate in predicting second and third volumetric virial coefficients for the monatomic gas argon, the pseudospherical gas methane as well as for the non-spherical nitrogen gas. The calculations involved employ the assumption that the dominant contribution to the non-pairwise-additive part of the potential of three molecules is the Axilrod-Teller triple-dipole term. This assumption has been confirmed for the case of argon. For the spherical substances studied the potentials derived from the fit are shown to be good approximations of the true potential.

The same method has been applied to an argon-nitrogen mixture yielding second and third interaction volumetric virial coefficients. The accuracy of the second interaction volumetric virial coefficients obtained is estimated to be better than that of the values previously available, while third interaction volumetric virial coefficients are reported for first time over a wide temperature range.

TABLE OF CONTENTS

LIST OF FIGURES

LIST OF TABLES

ACKNOWLEDGEMENTS

I would like to express my gratitude to Professor Bill Wakeham for his encouragement, sound advice and excellent guidance. His moral support and understanding have been to me an inspiration and continuous driving force.

I must also thank Dr. Martin Trusler for providing to me the opportunity to get involved in this research area and for his kind help and advice when performing the experimental measurements.

I am grateful to Professor Mark Assael for encouraging me to pursue postgraduate studies.

The financial support of the EEC grant No. ERBSC1*CT900610 is also greatly acknowledged.

I am indebted to Professor Julia Higgins and Drs. Stephen Richardson and Graham Saville for their kind and firm support.

I would also like to thank the members of my thesis committee, Drs. G. Saville and G. C. Maitland.

Special thanks go to all members of the Fluids Group and my friends in London.

I would like to thank Stratos for always being there when I needed moral support and encouragement.

Finally, I would like to thank my parents, Prodromos and Efi, for their love, understanding. To them I dedicate this effort.

CHAPTER 1

INTRODUCTION

Accurate speed of sound data in gases are largely sought by the gas industry for calibration of flowmeters using sonic nozzles. The speed of sound data are of equally great importance for scientific purposes. The thermodynamic property of the speed of sound is particularly sensitive to the accuracy of volumetric data and therefore speed of sound data are used for testing equations of state.

In this work extremely accurate acoustic measurements have been performed for gaseous methane, propane and a methane-propane mixture, using a spherical resonator, the description of which is found in chapter 4. Employing the acoustic model developed in chapter 3 the speed of sound was determined from the acoustic measurements. Depending mainly on the purity of the substances measured the speed of sound has been obtained with an estimated accuracy from 20 to 200 parts per million, as the analysis in chapter 5 shows. In chapter 6 a new method is presented by which one can obtain an equation of state using solely speed of sound measurements. The method is based on integrating the speed of sound data to obtain the compression factor using initial values at the lowest temperature of measurements. The propagation of error in this method has been studied both numerically and analytically. It has been found that the method is of increasing accuracy when the temperature increases, a fact which allows the implementation of the method to a variety of substances provided initial values of the compression factor and its derivative with respect to the temperature exists at the lowest temperature of the integration.

The speed of sound data when fitted into a virial series in the density yield acoustic virial coefficients which are related to the volumetric virial coefficients through ordinary

differential equations. Accordingly, the functional relationship between the volumetric virial coefficients and the intermolecular pair-potential, discussed in chapter 2, yields, through these differential equations, the functional relationship between the acoustic virial coefficients and the intermolecular pair-potential. Employing this relationship we have fitted simultaneously the second and third acoustic virial coefficients to a simple but flexible potential model in order to obtain the potential which best represents the two acoustic virial coefficients.

The third volumetric virial coefficients are related in addition to the pair-potential, to the non-pairwise-additive part of the potential of three interacting molecules. This part of the potential in the present work has been approximated by the Axilrod-Teller triple-dipole term, assuming that the dominant contribution to the non-pairwise-additive part of the three-molecule-potential arises from the dispersion. This assumption which has been already tested for argon, was reconfirmed using accurate values of the third acoustic virial coefficients in conjuction with the most accurate available potential and was employed next for the analysis of the other substances.

Subsequently, the potential which was found to represent best the second and third acoustic virial coefficients was employed for the calculation of the second and third volumetric virial coefficients and, independently, the viscosity of the dilute gas. The excellent agreement between the calculated and experimental values obtained for these properties for the spherical substances studied is a strong indication that potentials derived using only accurate second acoustic virial coefficients are very good approximations of the true potentials.

CHAPTER 2

BACKGROUND IN INTERMOLECULAR FORCES

2.1 Introduction.

The forces which act between pairs or greater clusters of molecules determine , to a large extent, the thermophysical properties of bulk materials. Statistical mechanical theory provides a direct final link between those intermolecular forces and the properties. Thus, in principle, if the intermolecular pair potentials for all molecular interactions in a system are known it should be possible to predict the properties of the material. Thĕ existence of such a procedure would mean that the needs of the chemical industry for thermophysical property data on a wide range of systems over a wide range of conditions could be met solely by calculation. In practice, the only intermolecular pair-potentials known with exactitude at present are these for monatomic species and thus the procedure set out above cannot yet be carried out. Instead it is useful to exploit measurements of some of the thermophysical properties of fluids in order to determine intermolecular potentials so that others may then be calculated without measurement.

In this chapter we consider the origins of intermolecular forces and their quantitative nature as well as the sources of information about them that are available. In particular, in the context of the current work, we consider the use of the accurate measurements of acoustic virial coefficients made in this work to the determination of intermolecular forces.

2.2 Intermolecular forces

The intermolecular pair-potential energy for a system of two atoms describes the departure of the total energy of the two-atom system from its value when the two atoms

are infinitely separated. This energy difference is equal to the work needed to bring two atoms together from infinite separation to a separation r:

$$U(r) = -\int_{\infty}^{r} F(r)\,dr \qquad (1)$$

where $F(r) = -dU/dr$ is the total intermolecular force at a separation r. By convention the intermolecular force is positive when it is repulsive and negative when it is attractive.

The origins of intermolecular forces lie in electromagnetic interactions between charges on the electrons and nuclei of the molecules. According to the semi-classical approach, the electrons of an atom are supposed to be in continuous orbit about the nucleus so that these forces are expected to have a time-dependence, related to the velocity of the electronic motion. In the development of the above relation we assumed that the two atom were held stationary at the separation r, so that the resulting intermolecular force is the time average of the time-fluctuating forces. However, according to the molecular theory the atoms in matter are in continuous motion and not stationary. Since the electron velocities are always much larger than the atom velocities, we can indeed consider the two atoms to be stationary. This is the Born-Oppenheimer approximation, which results in a unique, velocity independent intermolecular pair-potential [1].

The essential characteristics of an intermolecular pair-potential for a non-reactive system are taken to be:

- the separation σ at which the potential energy function crosses zero,
- the separation r_m at which the potential attains its minimum value and
- the minimum value of the energy $-\varepsilon$ itself known as the potential well depth.

These characteristics are shown in figure 2.1 for a typical intermolecular pair-potential curve.

For a system of two molecules, there are fluctuations in the intermolecular pair-potential arising from vibrations and rotations of the molecule. Within the 'rigid-molecule'

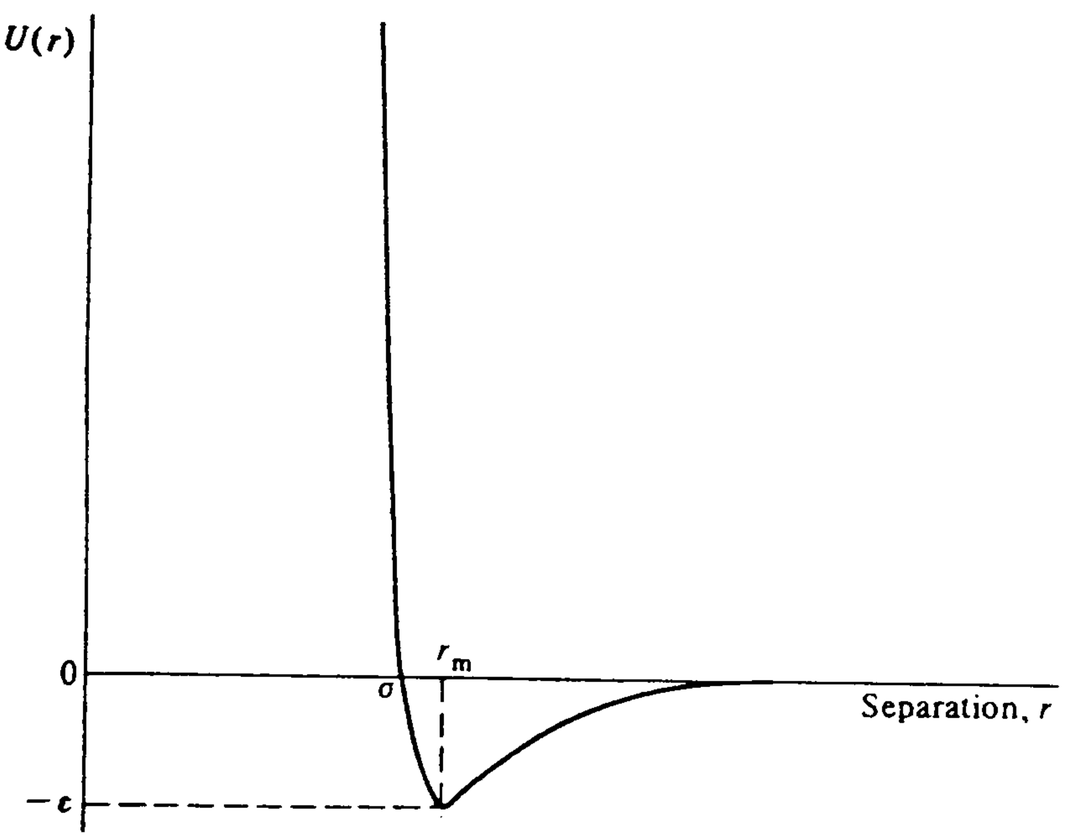

Figure 2.1. The intermolecular pair-potential of a spherically symmetric system as a function of the separation.

approximation, according to which there is no internal rotation of the molecules and the molecules are in their ground electronic and ground vibrational states [2], the potential depends only on the intermolecular separation r, and the relative orientation ω and we write $U(r,\omega)$. For the general case of any space-fixed coordinate-system XYZ, the intermolecular pair-potential is expressed as $U(\bar{r},\omega_1,\omega_2)$, where $\bar{r}=\bar{r}_2-\bar{r}_1$ is the vector of the molecular separation with respect to that system, and ω_1 and ω_2 the orientations (the Euler angles [2]) of molecules 1 and 2 respectively, with respect to that system. If the orientations of the two interacting molecules refer to the vector $\bar{r}=\bar{r}_1-\bar{r}_2$ as polar axis, we can express the intermolecular pair potential $U(\bar{r},\omega_1,\omega_2)$ as $U(r,\omega'_1,\omega'_2)$, where r is the separation between the molecular centres and ω'_1 and ω'_2 are the orientations of the two molecules with respect to the new coordinate system. As the molecular centre one often chooses the centre of mass, so that all molecular parameters, moments of inertia, multipole moments, etc., relate to one origin.

2.2.1 Origins of intermolecular forces

The forces between particles are classified into (1) strong nuclear forces, which are responsible for the binding of the neutrons and protons inside the nucleus and are significant over a range of order 10^{-4} nm, (2) weak nuclear forces, known to be electromagnetic in origin, acting in a similar short range, (3) electromagnetic forces and (4) gravitational forces [1].

Since the molecular dimensions are of order 0.5 nm, the nuclear forces cannot contribute to the intermolecular force. On the other hand, gravitational forces, which are extremely long range, contribute a force some thirty orders of magnitude smaller than the observed intermolecular force, so that they are not responsible for intermolecular forces. Thus, the intermolecular forces must be electromagnetic in origin [1].

The qualitative diagram contained in figure 2.1, shows that the total intermolecular force at short range is repulsive, while at long range it is attractive. Therefore we can

discern at least two sources of contribution to the total intermolecular force and the corresponding intermolecular potential [1].

Qualitatively, the origin of repulsive forces is simpler to explain. When the electron clouds of two molecules approach each other sufficiently closely that they overlap, the Pauli excusion principle prohibits some electrons from occupying the overlap region reducing, as a consequence, the electron density in that region. The positively charged nuclei are thus incompletely shielded and therefore exert on each other a strong repulsive force. Such short range forces are referred to as overlap forces [1]. Modern methods of quantum chemistry permit numerical evaluation of these overlap forces for relatively simple molecules by means of appropriate solutions of the Schroedinger equation.

The long range attractive component of the intermolecular force arises in a completely different manner and is significant when the overlap of the electron clouds is small. There are three possible contributions to the attractive force depending on the nature of the interacting molecules:

(a) Electrostatic contributions:

The electrostatic forces are important only between molecules possessing a permanent dipole moment such as HCl. As expected these forces are strongly dependent on the relative orientations of the two interacting molecules and therefore sometimes are called orientation forces. Since the interaction between the two dipoles takes place without a distortion of the electron-charge distribution on either molecule, the resulting energy is termed a first-order energy [1].

The electrostatic energy of two dipoles, having a linear charge distribution and total charges $Q = Q_1 + Q_2 = 0$ and $Q' = Q_1' + Q_2' = 0$, for dipole 1 and dipole 2 respectively, is, after averaging for all possible orientations using the Boltzmann weighting $\exp(-U_{el} / kT)$, given by the sum of terms [1]:

$$\langle U_{el}\rangle_{\mu\mu'} = -\frac{2}{3}\frac{\mu^2\mu'^2}{r^6 kT\ (4\pi\varepsilon_0)^2} + \cdots \tag{2}$$

$$\langle U_{el}\rangle_{\mu\Theta} = -\frac{1}{r^8 kT\ (4\pi\varepsilon_0)^2}(\mu^2\Theta'^2 + \mu'^2\Theta^2) + \cdots \tag{3}$$

$$\langle U_{el}\rangle_{\Theta\Theta'} = -\frac{14}{5}\frac{\Theta^2\Theta'^2}{r^{10} kT\ (4\pi\varepsilon_0)^2} + \cdots \tag{4}$$

where ε_0 is the permittivity of free space, μ and μ' are the dipole moments and Θ and Θ' are the quadrapole moments, of dipole 1 and dipole 2 respectively. If we consider the charges Q_1 and Q_2 of dipole 1 lying on the z-axis, at distances $-z_1$ and z_2 from the origin of the axis taken to be the centre of mass of the dipole, the dipole moment of 1 is defined as $\mu = -Q_1 z_1 + Q_2 z_2$ and the quadrapole moment of 1 as $\Theta = Q_1 z_1^2 + Q_2 z_2^2$. The terms $\langle U_{el}\rangle_{\mu\mu'}$, $\langle U_{el}\rangle_{\mu\Theta}$ and $\langle U_{el}\rangle_{\Theta\Theta'}$ are called the dipole-dipole, dipole-quadrapole and quadrapole-quadrapole contributions to the electrostatic energy respectively. All these contributions to the electrostatic energy are seen to be attractive and they vary as r^{-6}, r^{-8} and r^{-10} respectively where r is the distance between the centres of mass of the two dipoles [1].

(b) Induction contributions:

These forces arise from the interaction of a multipole on a molecule with a non-polar molecule. For example a dipole moment on one molecule distorts the electron charge distribution of the other molecule producing an induced dipole moment within it. This induced dipole then interacts with the inducing dipole to produce an attractive force. Because this contribution to the potential energy arises from distortion of the electron clouds it is termed a second-order energy. When two polar molecules interact the induction force is simultaneously present.

The induction energy between a dipolar molecule and a non-polar molecule after averaging over all possible orientations, using the Boltzmann weighting, $\exp(-U_{ind}/kT)$, is given by [1]:

$$\langle U_{\text{ind}} \rangle = -\frac{\mu^2 \alpha'}{(4\pi\varepsilon_0)^2 r^6} \tag{5}$$

where μ is the dipole moment of one molecule and α' is the static polarizability of the other. This expression is not temperature dependent, unlike the corresponding leading term in the electrostatic energy. When two polar molecules interact the orientationally averaged induction energy is [1]:

$$\langle U_{\text{ind}} \rangle_{\mu\mu'} = -\frac{\mu^2 \alpha' + \mu'^2 \alpha}{(4\pi\varepsilon_0)^2 r^6} + \cdots \tag{6}$$

where α and α' are the static polarizabilities and μ and μ' the dipole moments of the two dipoles respectively. We see that in both cases the induced energy varies as r^{-6}.

(c) Dispersion contributions:

When two molecules possessing no permanent electric dipole or higher order moments interact, electrostatic and induction contributions to the intermolecular potential energy are absent and the interaction arises solely from the dispersion forces. The electrons of a molecule are in continuous motion so that the electron density oscillates continuously in time and space. Thus, at any instant, any molecule possesses an instantaneous dipole which fluctuates as the electron density fluctuates. This instantaneous dipole induces an instantaneous dipole in a second molecule. The induced dipole and the inducing dipole interact then to produce an attractive energy called the dispersion energy, which is, accordingly, a second-order energy.

According to the simplified Drude model [1], which treats each molecule as a simple oscillator, or using exact quantum-mechanical methods, we obtain the expression of the dispersion energy between two identical spherically symmetric molecules as follows:

$$U_{\text{disp}} = \frac{C_6}{r^6} + \frac{C_8}{r^8} + \frac{C_{10}}{r^{10}} + \cdots \tag{7}$$

where the coefficients C_6, C_8 and C_{10} correspond to the induced dipole-dipole, dipole-quadrapole and quadrapole-quadrapole interactions. The coefficient of the leading term is given by:

$$C_6 = -\frac{3}{4}\frac{\alpha^2 \hbar\omega_0}{(4\pi\varepsilon_0)^2} \qquad (8)$$

where ω_0 is the angular frequency of the simple oscillator and $\hbar = h / 2\pi$, with h being Planck's constant. London [1] estimated first the magnitude of C_6, by assuming that the angular frequency of the oscillator model ω_0 was that corresponding to the energy of ionization of the molecule from its ground state, $E_I = \hbar\omega_0$. This assumption was supported by the fact that an identical assumption was found to describe reasonably well the variation of the refractive index of a gas with the frequency of electromagnetic radiation (the so-called effect of dispersion). Accordingly we write:

$$C_6 \approx -\frac{3}{4}\frac{\alpha^2 E_I}{(4\pi\varepsilon_0)^2} \qquad (9)$$

The coefficient C_6, called the two body dispersion energy coefficient, calculated in this manner for argon was found to be only 30 per cent smaller than the actual value. A full quantum-mechanical treatment yield expressions for C_6, C_8, and C_{10}, from which they can be calculated using experimental data information on multipole oscillator-strengths [1].

The dispersion energy is the only contribution to the intermolecular pair-potential energy arising from the long-range forces for non-polar molecules, while it constitutes the largest contribution to the attract ive force it for the most polar molecules, except the most highly polar such as H_2O [1].

2.2.2 Representation of the intermolecular pair-potential

Many semiempirical models have been proposed in order to represent intermolecular pair-potential functions of spherically symmetric molecules [1], since an exact analytical expression is not yet feasible. One of the most popular potential models is the Lennard-Jones (n-6) potential:

$$U(r) = \varepsilon / (n-6)\,[6\,(r_m / r)^n - n\,(r_m / r)^6] \qquad (10)$$

The characteristic of all these potential models is that they consist of two parts, a repulsive term and an attractive part usually varying as r^{-6} . The latter term is consistent with the theory outlined above but there is no justification for the form of the repulsive term.

The representation of the intermolecular potentials of non-spherical molecules involves a consideration of the orientation dependence. One way of representing the intermolecular pair-potential of two non-spherical molecules $U\ (\bar{r}, \omega_1, \omega_2)$, is the site-site model. This model assumes that the intermolecular pair-potential is the sum of the pairwise potentials $U_{\alpha\beta}$ between individual sites on the two molecules. The sites are often coincident with the that make up the molecules:

$$U\ (\bar{r}, \omega_1, \omega_2) = \sum_{\alpha\beta} U_{\alpha\beta}(r_{\alpha\beta}) \tag{11}$$

For some applications it is convenient to separate the intermolecular pair-potential into isotropic and anisotropic parts:

$$U\ (\bar{r}\omega_1\omega_2) = U_0(r) + U_a(\bar{r}\omega_1\omega_2) \tag{12}$$

where the isotropic potential U_0 depends only on the separation r. This decomposition is of course not unique, but the most convenient choice for U_0 is the unweighted orientational average of the full potential:

$$U_0(r) = \left\langle U\ (\bar{r}\omega_1\omega_2) \right\rangle_{\omega_1\omega_2} \tag{13}$$

Accordingly, it should be:

$$\left\langle U_a(\bar{r}\omega_1\omega_2) \right\rangle_{\omega_1\omega_2} = 0 \tag{14}$$

All potentials defined by equations (12) and (13) satisfy the condition of (14) [2].

An alternative means of representing non-spherical potentials which has been proved very useful for theoretical calculations, follows from a spherical harmonic expansion of the potential $U\ (\bar{r}, \omega_1, \omega_2)$ [2]. Analytic statistical mechanical calculations are easily carried out, since the properties of the spherical harmonics, integration,

differentiation, rotation, etc., are well established. For molecules of an arbitrary shape, the spherical harmonic expansion of the potential is written:

$$U(\bar{r},\omega_1,\omega_2) = \sum_{l_1 l_2 l} \sum_{m_1 m_2 m} \sum_{n_1 n_2} U(l_1 l_2 l; n_1 n_2; r) \times C(l_1 l_2 l; m_1 m_2 m)\, D^{l_1}_{m_1 n_1}(\omega_1)^* D^{l_2}_{m_2 n_2}(\omega_2)^* Y_{lm}(\omega)^* \quad (15)$$

where $[l = 0,1,2,\cdots; m = -l,\cdots,+l; n = -l,\cdots,+l]$, $C(l_1 l_2 l; m_1 m_2 m)$ is a Clebsch-Gordan coefficient, $D^{l}_{mn}(\omega)^*$ (* indicates the conjugate) is a generalized spherical harmonic, $Y_{lm}(\omega)$ is a spherical harmonic and ω is the orientation (the polar angles [2]) of $\bar{r}$ with respect to the chosen *XYZ* coordinate system. The separation-dependent coefficients of the above expansion, $U(l_1 l_2 l; n_1 n_2; r)$, can be obtained [2] for each of the contributions to the intermolecular pair-potential (electrostatic or multipole, induction, dispersion, overlap), so that the full potential $U(\bar{r}\omega_1\omega_2)$ can be obtained by performing the summation of (15). Employing symmetry properties of the system of molecules interacting equation (15) can be substantially simplified. For example for linear molecules equation (15) it is reduced to [2]:

$$U(\bar{r}\omega_1\omega_2) = \sum_{l_1 l_2 l} \sum_{m_1 m_2 m} U(l_1 l_2 l; r)\, C(l_1 l_2 l; m_1 m_2 m) \times Y_{l_1 m_1}(\omega_1) Y_{l_2 m_2}(\omega_2) Y_{lm}(\omega)^* \quad (16)$$

where there is no n_i dependence. This spherical harmonic expansion of the potential has been applied in attempts to determine the intermolecular pair-potential for the linear molecule of nitrogen, up to $l_1 = l_2 = 6$ and $l = 12$ giving good convergence [2,3].

2.2.3 Non-additivity of the intermolecular potential

It is often assumed that the total intermolecular potential energy $U_N(\bar{r}^N, \omega^N)$, for *N* molecules, where $\bar{r}^N \equiv \bar{r}_1, \bar{r}_2, \cdots, \bar{r}_N$ and $\omega^N \equiv \omega_1, \omega_2, \cdots, \omega_N$, is simply the sum of the intermolecular potentials for isolated pairs of molecules, i.e.

$$U_N(\bar{r}^N, \omega^N) = \sum_{i<j} U(\bar{r}_{ij}, \omega_i, \omega_j) \quad (17)$$

where $U\ (\bar{r}_{ij}\ ,\omega_i\ ,\omega_j\ )$ is the potential for a pair of molecules i and j isolated from the other molecules, with the centre of j at $\bar{r}_{ij} = \bar{r}_j - \bar{r}_i$ from i, and orientations ω_i and ω_j . The assumption of pairwise additivity is not exact because the presence of additional molecules near a pair distorts the electron-charge-distributions in the particular molecules i and j, and thus changes the intermolecular interaction between this pair from that appropriate when the pair is isolated. Thus, more precisely we write:

$$U_N\ (\bar{r}^N, \omega^N\ ) = \sum_{i<j} U\ (ij\ ) + \sum_{i<j<k} U\ (ij\ k\ ) + \cdots \qquad (18)$$

where $U\ (ij\ ) = U\ (\bar{r}_{ij}\ ,\omega_i\ ,\omega_j\ )$, $U\ (ij\ k\ ) = U\ (\bar{r}_{ij}\ ,\bar{r}_{ik}\ ,\bar{r}_{jk}\ ,\omega_i\ ,\omega_j\ ,\omega_k\ )$, etc. The term $U\ (ij\ k\ )$ is the additional part of the potential not included in the sum of the isolated pair terms $U\ (ij\ ) + U\ (i\ k\ ) + U\ (j\ k\ )$, and so on. For monatomic gases it seems that a description of most thermophysical properties can be achieved if the above equation is truncated at the triplet term. For polyatomic fluids the situation is not yet clear [2].

The influence of the three-body term on physical properties has been studied for atomic fluids. In these studies the long-range Axilrod-Teller [1,2] triple-dipole dispersion term was found to be the most important part of the three-body interaction. An explanation of this is that configurations where three molecules overlap are rare, because of the strongly repulsive nature of the overlap potentials [2], so that the additional energy arises largely from the long range attractive contribution.

The effect of the three-body term on the internal energy of the liquid is small even at the triple point; being only a few per cent [2] of the total configurational energy; for less dense fluids the effect is smaller. However, some properties are much more sensitive to the three-body forces. For example, the Axilrod-Teller [1,2] three-body interaction was shown to have a large effect on the third virial coefficient, especially at the lower temperatures [2]. The three-body interaction also has a large effect on other properties for atomic liquids, such as the surface energy and surface tension. The neglect of the three-

body forces produces an error of 25 per cent in the surface tension and 10 per cent in the surface energy of liquid argon.

The Axilrod-Teller triple-dipole term is the leading correction term to the dispersion energy arising from the interaction of three molecules. For the particular case of spherically symmetric molecules it is given by:

$$\Delta U = \nu_{123}(r_{12}r_{13}r_{23})^{-3}(1 + 3\cos\theta_1\cos\theta_2\cos\theta_3) \tag{19}$$

where θ_i are the interior angles of the three-body triangle and

$$\nu_{123} = \frac{3}{4}\alpha C_6 \tag{20}$$

In equation (27) α is the zero frequency polarizability and C_6 the two-body dispersion energy coefficient.

2.3 Sources of information about the intermolecular pair-potential

In this section we consider the properties which have been proved of greatest value in the determination of intermolecular pair-potentials for simple molecules.

2.3.1 Second volumetric virial coefficients

The volumetric virial coefficients are the coefficients obtained by the expansion of the compressibility factor in density series:

$$z = \frac{p}{\rho_n RT} = 1 + B\rho_n + C\rho_n^2 + \cdots \tag{21}$$

where z is the compressibility factor, p is the pressure, T is the temperature, R is the gas constant, ρ_n is the amount of substance density and, B and C are the second and third volumetric virial coefficients respectively. These coefficients represent the effect of the intermolecular interactions; in the absence of intermolecular interactions equation (21) reduces to the perfect-gas equation of state. In particular, the second virial coefficient expresses the effect of interactions between pairs of molecules and thus is directly related

to the intermolecular pair-potential. For spherically symmetric molecules the second virial coefficient $B(T)$ is given in terms of the intermolecular pair potential $U(r)$ as follows:

$$B(T) = 2\pi N_0 \int_0^\infty [1 - \exp(-U(r)/kT)]\, r^2 dr \qquad (22)$$

where N_0 is the Avogadro number. The calculation of B from an assumed intermolecular pair-potential is a straightforward procedure. The intermolecular pair-potential can be obtained from B, either by assuming a certain potential form and performing regression analysis to determine its parameters, or by inversion [4-9]. Since, the second virial coefficients are found to be quite insensitive to the potential form chosen, the first method does not lead to a unique potential. On the other hand, inversion techniques developed to determine the potential $U(r)$ from B require extremely high accuracy of the latter [4-9]. For non-spherical molecules the same two methods are available to determine the potential. However, the meaning of the spherical potential derived by an application of the inversion process is not yet understood. One suggestion has been made that the potential, U_B, obtained by inversion in such cases is related to the full anisotropic potential, $U(\bar{r}_\omega, \omega)$, by the equations:

$$U_B(\langle \bar{r}_\omega^{-3} \rangle^{1/3}) = \langle U(\bar{r}_\omega, \omega) \rangle \qquad (23)$$

where

$$\langle \bar{r}_\omega^3 \rangle = \frac{\int \bar{r}_\omega^3 d\omega}{\int d\omega} \qquad (24)$$

and $\bar{r}_\omega$ is the separation at which the potential for an orientation ω takes the value $U(\bar{r}_\omega, \omega)$.

We can see what type of information about the intermolecular pair-potential the second virial coefficients provide if we write equation (18) in the equivalent form:

$$B(T) = \frac{2\pi N_0 \exp(\varepsilon/kT)}{3T}\left[\int_0^\varepsilon \Delta \exp(-\varphi/T)\, d\varphi + \int_\varepsilon^\infty r^3 \exp(-\varphi/T)\, d\varphi\right] \qquad (25)$$

where $\varphi(r) = (U(r) + \varepsilon)/k$ and $\Delta = r_L^3 - r_R^3$, r_L and r_R being the separations of the inner and the outer walls of the potential energy well at the energy φ. The first term in

(25) corresponds to the contribution of the potential well to the virial coefficient at temperature T whereas the second term arises from the repulsive forces for $r < \sigma$. At high temperatures the first term is negligible compared with the second, so that $B(T)$ depends only on the repulsive region. Thus measurements of $B(T)$ in that region theoretically can be used to determine $U(r)$ explicitly. Unfortunately, the temperature range of the measurements restricts this method to the low energy repulsive region of the potential. At low temperatures $B(T)$ is dominated by the first term so that measurements can provide information about the potential well [1].

2.3.2 Transport properties of dilute gases

All transport processes are associated with the flux of a dynamic property owing to the concentration gradient of this property. In the transport mechanism collisions between the molecules are directly involved. The outcome of these molecular collisions is controlled by the intermolecular forces acting between the molecules. When the gas is dilute the collisions occur only between pairs of molecules, so that the scattering of the collisions is determined by the intermolecular pair-potential.

The transport properties of a gas of structureless, spherically symmetric molecules are related to the potential $U(r)$, through a series of collision integrals $\overline{\Omega}^{(l,s)}(T)$ defined by the equations [1]:

$$\overline{\Omega}^{(l,s)}(T) = [(s+1)!(kT)^{s+2}]^{-1} \int_0^\infty Q^{(l)}(E) E^{s+1} \exp(-E/kT)\, dE \tag{26}$$

$$Q^{(l)}(E) = 2\pi \left[1 - \frac{1+(-1)^l}{2(1+l)}\right] \int_0^\infty (1-\cos^l \chi)\, b\, db \tag{27}$$

$$\chi(b, E) = \pi - 2b \int_{r_c}^\infty \frac{dr/r^2}{[1 - b^2/r^2 - U(r)/E]^{1/2}} \tag{28}$$

where r_c is the closest distance of approach in a binary collision having an impact parameter b and a relative kinetic energy E, $\chi(b, E)$ is the scattering angle and $Q^{(l)}(E)$ is a transport cross-section. Measurements of the transport properties of a gas

are equivalent to measurements of the appropriate collision integral. Thus, the viscosity is given by:

$$\eta(T) = \frac{5(\pi mkT)^{1/2}}{16\,\overline{\Omega}^{(2,2)}(T)} f_\eta \tag{29}$$

where m is the molecular mass and f_η a correction factor near unity which accounts for kinetic theory approximations beyond the first. Because f_η, is quite insensitive to the pair-potential, the viscosity can be used to evaluate the collision integral $\overline{\Omega}^{(2,2)}(T)$ at each temperature.

One method of obtaining the potential from the viscosity, is to assume a certain potential-function-model with some disposable parameters and perform non-linear regression analysis to determine these parameters. However, this method depends always on the form of the potential function chosen. Inversion techniques have also been developed [4-8], to yield the potential $U(r)$ directly from the collision integral $\overline{\Omega}^{(2,2)}(T)$.

Application of the inversion process to the measured collision integrals of a polyatomic system necessarily yields a spherically symmetric result. The relationship between the effective spherical potential U_Ω, obtained by inversion, and the true non-spherical potential is not yet fully understood. However, one suggested form of the relation is [4-7]:

$$U_\Omega(\langle \bar{r}_\omega^{-2} \rangle^{1/2}) = \langle U(\bar{r}_\omega, \omega) \rangle \tag{30}$$

where

$$\langle \bar{r}_\omega^{-2} \rangle = \frac{\int \bar{r}_\omega^{-2} d\omega}{\int d\omega} \tag{31}$$

and $\bar{r}_\omega$ is the separation at which the potential for an orientation ω takes the value $U(\bar{r}_\omega, \omega)$.

The viscosity of a gas is dominated by collisions at an energy $\approx 3kT$. Low temperature measurements can be therefore used to test the intermolecular potential

energy function at long range ($r > r_m$). On the other hand at high temperatures the viscosity is dominated by the low-energy repulsive region of the potential and thus experimental measurements can be used to determine the potential in that region.

Other transport properties can also yield information of the pair potential but the available experimental techniques were, until recently, not as accurate as those for the viscosity.

2.3.3 Molecular beam scattering

As already discussed the progress of collisions in a dilute gas is determined by the intermolecular pair-potential. The techniques of molecular beam scattering allows the study of molecular collisions without the energy averaging implicit in the measurement of a transport property. A molecular beam is a well-collimated stream of atoms or molecules which are at sufficiently low density and have sufficiently low velocities relative to each other so that they do not collide together, so that the spatial and velocity broadening of the beam is minimized. In practical applications of molecular beam scattering the beam produced in a supersonic moves in high vacuum in order to reduce the frequency of unwanted collisions with the beam. The beam impinges on a target of another set of molecules or a second beam from which the scattering can be monitored by a suitable detector. Statistically such molecular beam experiments are equivalent to carrying out a large number of collisions between just two molecules over a range of impact parameters; the impact parameter represents the distance by which the two molecular centres would miss if there were no interaction. By using monoenergetic molecular beams, which is a recent technological development [1], one can obtain the integral scattering cross-section $Q(E)$ and the differential scattering cross-section $\sigma(\chi, E)$. The fraction of molecules in an incident beam of energy E which suffer any scattering, which is also the probability of scattering, is determined by the integral cross-section $Q(E)$. The fraction of molecules which are scattered into a unit solid angle about the deflection angle χ is determined by

the differential scattering cross-section $\sigma(\chi, E)$. A full quantum mechanical analysis of the dynamics of two-molecule encounter can relate both $\sigma(\chi, E)$ and $Q(E)$ to the intermolecular pair-potential [1].

2.3.4 Spectroscopy of van der Waals dimers

Two molecules under appropriate conditions can form physically bound dimers. For example, when three molecules approach each other with low energy one of these molecules can remove kinetic energy of the other two which themselves become trapped in their intermolecular potential well, thus forming a dimer. The intermolecular pair-potential energy of the two molecules differs from the 'effective' intermolecular pair-potential of the dimer by a factor depending on the angular momentum of the dimer and the separation of the two molecules forming the dimer (for the particular case of spherically symmetric interactions). Within the well of that 'effective' potential a number of discrete vibration and rotation states exist as for a chemically bound molecule. The energies and spacing of these states are characteristic of the potential well, which thus can be determined. The physically bound dimer system, called often Van der Waals dimer, has many similarities with a chemically bound system and theoretically its rotation and vibration spectra can be studied accordingly. However, only just recently experimental techniques have been developed which make this study possible, the main reasons being the very small concentration of van der Waals dimers in given species, the extremely short life of the dimers under normal conditions and the fact that the dimers of the inert gas atoms possess no dipole moment and therefore they are not active in the infrared region of the spectrum. In order to prolong the dimer's life high vacuum is required, which on the other hand generates the need of an extremely long path-length in the spectrometer.

The spectroscopy of the van der Waals dimers is a very good source of information about the potential well. It is a very promising method but for the time being is restricted to very simple molecules [1].

2.3.5 Solid state properties

The lattice energy, the dimensions and properties such as the compressibility of molecular crystals can be directly related to the intermolecular forces. The arrangement of the molecules in the lattice represents a balance of the repulsive and attractive forces, which is such that the total potential energy is minimized. The calculation of the intermolecular pair-potential from solid state properties involves an assumption about the pair-potential model and should take into account the non-pairwise-addititivity of the potential [1]. The solid state properties are thus mostly regarded as a test of the intermolecular pair-potentials obtained from other sources.

2.3.6 Ab initio calculations

Another way to establish the intermolecular pair-potential is quantum-mechanical calculations called 'ab initio' calculations. In order to obtain the pair-potential by the 'ab initio' calculations one requires the wave function for the two interacting monomers in their ground and all excited states. In general, these wave functions are not known exactly for atoms with many electrons, because of the impossibility of obtaining an exact solution of the Schroedinger wave equation for these systems [1]. However, these wave functions can be obtained for atoms or simple molecules like nitrogen, using theoretical models such as the uncoupled Hartee-Fock perturbation method, or the time-dependent uncoupled Hartee-Fock method [3]. In this manner the 'ab initio' calculations yield the full anisotropic interactions of the pair-potential. Unfortunately, for more complicated molecules the 'ab initio' calculations yield very poor results [1,2] at present.

2.3.7 Molecular properties

A number of indirect methods are available for the experimental determination of dipole, quadrapole and higher moments (used in the calculation of the electrostatic

contribution to the pair-potential), including measurements of pressure and dielectric second virial coefficients, heats of sublimation and other crystal properties, pressure-broadening in microwave, infrared and Raman spectra, collision-induced vibrational, rotational and translational absorption spectra, ion-molecule scattering in gases, non-linear light scattering and molecular beam scattering [2]. All these methods have the disadvantage that the values of the moments depend on the assumed form of the intermolecular pair-potential. In addition they yield only the magnitude, and not the sign, of the moment [2].

2.4 Intermolecular forces and virial coefficients

The second and third volumetric virial coefficients of pure substances and mixtures are directly related to the intermolecular pair potentials (as we have already seen for the second). In the following it will be shown how these coefficients are obtained from the canonical partition function and the way they are related to the intermolecular pair potentials. Finally, the acoustic virial coefficients will be presented which constitute a new source of information about intermolecular pair-potentials.

2.4.1 Volumetric virial coefficients from the partition function

For a system of N indistinguishable molecules the canonical partition function Q [2,10] can be separated into a molecular part Q_{mol} and a configurational integral Q_{N} as follows:

$$Q = Q_{\mathrm{mol}} Q_{\mathrm{N}} / N ! \tag{32}$$

The molecular part depends only on one-molecule properties such as mass, moment of inertia etc. The configurational integral counts for the presence of the intermolecular forces and, for the simplified case of spherical molecules, which will be of interest here, is given by:

$$Q_N = \int_{(V)} \exp(-U_N / kT)\, d\bar{r}^N \qquad (33)$$

where N is the number of molecules, $U_N = U_N(\bar{r}_1, \bar{r}_2, \cdots, \bar{r}_N)$ is the total intermolecular potential of the N molecules, $\bar{r}_i = \bar{r}_i(x_i, y_i, z_i)$ is the position vector of the i^{th} molecule and $d\bar{r}^N = d\bar{r}_1\, d\bar{r}_2 \cdots d\bar{r}_N$ where $d\bar{r}_i = dx_i dy_i dz_i$. The N-fold volume integral is performed over all possible positions $\bar{r}$ of every molecule in the system.

The first term Q_1 of the Q_N series is simply

$$Q_1 = \int_{(V)} \exp(-U_1 / kT)\, d\bar{r}_1 = V \qquad (34)$$

since the intermolecular potential for one molecule U_1 is by definition zero. The second term, which involves the intermolecular potential of two molecules U_2 is given by:

$$Q_2 = \int_{(V)} \exp(-U_2 / kT)\, d\bar{r}_1\, d\bar{r}_2 \qquad (35)$$

and the third term which involves the intermolecular potential of three molecules U_3 is given by

$$Q_3 = \int_{(V)} \exp(-U_3 / kT)\, d\bar{r}_1 d\bar{r}_2 d\bar{r}_3 \qquad (36)$$

Statistical mechanics [2,10] also leads to the result that the pressure is related to the canonical partition function as follows:

$$p = kT \left.\frac{\partial \ln Q}{\partial V}\right|_{N,T} \qquad (37)$$

where k is the Boltzmann constant. Since the molecular part of the partition function is not volume dependent, the above equation can be written

$$p = kT \left.\frac{\partial \ln Q_N}{\partial V}\right|_{N,T} \qquad (38)$$

Expanding equation (38) in density series and comparing with (21) we obtain the relations for the second and third volumetric virial coefficients [10]:

$$B = -\frac{N_0}{2V}(Q_2 - Q_1^2) \qquad (39)$$

$$C = -\frac{N_0^2}{3V^2}[V(Q_3 - 3Q_2Q_1 + 2Q_1^3) - 3(Q_2 - Q_1^2)^2] \qquad (40)$$

2.4.1.1 Second volumetric virial coefficient

In order to calculate the second volumetric virial coefficient from equation (39), one needs to obtain U_2 . According to the assumption of spherical molecules, U_2 involves only central forces and one can write $U_2 = U_{12}(r_{12})$, where $r_{12} = |\bar{r}_1 - \bar{r}_2|$ is the two molecule separation. After some algebra equation (39) becomes:

$$B = 2\pi N_0 \int_0^\infty [1 - \exp(-U_{12} / kT)] r_{12}^2 dr_{12} \tag{41}$$

2.4.1.2 Third volumetric virial coefficient

In order to obtain the third virial coefficient one needs the quantity U_3 . The intermolecular potential of three molecules is given as the sum of pairwise additive terms, U_{ij} , plus an extra term, ΔU , to account for the non-additivity, as discussed previously:

$$U_3 = U_{12} + U_{13} + U_{23} + \Delta U \tag{42}$$

Inserting equation (32) into the expression for Q_3 , and substituting to (40), one obtains the expression for the third volumetric virial coefficient as a sum of two terms related to the intermolecular pair potential as follows:

$$C = C^{add} + \Delta C \tag{43}$$

$$C^{add} = -\frac{8\pi^{-2} N_0^{\,2}}{3} \iiint [1 - \exp(-U_{12} / kT)][1 - \exp(-U_{13} / kT)] \tag{44}$$
$$\times [1 - \exp(-U_{23} / kT)] r_{12} r_{13} r_{23} dr_{12} dr_{13} dr_{23}$$

$$\Delta C = -\frac{8\pi^2 N_0^{\,2}}{3} \iiint \exp[-(U_{12} + U_{13} + U_{23}) / kT] \tag{45}$$
$$\times [\exp(-\Delta U / kT) - 1] r_{12} r_{13} r_{23} dr_{12} dr_{13} dr_{23}$$

where U_{ij} and r_{ij} are the pair potential and the separation between molecules i and j respectively.

2.4.1.3 Volumetric virial coefficients of mixtures

The volumetric virial coefficients for mixtures can be easily obtained from the grand partition function approach [10]. The expression derived for the second volumetric second virial coefficients of a binary mixture is the following

$$B_M = x_1^2 B_{11} + 2x_1 x_2 B_{12} + x_2^2 B_{22} \tag{46}$$

where B_M is the volumetric second virial coefficient of the mixture, x_i and B_{ii} are the mole fraction and the volumetric second virial coefficient of the pure component i, and B_{ij} is the volumetric interaction second virial coefficient, for interactions between two molecules of components i and j.

The expression derived for the volumetric third virial coefficient for a binary mixture is given by:

$$C_M = x_1^3 C_{111} + 3x_1^2 x_2 C_{112} + 3x_1 x_2^2 C_{122} + x_2^3 C_{222} \tag{47}$$

where C_M is the volumetric third virial coefficient of the mixture, C_{iii} is the volumetric third virial coefficient of the pure component i and C_{iij} is the volumetric interaction third virial coefficient, for the interactions of two molecules of component i with one molecule of component j.

2.4.2 Acoustic virial coefficients

The fundamental equation of the speed of sound (discussed in chapter 3)

$$u^2 = (\partial p / \partial \rho)_s \tag{48}$$

where u is the speed of sound, ρ is the mass density and s denotes entropy, after standard thermodynamic manipulations yields:

$$u^2 = (RT / M)\{[z + \rho_n(\partial z / \partial \rho_n)_T] + (R / c_{v,m})[z + T(\partial z / \partial T)_\rho]^2\} \tag{49}$$

with

$$c_{v,m} = c_{v,m}^0 + \int_0^{\rho_n} (\partial c_{v,m} / \partial \rho_n)_T \, d\rho_n \tag{50}$$

and

$$(\partial c_{v,m} / \partial \rho_n)_T = -(R / \rho_n)[2T(\partial z / \partial T)_\rho + T^2(\partial^2 z / \partial T^2)_\rho] \quad (51)$$

where M is the molar mass, $c_{v,m}$ is the molar isochoric heat capacity and $c^0_{v,m}$ is the value of $c_{v,m}$ at zero density.

By substituting the virial expression of the compressibility factor (21) into equation (49) we obtain the following relation for the speed of sound

$$u^2 = A_0(1 + \beta_a \rho + \gamma_a \rho^2 + \cdots) \quad (52)$$

with

$$A_0 = \frac{RT\gamma^{pg}}{M} \quad (53)$$

where A_0 is the value of u^2 at zero density, γ^{pg} is the perfect gas heat capacity ratio and β_a and γ_a are the second and third acoustic virial coefficients respectively.

The second and third acoustic virial coefficients are related to the volumetric virial coefficients by the differential equations [11] as can be shown by:

$$\beta_a = 2B + 2(\gamma^{pg} - 1)T\frac{dB}{dT} + \frac{(\gamma^{pg} - 1)^2}{\gamma^{pg}}T^2\frac{d^2B}{dT^2} \quad (54)$$

$$\gamma_a = \frac{(\gamma^{pg} - 1)}{\gamma^{pg}}\left[B + (2\gamma^{pg} - 1)T\frac{dB}{dT} + (\gamma^{pg} - 1)T^2\frac{d^2B}{dT^2}\right]^2 + \frac{(1+2\gamma^{pg})}{\gamma^{pg}}C + \frac{(\gamma^{pg})^2 - 1}{\gamma^{pg}}T\frac{dC}{dT} + \frac{(\gamma^{pg} - 1)^2}{2\gamma^{pg}}T^2\frac{d^2C}{dT^2} \quad (55)$$

Taken together with equations (41) and (43), these equations relate the second and third acoustic virial coefficients to the intermolecular potential between the molecules in the fluid.

2.5 Intermolecular forces from the speed of sound

Until recently [12-14] the analysis of the speed of sound data have been constrained to simple fits of the square of the speed of sound to pressure or density series in order to obtain the perfect gas heat capacity and the second and third acoustic virial coefficients. Where available , accurate potentials have been used [12,15] to check the validity of the second acoustic virial coefficient data, such as HFD-B2 [16] and BBMS [17] for argon. Some attempts have been made [18-21] to derive second volumetric virial coefficients by fitting second acoustic virial coefficients to the crude, but flexible, square-well potential model [1]. This potential model was regarded suitable for fitting second virial coefficients over a limited temperature range [22]. More recently Ewing and Trusler [23,24] calculated second volumetric virial coefficients for nitrogen from a fit to a site-site Maitland-Smith [25] potential model function. The same authors modified the HFD-B2 potential for argon to fit the second acoustic virial coefficient data. They also calculated interaction second virial coefficients for argon-nitrogen mixtures using again a site-site potential model for the argon-nitrogen interactions.

In a subsequent work [16] the calculation of the whole p,ρ,T surface has been performed , through numerical integration of the differential equation relating the speed of sound with the compressibility factor. The method has been found to be successful but the requirement of initial values for the integration restricts its applicability to substances for which the compressibility factors and their derivatives with respect to the temperature are available at the lowest temperature of the numerical integration.

2.6 References

[1] G. C. Maitland, M. Rigby, E. B. Smith and W. A. Wakeham, *Intermolecular forces* (Clarendon, Oxford, 1981).

[2] C. G. Gray and K. E. Gubbins, *Theory of Molecular Fluids*Volume 1 (Clarendon, Oxford, 1984).

[3] A. van der Avoird, P. E. S. Wormer and A. P. J. Jansen, J. Chem. Phys. **84**, 1629

[4] G. C. Maitland, V. Vesovic and W. A. Wakeham, Mol. Phys. **54**, 287 (1985).

[5] G. C. Maitland, V. Vesovic and W. A. Wakeham, Mol. Phys. **54**, 301 (1985).

[6] G. C. Maitland, M. Mustafa, V. Vesovic and W. A. Wakeham, Mol. Phys. **57**, 1015 (1986).

[7] V. Vesovic and W. A. Wakeham, Mol. Phys. **62**, 1239 (1987).

[8] J. P. M. Trusler, Mol. Phys. **64**, 1153 (1988).

[9] J. P. M. Trusler, Mol. Phys. **57**, 1075 (1986).

(1986).

[10] E. A. Mason and T. H. Spurling, *The Virial Equation of State* (Pergamon, Oxford, 1969).

[11] J. P. M. Trusler, *Physical Acoustics and Metrology of Fluids* (Adam Hilger, Bristol, 1991), p. 76.

[12] M. B. Ewing, M. L. McGlashan and J. P. M. Trusler, J. Chem. Thermodyn. **17**, 549 (1985).

[13] M. B. Ewing, M. L. McGlashan and J. P. M. Trusler, J. Chem. Thermodyn. **18**, 511 (1986).

[14] J. B. Mehl and M. R. Moldover, J. Chem. Phys. **74**, 4062 (1981).

[15] M. B. Ewing, A. A. Owusu and J. P. M. Trusler, Physica **A 156**, 899 (1989).

[16] R. A. Asiz and M. J. Slaman, Mol. Phys. **58**, 679 (1986).

[17] G. C. Maitland and E. B. Smith, Mol, Phys. **22**, 861 (1971).

[18] M. B. Ewing, A. R. H. Goodwin, M. L. McGlashan and J. P. M. Trusler, J. Chem. Thermodyn. **19**, 721 (1987).

[19] M. B. Ewing, R. H. Goodwin, M. L. McGlashan and J. P. M. Trusler, J. Chem. Thermodyn. **20**, 243 (1988).

[20] M. B. Ewing, R. H. Goodwin and J. P. M. Trusler, J. Chem. Thermodyn. **21**, 867 (1989).

[21] M. B. Ewing and J. P. M. Trusler, J. Chem. Phys. **90**, 1106 (1989).

[22] M. E. Boyd and R. D. Mountain, Phys. Rev. **A 2**, 2164 (1970).

[23] M. B. Ewing and J. P. M. Trusler, Physica **A 184**, 415 (1992).

[24] M. B. Ewing and J. P. M. Trusler, Physica **A 184**, 437 (1992).

[25] G. C. Maitland and E. B. Smith, Chem. Phys. Lett. **22**, 443 (1973).

[26] J. P. M. Trusler and M. Zarari, J. Chem. Thermodyn. **24**, 973 (1992).

CHAPTER 3

ACOUSTIC MODEL

3.1 Introduction.

The objective of this chapter is to introduce the basic concepts and the methodology involved in deriving the speed of sound in a fluid from the acoustic measurements performed with the apparatus described in chapter 4.

An acoustic model is presented which relates the speed of sound to the resonance frequencies and halfwidths of the spherical resonator employed; suitable corrections are applied to account for the non-idealities in the fluid and the apparatus.

3.2 The speed of sound as a thermodynamic property.

The fundamental relation between the speed of sound u and the thermodynamic property $(\partial p / \partial \rho)_s$ is [1]:

$$u^2 = (\partial p / \partial \rho)_s \qquad (1)$$

where p is the pressure, ρ is the mass density and s denotes entropy. Generally the speed of sound depends on the frequency and amplitude of the sound wave. It will be shown that the above expression is exact only in the limit of small amplitudes and frequencies. In practice the former limit is easily achieved while the latter is usually achieved.

3.3 Wave equation of an idealized fluid

The starting point for the description of an acoustic process is the derivation of an equation for the transmission of an acoustic pressure wave through an idealized fluid. The fluid is ideal in the sense that its thermal conductivity and viscosity are negligibly small.

Under the additional assumption that local equilibrium in the fluid is achieved instantaneously, the acoustic process is also an adiabatic one. Thus, with the aid of an adiabatic equation of state for the fluid, the equation of continuity and a momentum conservation equation (Euler's equation for an inviscid fluid) it is possible to derive a wave equation for the propagation of sound in a fluid. In the particular case where the disturbances caused by the propagation are small this equation is particularly simple as is shown in the next section.

3.3.1 The equation of state

Small adiabatic acoustic disturbances result in small fluctuations in the pressure and the density from their equilibrium values (p_e and ρ_e). The disturbances in the instantaneous pressure, p, and density, ρ, are related through the partial derivative $(\partial p / \partial \rho)_s$ as follows:

$$p - p_e = (\partial p / \partial \rho)_s (\rho - \rho_e) \tag{2}$$

The fluctuation in the pressure $p_a = p - p_e$ is called the acoustic pressure and the fluctuation in the density $\rho_a = \rho - \rho_e$ is called the acoustic density. Equation (2) written in terms of the acoustic quantities, yields:

$$p_a = (\partial p / \partial \rho)_s \rho_a \tag{3}$$

which is a linear relationship between the acoustic pressure and density. Fluctuations in the temperature, T, are determined accordingly by the equation, $T_a = (\partial T / \partial \rho)_s \rho_a$, but this expression will not be needed in the analysis following.

The fluctuations caused in any property of the fluid by the acoustic disturbances such as p_a and ρ_a, are assumed to be small enough that second order terms can be considered negligible.

3.3.2 The equation of continuity

The mass balance over a volume element ΔV fixed in space, through which the fluid is flowing yields the equation of continuity for the density. Assuming there is no mass production within that volume element, the equation of continuity is given by [2-4]:

$$\frac{\partial \rho}{\partial t} = -\nabla \cdot (\rho \bar{u}) \tag{4}$$

or

$$\frac{\partial \rho_a}{\partial t} = -\rho \nabla \cdot \bar{u} - \bar{u} \cdot \nabla \rho = -\rho \nabla \cdot \bar{u} - \bar{u} \cdot \nabla \rho_a \tag{5}$$

where $\bar{u}$ is the vector of the fluid velocity. Since the fluid velocity at equilibrium, $\bar{u}_e$, is zero, $\bar{u} = \bar{u}_e + \bar{u}_a = \bar{u}_a$ so that the second order term $-\bar{u} \cdot \nabla \rho_a$ can be neglected. Thus equation (5) reduces to:

$$\frac{\partial \rho_a}{\partial t} + \rho \nabla \cdot \bar{u} = 0 \tag{6}$$

which is the linearized continuity equation. This equation provides a functional relationship between the fluid velocity $\bar{u}$ and the acoustic density ρ_a to be used in the following for the derivation of the wave equation.

3.3.3 Euler's equation

The momentum balance over a volume element fixed in space ΔV yields the so-called equation of motion of the fluid [2,4]. In the absence of viscosity and external forces the equation of motion [2,4] reduces to Euler's equation:

$$\frac{\partial \bar{u}}{\partial t} + (\bar{u} \cdot \nabla)\bar{u} = -\frac{1}{\rho}\nabla p \tag{7}$$

By neglecting the small second order term $(\bar{u} \cdot \nabla)\bar{u} = (\bar{u}_a \cdot \nabla)\bar{u}_a$ equation (7) yields the linear Euler's equation:

$$\rho \frac{\partial \bar{u}}{\partial t} = -\nabla p_a \tag{8}$$

3.3.4 Wave equation

The three equations, equation of state, equation of continuity and Euler's equation, must be combined to yield a single differential equation with one variable. This equation will be shown to have a wave nature and therefore it is called the wave equation.

Taking the divergence of (8) and neglecting second order terms in the acoustic quantities we get:

$$\rho \nabla \cdot \frac{\partial \bar{u}}{\partial t} = -\nabla \cdot (\nabla p_a) = -\nabla^2 p_a \tag{9}$$

Employing the property $\nabla \cdot (\partial \bar{u} / \partial t) = \partial (\nabla \cdot \bar{u}) / \partial t$ equation (9) is written:

$$\rho \frac{\partial (\nabla \cdot \bar{u})}{\partial t} = -\nabla^2 p_a \tag{10}$$

If we differentiate the linearized continuity equation, equation (6), with respect to time and combine it with equation (10) we obtain:

$$\frac{\partial^2 \rho_a}{\partial t^2} = \nabla^2 p_a \tag{11}$$

Use of the equation of state (3) to eliminate ρ_a yields:

$$\nabla^2 p_a = \frac{1}{c^2} \frac{\partial^2 p_a}{\partial t^2} \tag{12}$$

where c is given by

$$c = \sqrt{(\partial p / \partial \rho)_s} \tag{13}$$

Equation (12) is the linearized wave equation for the propagation of sound in fluids. Since the acoustic pressure p_a and acoustic density ρ_a are proportional according to (3), the acoustic density also satisfies the wave equation. Similar mathematical manipulations employing equations (6) and (8) demonstrate that the fluid velocity $\bar{u}$ and the acoustic temperature T_a also satisfy the wave equation [1].

3.3.5 Velocity potential

It is more convenient to express all the acoustic quantities in terms of a single quantity which is such that if it satisfies the wave equation, then so do all the acoustic quantities. It will be shown here that this quantity is the velocity potential.

Employing the properties $\nabla \times \nabla f = 0$ and $\nabla \times (\partial \bar{u} / \partial t) = \partial(\nabla \times \bar{u}) / \partial t$, equation (8) yields $\nabla \times \bar{u} = 0$. This means that the fluid velocity is irrotational and thus, it can be expressed as the gradient of a scalar function. This function is called the velocity potential which we denote by Ψ and we write:

$$\bar{u} = -\nabla\Psi \tag{14}$$

Combining equations (8) and (14) we get:

$$\nabla(\rho \partial\Psi / \partial t - p_a) = 0 \tag{15}$$

If we express the acoustic pressure in terms of the velocity potential by setting

$$p_a = \rho \frac{\partial \Psi}{\partial t} \tag{16}$$

then we can rewrite the wave equation, equation (12), neglecting second order terms in the acoustic quantities, as follows:

$$(\partial / \partial t)\,[\nabla^2\Psi - (1 / c^2)(\partial^2\Psi / \partial t^2)] = 0 \tag{17}$$

It is obvious now from (17) that if the velocity potential satisfies the wave equation then so does the acoustic pressure and, according to linear relationship of (4), so does the acoustic density. In addition by writing the wave equation for the fluid velocity

$$\nabla^2\bar{u} - (1 / c^2)\partial^2\bar{u} / \partial t^2 = -\nabla\,[\nabla^2\Psi - (1 / c^2)(\partial^2\Psi / \partial t^2)] = 0 \tag{18}$$

it is demonstrated that if the velocity potential satisfies the wave equation then so do the fluid velocity and all other acoustic quantities.

3.3.6 The wave nature of the wave equation solution

It was mentioned above that equation (12), has a wave nature and this is the reason it is called the wave equation. The wave nature of equation (12) as well as the physical interpretation of the constant c of equation (13) will be demonstrated in the following.

If all the acoustic variables are functions of only one spatial coordinate, then the phase of any variable is constant on any plane perpendicular to this coordinate and the waves are called plane waves. In that case equation (12) is written:

$$\frac{\partial^2 p_a}{\partial z^2} = \frac{1}{c^2}\frac{\partial^2 p_a}{\partial t^2} \tag{19}$$

The general solution of this partial differential equation (a general solution in 3-D is discussed by Landau and Lifshitz in [5]) is:

$$p_a(z,t) = f_1(ct - z) + f_2(ct + z) \tag{20}$$

We consider the solution $f_1(ct - z)$. At time t_1 the acoustic pressure at z_1 is $f_1(ct_1 - z_1)$. At time t_2 this particular acoustic pressure (or any other acoustic quantity, since all satisfy the wave equation) has moved a distance:

$$z_2 - z_1 = c\,(t_2 - t_1) \tag{21}$$

Since the particular acoustic pressure was chosen arbitrarily any acoustic pressure will move with the same speed c. This is also the case for all the acoustic quantities. Thus, we can say that in the limit of small amplitudes, so that the acoustic quantities can be considered small, and small frequencies, so that the assumption about equilibrium is valid, the speed of sound u in a non-dissipative, inviscid fluid is equal to $c = \sqrt{(\partial p / \partial \rho)_s}$. That forms the proof of equation (1).

3.4 Wave equation of a dissipative fluid

In a real fluid, of course, neither the viscosity nor the thermal conductivity are zero so that dissipative processes are possible. In this section we consider the wave equation for a dissipative fluid while retaining the assumption that the acoustic quantities all have a small magnitude.

3.4.1 Navier-Stokes equation

If the effects of friction are considered the momentum balance, which for the idealized case reduces to Euler's equation, results in Navier-Stokes equation [2]:

$$\rho\frac{\partial \bar{u}}{\partial} = -\nabla p + (4/3\ \ \eta + \eta_b)\nabla(\nabla\cdot\bar{u}) - \eta\nabla\times(\nabla\times\bar{u}) \qquad (22)$$

where η is the shear viscosity coefficient and η_b is called the bulk viscosity. According to equation (3) the acoustic density is proportional to the acoustic pressure as:

$$\rho_a = \kappa_s \rho p_a \qquad (23)$$

where $\kappa_s = 1/\rho(\partial\rho/\partial p)_s$ is the isentropic compressibility. By differentiating equation (23) with respect to time and neglecting second order terms in the acoustic quantities we get:

$$\partial\rho_a/\partial t = \kappa_s \rho \partial p_a/\partial t \qquad (24)$$

which combined with equation of continuity, equation (6), yields:

$$\frac{\partial p_a}{\partial t} = -\frac{1}{\kappa_s}\nabla\cdot\bar{u} \qquad (25)$$

From the above equation it is shown that the rate of change in the compression is proportional to $\nabla\cdot\bar{u}$. The acoustic disturbances cause sound waves and thus set the fluid into oscillation. Whenever a real body it is set into oscillation, as here the fluid is set by the acoustic disturbance, dissipative forces arise, which result in a damping of the oscillations [3]. These forces are assumed to be proportional to the rate of change of the property which oscillates; for a spring this property is the displacement, for a fluid we can consider the pressure. Thus, we may express this opposing force as

$$F_{opp} = -\lambda\frac{\partial p_a}{\partial t} = \frac{\lambda}{\kappa_s}\nabla\cdot\bar{u} \qquad (26)$$

where λ is the proportionality constant, and the term to be included in the stress tensor of the fluid is $-\eta_b\nabla\cdot\bar{u}$ [2]. The bulk viscosity η_b represents in this way a compressional resistance. For dilute monatomic gases the bulk viscosity is practically zero but it may be quite large in polyatomic gases at certain frequencies. The physical mechanism of its effect

is related to the time required to establish thermodynamic equilibrium between the translational and the rotation-vibration motions of the gas molecules [2,6,7].

Any vector function of position such as $\bar{u}$ can always be uniquely separated into a longitudinal (or lamellar) part $\bar{u}_l$, for which the curl is zero, and a transverse (or rotational) part $\bar{u}_t$, for which the divergence is zero [2]. Since the gradient of a scalar function is entirely longitudinal ($\nabla \times \nabla f = 0$ for any f), the Navier Stokes equation of motion, equation (22), can be split into two separate equations, one relating p_a to the longitudinal part of the fluid velocity, the other giving the behaviour of the transverse part, unrelated to pressure waves,

$$\rho \frac{\partial \bar{u}_l}{\partial t} = -\nabla p_a + (\eta_b + 4/3\,\eta)\nabla^2 \bar{u}_l \qquad (27)$$

$$\rho \frac{\partial \bar{u}_t}{\partial t} = -\eta \nabla \times (\nabla \times \bar{u}_t) = \eta \nabla^2 \bar{u}_t \qquad (28)$$

Thus the two parts of the velocity solution $\bar{u}_l$ and $\bar{u}_t$, can be solved for separately and need not be combined until we come to satisfy the boundary conditions. Equation (27) will be employed in the following for the derivation of the solution of the propagational mode of the wave equation. The transverse part solution will be shown to be important only near the boundaries.

3.4.2 Thermal conduction

Another matter we have to consider is the existence of non-zero thermal conductivity in a real fluid. The fluctuations in the pressure caused by sound are accompanied by fluctuations in the temperature. As soon as there are temperature gradients in the fluid, heat will flow irreversibly from regions of higher temperatures to those of lower temperatures. As a consequence the acoustic cycle is not purely adiabatic [2].

From Fourier's law of heat conduction, the heat flux is proportional to the temperature gradient:

$$J_{\mathrm{h}} = -\kappa \nabla T_{\mathrm{a}} \tag{29}$$

where κ is the coefficient of thermal conductivity and T_a is the fluctuation of the equilibrium thermodynamic temperature, which we call the acoustic temperature. Denoting the heat transferred per unit mass by q_a, and neglecting viscous dissipation terms, which are of second order in the fluid velocity $\bar{u}$, we apply the general equation of continuity [2] to the acoustic heat density ρq_{a}. To a first order approximation in the acoustic quantities we find [1]:

$$\rho \frac{\partial q_{\mathrm{a}}}{\partial t} = -\nabla \cdot J_{\mathrm{h}} = \kappa \nabla^2 T_{\mathrm{a}} \tag{30}$$

Since the rate of entropy production per unit mass is $ds=dq/T$, we write

$$\frac{\partial s_{\mathrm{a}}}{\partial t} = \frac{\kappa}{\rho T} \nabla^2 T_{\mathrm{a}} \tag{31}$$

where s_a is the fluctuation in the entropy from the equilibrium thermodynamic value or simply the acoustic entropy. Combining the above equation with the equation of state relating the change in entropy with the change in pressure and temperature

$$\mathrm{d}s = \left.\frac{\partial s}{\partial T}\right|_{\mathrm{p}} \mathrm{d}T + \left.\frac{\partial s}{\partial p}\right|_{\mathrm{T}} \mathrm{d}p$$

or for the acoustic problem:

$$s_{\mathrm{a}} = \left.\frac{\partial s}{\partial T}\right|_{\mathrm{p}} T_{\mathrm{a}} + \left.\frac{\partial s}{\partial p}\right|_{\mathrm{T}} p_{\mathrm{a}} \tag{32}$$

we obtain the second-order diffusion equation

$$D_{\mathrm{h}} \nabla^2 T_{\mathrm{a}} = (\partial / \partial t)\{T_{\mathrm{a}} - [(\gamma - 1) / \gamma \beta] p_{\mathrm{a}}\} \tag{33}$$

where $\beta = (\partial p / \partial T)_{\rho}$, $D_{\mathrm{h}} = \kappa / \rho c_{\mathrm{p}}$ is the thermal diffusivity, $c_{\mathrm{p}} = T(\partial s / \partial T)_{\mathrm{p}}$ is the isobaric heat capacity and γ is the ratio of the isobaric to the isochoric heat capacity.

3.4.3 Equation of continuity

Based on the separation of the fluid velocity into a longitudinal and a rotational part, since the divergence of the rotational part is zero, we can write the equation of continuity as

$$\frac{\partial \rho_a}{\partial t} + \rho \nabla \cdot \bar{u}_1 = 0 \tag{34}$$

where ρ_a is the acoustic density.

3.4.4 Equation of state

In order to relate the acoustic quantities of the pressure, density and temperature we write the thermodynamic equation of state

$$\rho_a = \left.\frac{\partial \rho}{\partial p}\right|_T p_a + \left.\frac{\partial \rho}{\partial T}\right|_p T_a = (\gamma / c^2)(p_a - \beta T_a) \tag{35}$$

where the constant c is as defined in equation (13).

3.4.5 The wave equation

So far we have involved four acoustic quantities, namely the acoustic pressure temperature and density and the particle velocity. There are also four equations available interrelating the acoustic quantities:

- Navier Stokes (22)
- equation of state (35)
- equation of continuity (34)
- second order diffusion equation (33)

Combining the equation of continuity (34) with equations (27) and (35) we obtain [1,2]

$$\nabla^2 p_a = \frac{\gamma}{c^2}[(\partial^2 / \partial t^2) - D_v(\partial / \partial t)\nabla^2](p_a - \beta T_a) \tag{36}$$

where $D_v = (4\eta / 3 + \eta_b) / \rho$.

This equation can be solved simultaneously with equation (33) to yield the solution for the acoustic pressure and temperature, and, with the aid of the equation of state (35), the solution for the density.

Also, combining (27) with (34) and (35) we obtain the expression for the longitudinal fluid velocity

$$\frac{\partial u_1}{\partial t} = -\nabla[(p_a / \rho) + (\gamma D_v / \rho c^2)(\partial / \partial t)(p_a - \beta T_a)] \quad (37)$$

Equation (36) is the wave equation modified for the effects of viscosity and thermal conduction. If there were no thermal conductivity then $D_h = 0$ and thus from equation (33) $T_a = (\gamma - 1)p_a / \gamma\beta$, which is equivalent to $\gamma(p_a - \beta T_a) = p_a$. If there were also no viscosity then $D_v = 0$, and equation (36) reduces to the simple wave equation of the idealized fluid, equation (12), for which we have illustrated that the speed of sound u=c. If the thermal conductivity were infinite then, from equation (33), $T_a = 0$. In that case, from equation (36), the speed of sound $u = c / \sqrt{\gamma}$, the isothermal speed of sound. For intermediate cases the pressure and temperature are coupled together.

3.4.6 Simple-harmonic wave motion

The wave equation is a partial differential equation and, in order to solve it, we must make assumptions about the form of the solution. For the case that the acoustic disturbance is simple-harmonic, which is our case, the solution we have to consider is that for simple-harmonic wave motion. In addition, since any wave may be expanded into harmonic components of various frequencies using a Fourier series analysis a treatment using simple-harmonic wave motion places no constraints whatsoever on the solutions we obtain. In a simple harmonic wave motion all the small acoustic quantities vary with time as $\exp(i\omega t)$, where ω is the angular frequency of the sound.

Accordingly, we can express the acoustic pressure p_a , as

$$p_a = P_a \exp(i\omega t) \quad (38)$$

where P_a is the amplitude of the acoustic pressure. By differentiating the above equation with respect to time we find:

$$\frac{\partial p_a}{\partial t} = i\omega p_a \quad (39)$$

Thus, if we express the wave equation as follows:

$$\nabla^2 p_a = (k / \omega)^2 \frac{\partial^2 p_a}{\partial t^2} \quad (40)$$

it is a prerequisite that the acoustic pressure satisfies also:

$$(\nabla^2 + k^2) p_a = 0 \tag{41}$$

where k is called the propagation constant. Equation (41) is called the Helmholtz equation and has eigenvalues $-k^2$ [1].

Equation (40) has the form of the wave equation for the idealized fluid, equation (12), in which ω / k is equal to the speed of sound c. It is now necessary to obtain the relationship between k and ω for the case of the dissipative fluid, known as the 'dispersion relation' [1].

It is convenient to introduce the dimensionless reduced propagation constant $\Gamma = kc / \omega$ [2] defined such that it takes the value unity for an ideal fluid. Inserting $-\Gamma^2$ for $(c^2 / \omega^2)\nabla^2$ and $i\omega$ for $\partial / \partial t$, as equations (39) and (41) imply, into equation (36) we obtain:

$$(\Gamma^2 + i\omega\tau_v\Gamma^2 - \gamma) p_a + (\gamma - i\omega\tau_v\Gamma^2)\beta T_a = 0 \tag{42}$$

where $\tau_v = D_v / c^2$. Similarly, from equation (33) we obtain,

$$(1 - i\omega\tau_h\Gamma^2) T_a - [(\gamma - 1) / \gamma\beta\ ] p_a = 0 \tag{43}$$

where $\tau_h = D_h / c^2$. Combining equations (42) and (43) we find,

$$\Gamma^4(\gamma\omega^2\tau_v\tau_h - i\omega\tau_h) + \Gamma^2(1 + i\gamma\omega\tau_h + i\omega\tau_v) - 1 = 0 \tag{44}$$

There are two solutions for Γ^2 :

$$\Gamma^2 = \frac{-i}{2\omega\tau_h} \frac{1 + i\omega\tau_v + i\gamma\omega\tau_h \pm D}{1 + i\gamma\omega\tau_v} \tag{45}$$

where D is given by

$$D^2 = (1 + i\omega\tau_v - i\gamma\omega\tau_h)^2 + 4i\ (\gamma - 1)\omega\tau_h \tag{46}$$

Usually the effects of thermal conductivity and viscosity are slight and the quantities $\omega\tau_h$ and $\omega\tau_v$ correspondingly small so that second order terms involving these quantities can be neglected. Thus, in a first order approximation, equations (45) and (46) yield the solution for -D:

$$\Gamma^2 = 1 - i\left[\omega\tau_v + (\gamma - 1)\omega\tau_h\right] \tag{47}$$

or

$$k^2 = \frac{\omega^2}{c^2} - \frac{\omega^2}{c^2} i\,[\omega\tau_v + (\gamma - 1)\omega\tau_h] \tag{48}$$

This solution is called the propagational mode of sound and the propagation constant k is generally a complex quantity given by

$$k = \frac{\omega}{u_p} - i\alpha \tag{49}$$

where u_p is called the phase speed and α is the sound absorption coefficient.

In order to make equation (49) clear we consider the solution of the wave equation for simple harmonic motion:

$$p_a = A\ \exp[i\ (\omega t - kz)] \tag{50}$$

If k is complex it can be written $k = \mathrm{Re}(k) + \mathrm{Im}(k)$ and therefore equation (50) yields

$$p_a = A\ \exp[\mathrm{Im}(k)z]\ \exp[i\omega t - i\,\mathrm{Re}(k)z] \tag{51}$$

As is clear from (51) ,the amplitude of the sound wave decreases (if Im(k) is negative quantity) with distance z from the source as $\exp[\mathrm{Im}(k)z]$ .Therefore we can identify $\alpha = -\mathrm{Im}(k)$ as the sound absorption coefficient. It can be also easily shown (using the same method employed in 3.3.6) that the phase of the sound wave $\omega t - \mathrm{Re}(k)z$ travels with speed $u_p = \omega / \mathrm{Re}(k)$ so that $\mathrm{Re}(k) = \omega / u_p$.

From equations (48) and (49), by equating real and imaginary parts and assuming that the square of the sound absorption coefficient is a negligible quantity, we find that $u_p = c = u$, where $u = \omega / k$ is the speed of sound in the fluid, which is identical with that for the idealized fluid, but the amplitude of the sound wave is minimized by the sound absorption coefficient given by:

$$\alpha = (\omega^2 / 2c)[\tau_v + (\gamma - 1)\tau_h] \tag{52}$$

The derivation given here has been performed for the propagational mode. The wave equation, equation (40), generalized for all the acoustic quantities, has solutions for all the different modes of k. The total solution for the acoustic quantities is obtained by the summation of the solutions corresponding to the different modes [1]. In the following we

will derive the solution for the acoustic quantities for each of the modes involved separately.

3.4.6.1 Propagational mode

By substitution of the value of Γ obtained for the propagational mode, equation (47), into equations (43) and (37), we obtain the contributions of the propagational mode to the acoustic temperature and longitudinal velocity:

$$T_p = [(\gamma - 1) / \gamma\beta\,](1 + i\omega\tau_h)\, p_p \tag{53}$$

$$\bar{u}_{l,p} = (i / \omega\rho)\,(1 + i\omega\tau_v)\,\nabla p_p \tag{54}$$

where the notation p in the acoustic quantities implies the propagational mode solutions. The propagational mode solution is the only significant solutions in the bulk of the fluid (away from the boundaries) [8,9].

3.4.6.2 Thermal mode

The second solution of equation (45) is obtained for $+D$. A first order approximation to equation (45) yields

$$\Gamma_h^2 = -i / (\omega\tau_h) \tag{55}$$

This solution is called the thermal mode. The reduced propagation constant Γ_h has equal real and imaginary parts. This results in a rapid attenuation of the thermal waves. Substituting equation (55) into equations (42) and (37) we obtain the contribution of the thermal mode to the acoustic pressure and longitudinal velocity:

$$p_h = -i\gamma\beta\omega\,(\tau_h - \tau_v)\, T_h \tag{56}$$

$$\bar{u}_{l,h} = (\gamma\beta\tau_h / \rho)\,\nabla T_h \tag{57}$$

where the subscript h indicates the thermal mode solutions.

The thermal and the shear waves treated below are found [8,9] to be important only near to the boundaries enclosing the fluid and not in the bulk of the fluid. The thermal

wave solution will be used in order to satisfy the boundary condition that the temperature is continuous at the boundary.

3.4.6.3 Shear mode

A third solution can be derived from the rotational part of the fluid velocity. Inserting $-\Gamma_s^2$ for $(c^2/\omega^2)\nabla^2$ and $i\omega$ for $\partial/\partial t$ in equation (28)

$$\Gamma_s^2 = -i/(\omega\tau_s) \tag{58}$$

where $\tau_s = D_s/c^2$, and $D_s = n/\rho$ is the kinematic viscosity. There is no corresponding contribution to the acoustic temperature or pressure. This third solution is called the shear mode. As for the thermal mode, the reduced propagation constant Γ_s has equal real and imaginary part, which indicates rapid attenuation of this mode.

3.5 Wave equation solutions for a spherical cavity

When sound waves are produced in a region completely enclosed by walls, all wave motion is a standing-wave motion determined by the geometry and nature of the enclosing walls. If the excitation frequency of the sound source in such a cavity coincides with the natural frequency of the enclosure then resonance occurs. When the enclosure is of simple geometry and the wall properties are known, solutions of the wave equation can be found that satisfy the boundary conditions at the walls. Since we shall be employing a spherical enclosure, described in chapter 4, for the measurements reported here we must consider the eigenvalues of the wave equation for a spherical cavity.

3.5.1 Free oscillations - Normal modes

As we have already seen in section (3.3.5) all acoustic quantities can be expressed in terms of the velocity potential $\Psi(\bar{r},t)$, where $\bar{r}$ is the position vector. If a velocity potential can be found which satisfies the wave equation *and* the boundary conditions

imposed by the enclosure, then the problem is solved and all the acoustic quantities can be calculated. For the velocity potential to satisfy the wave equation

$$[\nabla^2 + (k / \omega)^2(\partial^2 / \partial t^2)]\Psi(\bar{r},t) \tag{59}$$

it should be an eigenfunction of the Helmholtz equation

$$(\nabla^2 + k^2)\Psi(\bar{r},t) = 0 \tag{60}$$

Since the time dependence of a simple harmonic standing wave is spatially uniform the velocity potential can be written:

$$\Psi(\bar{r},t) = A\ \Phi(\bar{r})\exp(i\omega t) \tag{61}$$

where $\Phi(\bar{r})$ is a dimensionless spatial distribution function of the wave field and A is a constant determining the overall amplitude. It is obvious that if $\Psi(\bar{r},t)$ is an eigenfunction of the Helmholtz equation then so is $\Phi(\bar{r})$ and therefore equation (60) can be simplified to

$$(\nabla^2 + k^2)\Phi(\bar{r}) = 0 \tag{62}$$

In the following we will find the solutions $\Phi_N(\bar{r})$ of the wave equation and the corresponding eigenvalues $-K_N^2$ of the Helmholtz equation that satisfy the boundary conditions (N stands for a triplet of numbers n_1, n_2, n_3 as required for a three dimensional wave).

If the motion of any element of the non-rigid enclosure is assumed to depend only on the acoustic pressure acting there, then the boundary is said to be of local reaction. The boundary conditions at an interface between a fluid and solid walls are that: (1) the tangential component of the fluid velocity on the surface is zero, and (2) that the boundary is of local reaction [1,2]. The latter is not a boundary condition itself, rather it is a prerequisite for the separation of wall motion from fluid motion.

Based on the second boundary condition we can write [1,2]:

$$u_n(\bar{r}_s) = p_a(\bar{r}_s)\, Y\ (\bar{r}_s, \omega) \tag{63}$$

where $u_n(\bar{r}_s)$ is the outward pointing normal component of the fluid velocity at position $\bar{r}_s$ on the surface S, $p_a(\bar{r}_s)$ is the acoustic pressure and

$$Y(\bar{r}_s, \omega) = y(\bar{r}_s, \omega) / (\rho u) \tag{64}$$

is the acoustic admittance of the surface, $y(\bar{r}_s)$ being the dimensionless specific acoustic admittance of the surface, since ρu is the characteristic acoustic impedance of the fluid. When the acoustic admittance is zero then the surface is said to be rigid. In that case the fluid velocity vanishes at the boundary. When the acoustic admittance is infinite, the pressure vanishes at the boundary, which is then said to have pressure release [1].

Using equations (14) and (16), which relate the velocity and the acoustic pressure to the velocity potential, equation (63) is written

$$\frac{\partial}{\partial n}\Phi_N(\bar{r}, \omega)\Big|_{\bar{r}=\bar{r}_s} = -i\,(\omega/u)\,\Phi_N(\bar{r}_s, \omega)\,y(\bar{r}_s, \omega) \tag{65}$$

We shall seek for an infinite set of solutions that are orthogonal, finite and continuous within R (the space enclosed by the surface S). These solutions define the normal modes of the cavity and it will be shown that they may be used to construct any physically-significant solution of the wave equation.

The orthogonality condition is interpreted as

$$\iiint_R \Phi_N(\bar{r}, \omega)\,\Phi_M^*(\bar{r}, \omega)\,dV = V\,\Lambda_N(\omega)\,\delta(N-M) \tag{66}$$

where * denotes the conjugate, $\Lambda_N(\omega)$ is the normalization constant and $\delta(N-M) = \delta(n_1-m_1)\,\delta(n_2-m_2)\,\delta(n_3-m_3)$ is the product of three Dirac delta functions.

The effect of the boundary conditions is to constrain k to discrete values K_N. Thus, from equation (49), where $u_p = c = u$, we obtain for $k = K_N$ the corresponding complex eigenfrequencies F_N:

$$F_N = f_N + i g_N = \frac{u}{2\pi}(K_N + i\alpha) \tag{67}$$

Free oscillations of the fluid inside the enclosure can only occur at these discrete frequencies, called the natural frequencies of the cavity. The normal modes Ψ_N will oscillate with a time dependence $\exp(i\,2\pi F_N t) = \exp(i\,2\pi f_N t)\exp(-\,2\pi g_N t)$. Thus the free oscillations will decay with time as $\exp(-\,2\pi g_N t)$.

The normal-mode solutions are employed in the following in order to derive the steady state response of the cavity to a simple-harmonic source of sound.

3.5.2 Forced oscillations - Steady-state response of the cavity

The normal modes define only the form of the free oscillations allowed within the cavity whereas we require the steady-state response (forced oscillations). However, it will be shown that all the acoustic properties of the cavity, including both the transient and steady-state response to a source of sound, can be expressed in terms of the normal-mode solutions. In this section we consider the response of the cavity to a continuous simple-harmonic source of sound, the case in which we are interested in the present work. The velocity potential for a cavity driven in the steady state by an infinitesimally small source of strength S_ω placed at position $\bar{r}_0$ will be denoted by [1,2]

$$\Psi_\omega(\bar{r}|\bar{r}_0,t) = S_\omega G_\omega(\bar{r}|\bar{r}_0)\exp(i\omega t) \tag{68}$$

where $G_\omega(\bar{r}|\bar{r}_0)$ is the spatial distribution function of the wave field produced by the source. The spatial distribution of the wave field $G_\omega(\bar{r}|\bar{r}_0)$ of the driven cavity differs from that of the undriven cavity because it is discontinuous at the source point. Therefore it is not a solution of the homogeneous Helmholtz equation, and obviously the velocity potential is not a solution of the homogeneous wave equation. However, $G_\omega(\bar{r}|\bar{r}_0)$ satisfies the inhomogeneous equation [2]

$$(\nabla^2 + k^2)G_\omega(\bar{r}|\bar{r}_0) = -\delta(\bar{r}-\bar{r}_0) \tag{69}$$

From the boundary conditions we obtain, in the same way as for the undriven cavity,

$$\frac{\partial}{\partial n}G_\omega(\bar{r}|\bar{r}_0)\bigg|_{\bar{r}=\bar{r}_S} = -i(\omega/u)\,G_\omega(\bar{r}_S|\bar{r}_0)\,y(\bar{r}_S,\omega) \tag{70}$$

Whatever the form of G_ω, it can be expanded in infinite series of orthogonal functions. Thus in terms of the normal modes of the cavity, which are the natural choice of orthogonal functions, the expansion yields [2]:

$$G_\omega(\bar{r}|\bar{r}_0) = \sum_N \frac{\Phi_N(\bar{r},\omega)\Phi_N^*(\bar{r}_0,\omega)}{V\,\Lambda_N[K_N^2(\omega)-k^2]} \tag{71}$$

Using equations (16), (68) and (71), we calculate the spatial distribution of the acoustic pressure of the driven cavity

$$p_\omega(\bar{r}|\bar{r}_0) = i\omega\rho S_\omega \sum_N \frac{\Phi_N(\bar{r},\omega)\Phi_N^*(\bar{r}_0,\omega)}{V\Lambda_N[K_N^2(\omega)-k^2]} \tag{72}$$

The amplitude of $p_\omega(\bar{r}|\bar{r}_0)$, $\left|p_\omega(\bar{r}|\bar{r}_0)\right|$, is maximum when $\left|K_N^2(\omega)-k^2\right|$ is minimum. The term $[K_N^2(\omega)-k^2]$ is given by

$$[K_N^2(\omega)-k^2] = (2\pi F_N/u - i\alpha)^2 - (2\pi f/u - i\alpha)^2 =$$
$$\frac{(2\pi)^2}{u^2}(f_N^2-f^2) - i\frac{4\pi\alpha}{u}(f_N-f) + i\frac{(2\pi)^2}{u^2}2f_N g_N + \frac{4\pi\alpha}{u}g_N \tag{73}$$

From the above relation it is obvious that, $\left|p_\omega(\bar{r}/\bar{r}_0)\right|$ is maximum, and thus any mode N is resonant, when the frequency of the source, f, is near to f_N, the real part of the natural frequency F_N. Figure 3.1 illustrates how the amplitude of $p_\omega(\bar{r}/\bar{r}_0)$ varies with frequency near resonance. The ratio $Q_N = f_N/2g_N$, which is the quality factor of the mode N [1], typically has large values of the order 10^3. Consequently, since α is also a very small quantity, the term $4\pi\alpha g_N/u$ can be considered negligibly small. Near resonance $f \approx f_N$ so that the term $-i(4\pi\alpha/u)(f_N-f)$ also becomes negligible. The imaginary term $i(2\pi/u)^2 2f_N g_N$ prevents the denominator from ever becoming zero.

The summation in (72) is to be carried out over all modes N with frequencies f_N near f. It is found that the number of modes within a certain frequency range increases when the frequency increases [1,2]. However, in the frequency range of interest, up to about 40000 Hz here, the modes are most likely to be well resolved and thus a single mode or a group of degenerate modes can be studied in near isolation, the only contribution of other nearby modes being a small background. Thus, using the approximation of equation (73), $(u/2\pi)^2(K_N^2-k^2) = F_N^2 - f^2$, equation (72) is rewritten as:

$$p_\omega = \sum_{N_1}^{N_2} \frac{A_N}{(F_N/f)^2-1} + B + C(f-f_0) + \cdots \tag{74}$$

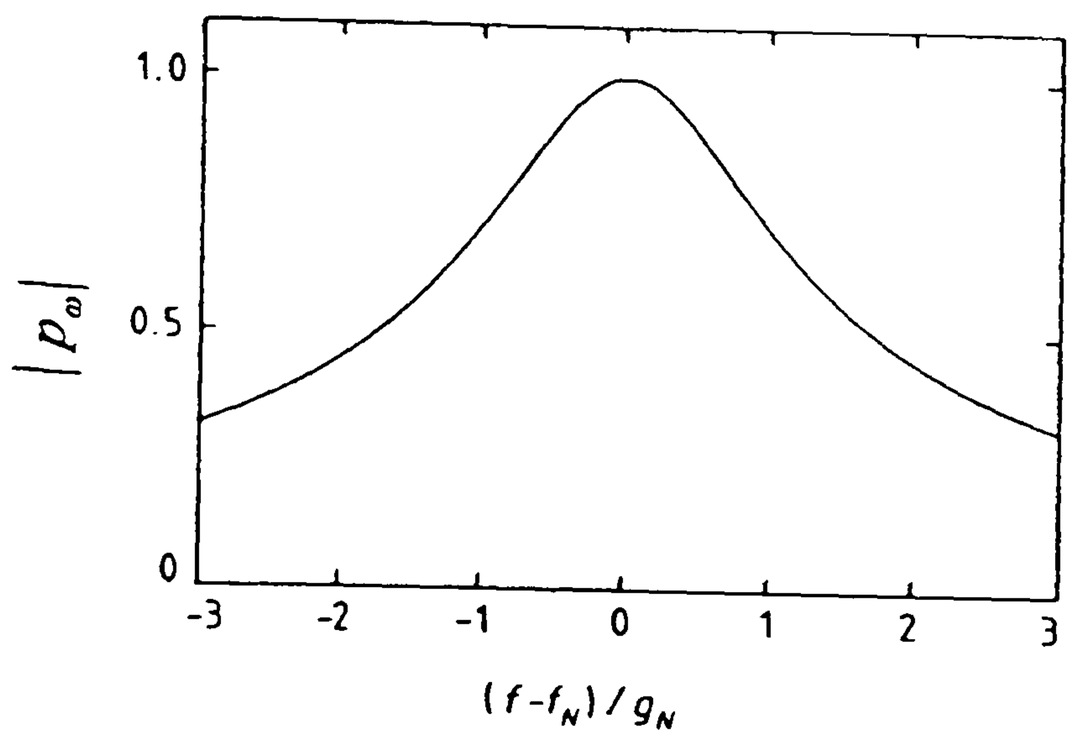

Figure 3.1. Amplitude of the acoustic pressure p_ω as a function of the frequency, near resonance.

where the summation is over the number of degenerate modes occuring at one frequency, and the terms after the summation are background contributions expanded in a Taylor series about some frequency f_0 near to the resonance frequency. The coefficients $A_N, B, C, \cdots$,which are complex constants for a fixed source, as well as the complex natural frequency F_N , can be determined by fitting (74) to experimental values of the phase and amplitude of the acoustic pressure at different driving frequencies.

Near resonance the term $[(F_N / f)^2 - 1]$ in equation (74) is almost equal to $2if_N[g_N + i(f - f_N)]$. If there is no background, at $f = f_N \pm g_N$ the amplitude of p_ω in (74) is reduced to $1/\sqrt{2}$ of its maximum at $f = f_N$ (see figure 3.1). Since these are the half-power points, g_N is referred to as the half-width of the resonance.

In order to obtain the speed of sound, u, from the values of F_N determined in this manner it is necessary to employ equation (67) together with independently determined values of K_N . The values of K_N for a real spherical cavity and their relation to those for an idealized cavity (zero surface admittance and perfect geometry) are considered in the next section.

3.5.3 Normal modes for idealized and real cavities.

So far we have derived the boundary conditions for the wave field in a driven and an undriven cavity. Based on these boundary conditions a relation has been obtained, between the normal modes of a cavity with idealized properties, i.e. cavities of perfect geometry and zero surface admittance, and the modes of the real cavity. The effects of the imperfection for the real cavity have been evaluated as perturbations [1,2].

For the idealized case the eigenfunctions of the Helmholtz operator are denoted by $\phi_N(\bar{r})$, the corresponding eigenvalues $-k_N^2$ and the normalization constant Λ_N^0 . In a first order approximation, assuming that $\Phi_N(\bar{r}_s) = \phi_N(\bar{r}_s)$, where $\Phi_N(\bar{r}_s)$ are the eigenfunctions of the real cavity, the eigenvalues $-K_N^2$ of the real cavity are obtained in terms of those of the idealized cavity [1,2] as:

$$K_N = k_N + i/(2V\Lambda_N^0)\iint_S y(\bar{r}_s)\left|\phi_N(\bar{r}_s)\right|^2 dS \qquad (75)$$

In the derivation of this expression the effect of the imperfection in the geometry of the cavity, has not been taken into account. For the particular frequency modes of interest (radial modes) it can be shown [10] that to a first order approximation the shift in the eigenvalues vanish if shape changes which preserve the volume of the cavity are considered. In practice, it is relatively straightforward to ensure that deviations from perfect geometry are sufficiently small that the first-order result is adequate.

3.5.4 Ideal spherical cavity solutions

Given that it is possible to evaluate the eigenvalues for a real cavity from those of the ideal cavity, we now consider the eigenfunctions $\phi_N(\bar{r})$ and eigenvalues $-k_N^2$ for the idealized spherical cavity.

The region of the cavity is defined by a sphere of radius a centered at the origin and described in a spherical polar coordinate system. In this coordinate system the wavefunctions can be written as a product of three separable terms, with each term being a function of only one variable:

$$\phi_N(r,\theta,\xi) = R_N(r)P_N(\theta)Q_N(\xi) \qquad (76)$$

When this product is substituted in the Helmholtz equation it yields three independent equations:

$$(1/R)\frac{d^2R}{dr^2} + (2/rR)\frac{dR}{dr} + k^2 - l(l+1)/r^2 = 0 \qquad (77)$$

$$\frac{d^2P}{d\theta^2} + \frac{\cos\theta}{\sin\theta}\frac{dP}{d\theta} + [l(l+1) - m^2/\sin^2\theta]P = 0 \qquad (78)$$

$$\frac{d^2Q}{d\xi^2} + m^2Q = 0 \qquad (79)$$

The boundary condition for zero surface admittance of equation (65) is then:

$$\left.\frac{d\phi}{dr}\right|_{r=a} = \left.\frac{dR}{dr}\right|_{r=a} = 0 \qquad (80)$$

since the normal to the surface component is the radial component. By substituting x for kr in equation (77) we obtain the solution $R = j_l(x)$, which is the spherical Bessel function of order l. Thus equation (80) yields

$$\frac{d}{dr} j_l(kr)\Big|_{r=a} = 0 \tag{81}$$

The roots of this equation are $\nu_{ln} = k_N a$ and can be found in the literature [2].

The overall solution for the eigenfunctions and eigenvalues of the ideal spherical cavity is given by

$$\phi_N(r,\theta,\xi) = j_l(\nu_{ln} r / a) Y_{lm}(\theta,\xi) \tag{82}$$

$$k_N = \nu_{ln} / a \tag{83}$$

where $l = 0,1,2,\cdots$, $|m| = 0,\pm 1,\pm 2,\cdots,\pm l$, and $n = 1,2,3,\cdots$ .So the modes with a given l are $(2l+1)$-fold degenerate. The modes with l=0 are non-degenerate and are called radial modes. The spherical harmonic term, $Y_{lm}(\theta,\xi)$, originates from the solution of the two other equations (78) and (79). The eigenfunctions of equation (82) are orthogonal and the normalization constant obtained is [2]

$$\Lambda_N^0 = \frac{3}{2} \frac{1 - l(l+1) / \nu_{ln}^2}{(2l+1)} \frac{(l+|m|)!}{(l-|m|)!} j_l^2(\nu_{ln}) \tag{84}$$

Since the turning points of the Bessel function ν_{ln} are real quantities so too are the eigenvalues k_N of the ideal spherical cavity. For this special case equation (67) leads to the resonance frequencies

$$f_{ln} = \nu_{ln}(u / 2\pi a) \tag{85}$$

and the only contribution to the halfwidths g_{ln} is the bulk absorption term $g_b = (u / 2\pi)\alpha$.

3.5.5 Real spherical cavity solutions

The eigenfunctions and eigenvalues obtained for the ideal cavity will be used to obtain the eigenvalues and natural frequencies of a cavity with non-zero surface

admittance. The surface integral for the perturbed eigenvalues appearing in equation (75) yields for the radial modes,

$$\iint_S y(\bar{r}_s)\phi_N^2(\bar{r}_s)dS = y_s a^2 j_0^2(\nu_{0n})\int_0^{2\pi} d\xi \int_0^{\pi} \sin\theta d\theta \tag{86}$$

$$\text{and } V\Lambda_{0n} = 2\pi a^3 j_0^2(\nu_{0n}) \tag{87}$$

where y_s is the effective specific acoustic admittance of the surface, which has been derived assuming $y(\bar{r}_s)$ to be uniform all over the surface. Thus, from equation (67), we can derive the perturbed eigenvalues and the natural frequencies of the radial modes for a real cavity as

$$F_{0n} = f_{0n} + ig_{0n} = (u/2\pi a)(\nu_{0n} + iy_s + ia\alpha) \tag{88}$$

3.5.6 Perturbation terms

The effective specific acoustic admittance y_s has been calculated considering all possible contributions to it, and applying suitable boundary conditions [2,6]. The contributions were found to arise mainly from three sources; the existence of a thermal boundary layer at the interface between the fluid and the walls of the cavity, coupling of the fluid and the shell motion and existence of openings in the wall of the cavity. Thus, equation (88) results in

$$f_{0n} + ig_{0n} = (u/2\pi a)\nu_{0n} + (\Delta f_h + \Delta f_{sh} + \Delta f_o) + i(g_h + g_{sh} + g_o + g_b) \tag{89}$$

where the terms Δf_h , Δf_{sh} and Δf_o are the shifts to the resonance frequency away from the unperturbed value $(u/2\pi a)\nu_{0n}$ arising from the thermal boundary layer effect (subscript *h*) [11], the coupling of the fluid and shell motion (subscript *sh*) and from the openings on the resonator wall (subscript *o*) [11]. The terms g_h , g_{sh} and g_o are the corresponding contributions to the halfwidth. The bulk absorption term g_b is discussed previously.

3.5.6.1 Thermal boundary layer

The thermal boundary layer perturbation terms have been found to be [2,6]

$$\Delta f_h = -g_h(1 - 2l_h / \delta_h) \tag{90}$$

$$g_h = (\gamma - 1)(f / 2a)\delta_h \tag{91}$$

where $\delta_h = (D_h / \pi f)^{1/2}$ and $l_h = (\kappa / p)(\pi MT / 2R)^{1/2}(\gamma - 1) / (\gamma + 1)(2 - h) / h$, h being the thermal accommodation coefficient. Since δ_h varies as $\rho^{-1/2}$, and also l_h varies as p^{-1}, the shift to the resonance frequencies arising from the thermal boundary layer is most important at lower pressures. The term involving l_h is negligible except at very low pressures.

3.5.6.2 Coupling of fluid and shell motion

In the approximation that the shell is uniform and perfectly isotropic and its motion is radial and undamped, Greenspan [1,9,11] derived the following expression for the elastic response of the resonator's wall:

$$\Delta f_{sh} = -f\rho u^2 C_o / [1 - (f / f_{br})^2] \tag{92}$$

in which $C_o = a^{-1}(\partial a / \partial p)$ is the shell compliance

$$C_o = (1 + 2t_w^3) / 2(t_w^3 - 1)\rho_w u_w^2 \tag{93}$$

and

$$f_{br} = \{(t_w^3 - 1) / 2\pi^2(t_w - 1)(1 + 2t_w^3)\}^{1/2}(u_w / a) \tag{94}$$

is the lowest radially symmetric ('breathing mode') resonance frequency of the shell, t_w is the ratio of the outer and inner radii and the subscript w denotes properties of the wall material.

Since Δf_{sh} is directly proportional to the density, its significance is greater at higher pressures. The shell motion is assumed to be undamped and therefore there is no contribution to the halfwidth. The assumptions made in deriving the above perturbation term cannot be fulfilled in a real cavity. Thus, slight errors in the calculation of this term

are expected at the high pressures. However, the correction itself is always small so that the error propagated to the final speed of sound is even smaller.

3.5.6.3 Openings in the resonator wall

A further perturbation to the resonance frequencies arises from the opening of the fluid inlet tube. At measurement frequencies close to the tube resonance frequencies the specific acoustic admittance of the tube y_o can be very large [1,11]. However, by an appropriate choice of the tube dimensions the tube resonance frequencies can be shifted away from the measurement frequencies. It is then possible to arrange that perturbation term $\Delta f_o + ig_o$ is very much smaller than either the thermal boundary layer perturbation or the perturbation because of the coupling of the fluid and shell motion.

3.6 References

[1].J. P. M. Trusler, *Physical Acoustics and Metrology of Fluids* (Adam Hilger, Bristol, 1991).

[2] P. M. Morse and K. U. Ingard, *Theoretical Acoustics* (McGraw-Hill, New York, 1968).

[3].L. E. Kinsler, A. R. Frey, A. B. Coppens and J. V. Sanders, *Fundamentals of Acoustics* (John Wiley & Sons, New York, 1982).

[4]. R. B. Bird, W. E. Stewart and E. N. Lightfoot, *Transport Phenomena* (John Wiley & Sons, New York, 1960).

[5] L. D. Landau and E. M. Lifshitz, *Course of Theoretical Physics Volume 6, Fluid Mechanics* (Pergamon, Oxford, 1959).

[6] K. F. Herzfeld and T. A Litovitz, *Absorption and Dispersion of Ultrasonic Waves* (Academic Press, London, 1959).

[7] T. L. Cottrell and J. C. McCoubrey, *Molecular Energy Transfer in Gases* (Butterworths, London, 1961).

[8] J. B. Mehl and M. R. Moldover, J. Chem. Phys. **74**, 4062 (1981).

[9] M. R. Moldover, J. B. Mehl and M. Greenspan, J. Acoust. Soc. Am. **79**, 253 (1986).

[10] J. B. Mehl, J. Acoust. Soc. Am. **71**, 1109 (1982).

[11] M. B. Ewing, M. L. McGlashan, J. P. M. Trusler, Metrologia **22**, 93 (1986).

CHAPTER 4

EXPERIMENTAL METHOD

4.1 Introduction.

Speed of sound measurements in a number of different gases have been performed in this work. The measurements have been carried out in a spherical resonator. Spherical resonators have replaced cylindrical interferometers [1,2], as the preferred means of measurement of sound speed because they have proven much more precise [3-5].

It is now possible to manufacture spherical resonators which adhere exactly to the theoretical model set out in chapter 3. So far, spherical resonators have been used successfully for measurements of the sound speed in hydrocarbons such as methane [6,7], dimethylpropane [8], *n*-butane [9], *n*-pentane [10] and ethane [11], as well as in polar molecules such as methanol [12] and refrigerants such as CF_4 [13] and R134a [14]. Argon has also been studied frequently mostly as a calibration gas [15-16]. Speed of sound measurements in argon obtained in a spherical resonator at the triple point of water have been used to determine the universal gas constant more accurately than ever before [17]. Finally spherical acoustic resonators have been employed in field of thermometry for the measurement of the triple point of gallium [18].

The spherical resonator used in this work is the latest and most sophisticated development in a series of acoustic interferometers [1,2,4-6,13,19,20]. The whole system is able of operating at temperatures between 80 to 500 K and at pressures up to 20 MPa, which is the widest range of operation ever achieved with spherical resonators.

In the following section the entire apparatus is described. Details are also given of the experimental procedure followed in order to obtain the acoustic measurements. The

measurement and control of the temperature and the pressure, which are essential independent variables in the measurements are also discussed.

4.2 Apparatus

The apparatus used for speed of sound measurements in this work has been based on the design of Ewing and Trusler [13]. It consists of a stainless-steel spherical resonator housed in a thermostat (figure 4.1) with a high degree of temperature uniformity and stability. A short description of the various parts of the apparatus is presented in the following sections.

4.2.1 The sphere

The sphere was fabricated from two stainless-steel hemispheres of i.d. 80 mm and wall thickness 10.5 mm. The two hemispheres were joined together with a 6 mm deep electron-beam weld to form a vacuum- and pressure-tight seal around the equator. The outer surface of the sphere was also machined to spherical geometry, as the acoustic model requires (see chapter 3), except for the cylindrical bosses used to hold the sphere hemispheres during fabrication. These two pieces, shown at each pole (figure 4.1), were not removed for practical reasons.

Before welding the geometry of the inside surface of the sphere was investigated by studying the spectrum of microwave resonances [21], which indicated a deviation from sphericity of the order of 10 μm . This is the best that can be achieved using conventional machine-shop equipment and is more than adequate for speed of sound measurements of part-per-million accuracy. However, during the welding procedure the sphere suffered a slight distortion, as indicated from the subsequent observation of the microwave spectrum. The measured distortions, which were of the order of 100 μm , are sufficient to cause observable perturbations to the acoustic resonance frequencies.

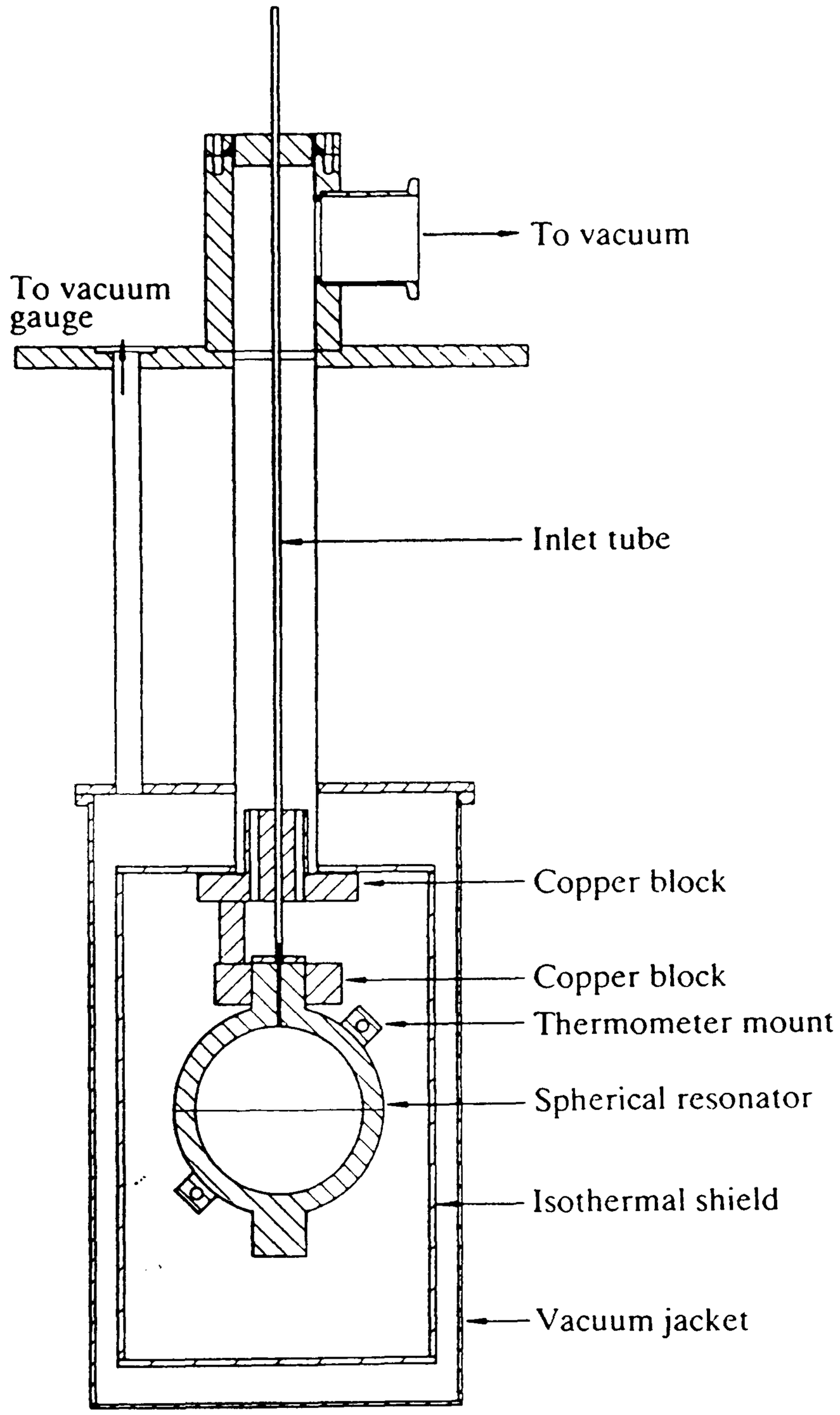

Figure 4.1. The spherical resonator and its thermal environment [6].

The effect of the geometric imperfections, which is still no greater than 50 parts per million in the speed of sound, may be minimized by the application of suitable corrections (see chapter 5).

The radius of the sphere at zero pressure was accurately obtained by calibration with argon gas (see chapter 5).

4.2.2 The gas-entry port

The gas-entry port was a 41 mm long stainless tube 1 mm in diameter embedded in the upper boss of the sphere. The upper face of the boss served as a flange to which the mating flange of the gas-inlet tube was bolted and sealed by a nitrogen-filled O-ring. The internal diameter of the gas-inlet tube (2.6 mm) was sufficient to accommodate the section of the gas-entry port protruding from the top of the boss.

The length of the gas-entry port was chosen to be nearly equal to the internal radius of the sphere. By virtue of this choice, the resonance frequencies of the tube are arranged not to interfere with the resonance frequencies of the radial modes of the sphere [13,22].

4.2.3 The thermostat

The thermostat was designed for operation up to 500 K. The gas-inlet tube and all the wires passing through the central access tube to the resonator were thermally anchored to the top copper block (figure 4.1). This block was equipped with a platinum resistance thermometer and heater which were used to control the heat flow to the sphere. The copper post interconnecting the top copper block with the lower copper block (figure 4.1) where the upper boss was clamped, served as a controlled heat leak. At steady state the temperature of the top copper block was approximately 60 mK below the set temperature.

In certain cases it was necessary to raise the temperature of the sphere rapidly. For this purpose a heater was attached around the equator of the sphere, being controlled by

the temperature reading of the two platinum resistance thermometers located on the northern and southern hemispheres, discussed in section 4.5. This control system will be referred to in the following as the servo control system.

The side and base of the isothermal aluminium shield, shown in figure 4.1, were both controlled at the set temperature. The thermostat was operated under vacuum to reduce the heat transfer between the resonator and the shield. Heat loss from the shield was further reduced by use of superinsulation consisting of 10 alternating layers of aluminium foil and glass fibre on the outside surface of the shield.

All temperature-control loops were operated under computer control using an a.c. resistance bridge, channel scanner (switch unit) and power supplies.

For operation below room temperature the whole thermostat system was immersed into a Dewar filled with liquid nitrogen.

4.3 Transducers

Two transducers have been used, one for the generation (source transducer) and one for the detection of sound (detector transducer). The transducers (figure 4.2) were located on the upper part of the resonator, 90° apart and symmetrically with respect to the resonator's polar axis. By locating the source transducer 90° apart from the detector transducer we reduce the interference between the lowest radial mode (0,2) and the nearby non-radial (3,1) mode which, in a perfect sphere, has a node at that point [3,23]. Both transducers were of essentially the same design, each consisted of a thin dielectric membrane clamped by a ceramic sleeve within a stainless-steel housing. The front of the housing exposed a circular area of the membrane of about 3 mm in diameter, arranged to be nearly flush with the resonator's surface.

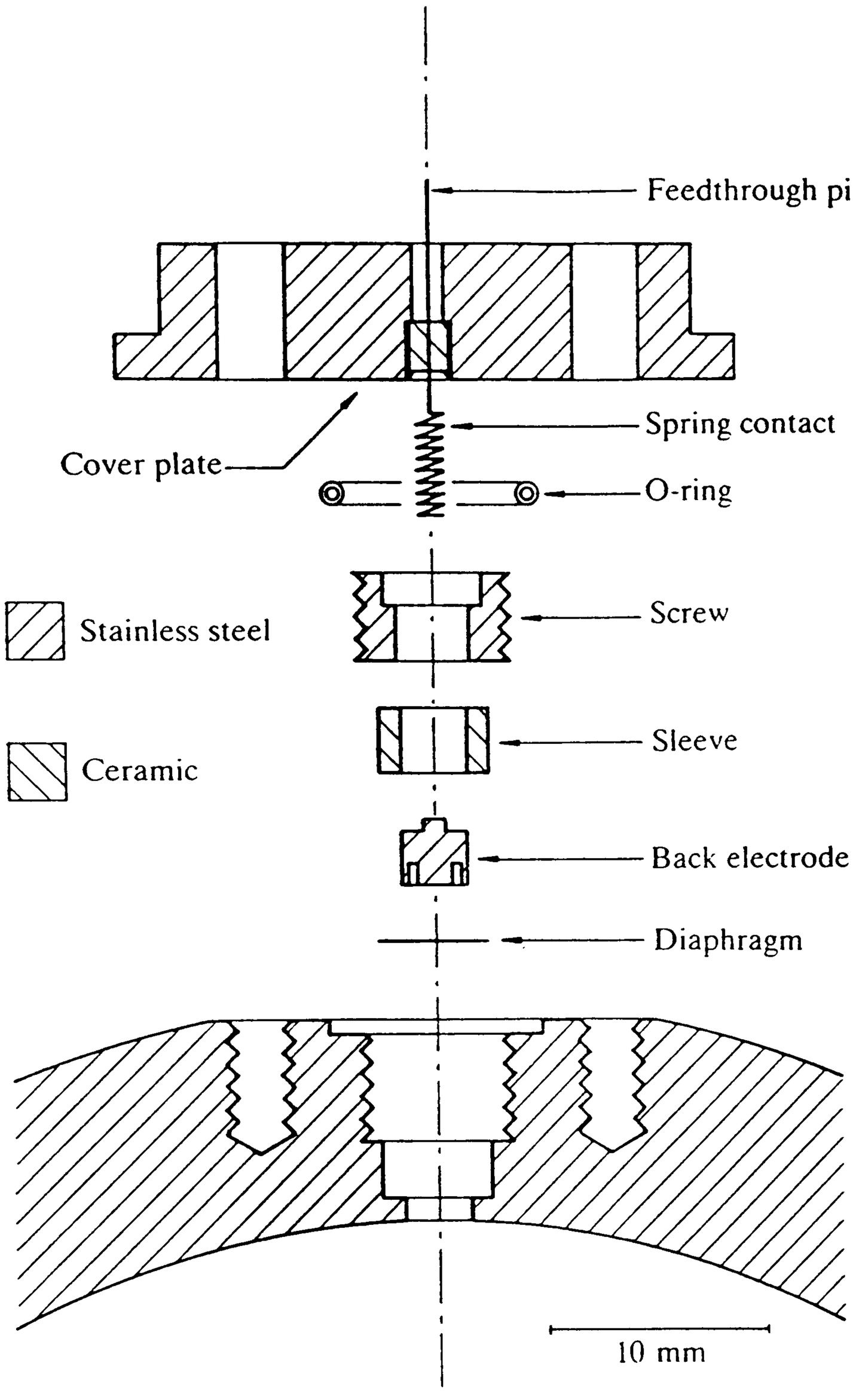

Figure 4.2. Electroacoustic transducer assembly fabricated in the wall of the resonator [6].

4.3.1 Source transducer

The moving element of the source transducer was a 12 μm thick Kapton membrane, coated with gold on the surface in contact with the resonator. The source transducer, which acts as a point source [24], was excited with a synthesized signal of frequency f, accurate to $\pm 1 \cdot 10^{-7} \cdot f$. The signal was fed to the source after amplification to 180 V r.m.s. Under these conditions, the source transducer electrostatic force drives the membrane to produce sound at a frequency $2f$.

4.3.2 Detector transducer

The moving element of the detector transducer was also a 12 μm thick Kapton membrane, gold coated on the surface in contact with the resonator, used with a dc bias of 100 V.

The detector had an active capacitance of only a few pF and it therefore acted as a very high impedance signal source when the source-membrane is set in motion by audio-frequency sound. Therefore a preamplifier was required very close to the detector to prevent division of the signal by the large ratio of stray-to-active capacitance that would result even from a few centimeters of coaxial cable [13]. Thus the output voltage of the transducer was buffered by a JFET follower (figure 4.3), soldered directly to the outside of the feedthrough pin (figure 4.2), and fed via a miniature coaxial cable, through the vacuum enclosure, to the lock-in amplifier, where its phase and amplitude were measured.

The simple JFET follower circuit discussed above is not suitable for operation at temperatures higher than 375 K because the signal-to-noise ratio becomes quite small. One solution to this problem is to place the preamplifier outside of the thermostated area. However, this is only feasible if the effective capacitance of the cable transferring the signal from the detector is very small. For this purpose a triaxial cable (guarded coaxial cable) has been constructed to transfer the signal from the feedthrough pin of the detector

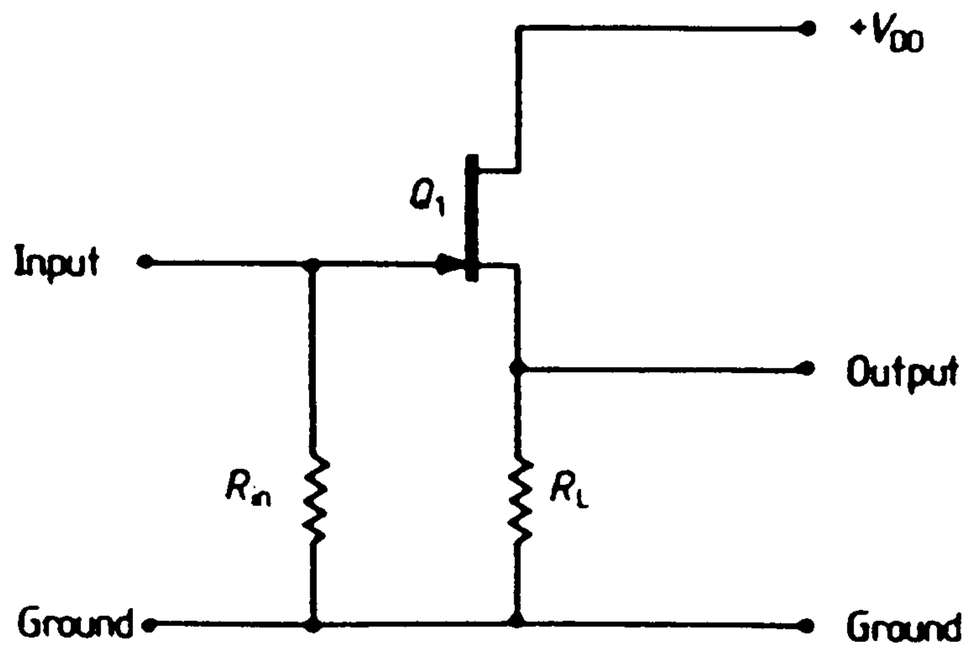

Figure 4.3. Preamplifier circuit used inside the thermostat.

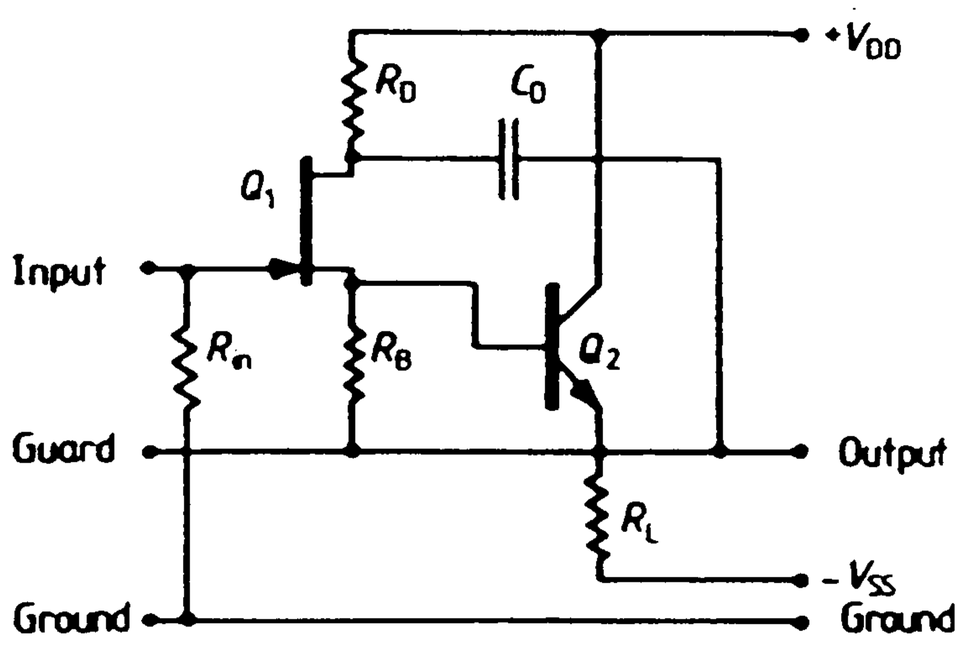

Figure 4.4. Preamplifier circuit used outside the thermostat.

to the preamplifier outside of the thermostat. The preamplifier circuit constructed for this case is shown in figure 4.4.

The amplitude of the signal received for both of the preamplifier arrangements was always much larger than the noise of the electronics.

4.4 .Excitation and detection of sound

The excitation signal was produced by a function synthesizer. During the measurements, the excitation frequency was increased in discrete steps of $g_N / 5$, from about $f_N - g_N$ to about $f_N + g_N$, where g_N is the halfwidth of the resonance (see chapter 3). At each point the amplitude and phase of the received signal was measured with the lock-in amplifier. In order to account for any possible drifts with a linear time-dependence, the resonances were first scanned with increasing frequency and then with decreasing frequency. The measured average of the signals obtained by the two scans corresponds to the conditions prevailing at the time the frequency step was reversed.

The theoretically predicted function which relates the resonance frequencies f_N and halfwidths g_N to the acoustic pressure has been already discussed in section 3.5.2. The acoustic pressure is transformed through the detector transducer to an electrical signal of amplitude and phase proportional to that of the acoustic pressure. Thus, for a resolved single mode the measured complex signals $w(f)$ are analyzed in terms of the function:

$$w(f) = \frac{A'}{(F_N / f)^2 - 1} + B + C(f - f_0) \qquad (1)$$

by non-linear regression analysis to determine F_N, A', B and C. The relative uncertainty in the resonance frequencies obtained was estimated in the analysis and found to be $\pm 1 \cdot 10^{-6}$.

4.5 Temperature measurements

The temperature of the gas was measured from the mean value of the reading of two capsule-type platinum resistance thermometers, located on the northern and southern hemispheres (figure 4.1).

These thermometers were calibrated on ITS-90 [25], by comparison with another thermometer calibrated on ITS-90 at the U.K. National Physical Laboratory. The thermometers were checked at the triple point of water before and after each set of measurements. Triple point cells of water were constructed for the calibration purposes based on the design of Ambrose et al. [26]

The temperature difference between the two platinum resistance thermometers located on the northern and southern hemispheres was always less than 5 mK, while the fluctuations in the mean temperature were never more than 0.5 mK, during a measurement. Since the calibration accuracy of these thermometers is about ± 5 mK the overall uncertainty in the temperature is estimated ± 7 mK .

4.6 Pressure measurements

For the pressure measurements two pressure transducers were used, one for pressures up to 20 MPa and one for pressures up to 1.4 MPa. The transducers were connected into the external tubing, which was maintained at room temperature.

(a) High pressure transducer:

The high pressure transducer was a resonant quartz-crystal manometer (Digiquarz model 43KT) with a precision of 40 Pa. When calibrated in pressure range 0 to 15 Mpa the manometer was found to have a reproducibility of $\pm$ 0.5 kPa, provided that the period of oscillation under vacuum was monitored regularly. The overall uncertainty in that pressure measurements was estimated to be $\pm$ 1 kPa.

(b) Low pressure transducer:

Since data were also taken at pressures as low as 20 kPa a high precision transducer was necessary for the low pressure range. The transducer used here was also a resonant quartz-crystal manometer (Digiquarz model 2200AT) of 1.4 MPa full scale. Its estimated accuracy is $\pm$ 0.01 per cent of full scale which is about $\pm$ 0.2 kPa.

4.7 Gas samples

The gaseous samples used for the measurements and their purities are discussed in the following.

(a) Argon:

'Zero grade' argon was supplied by British Oxygen with a specified mole fraction purity of at least 0.99998. Information provided by the manufacturer indicated that the main impurity is air. A mole-fraction of air even of 0.00002, would have a negligible effect upon the measured speed of sound in argon.

(b) Methane:

The methane gas was supplied by Union Carbide with a specified mole-fraction purity of at least 0.99995. Analysis with gaseous chromatography revealed no impurities. However, using as upper limits for the mole fractions of some possible impurities, the detection thresholds in g.c., it was found that the possible shift to the speed of sound could not be more than a few parts per million.

(c) Propane:

The propane gas was supplied by Union Carbide with a specified purity of at least 0.9995. Analysis with gaseous chromatography showed that the largest impurity was methane. The effect of this impurity in the speed of sound is discussed analytically in chapter 5.

(d) Methane-propane:

Two sets of measurements were performed with a methane-propane mixture, one set along isochores, reaching up to $5\ \mathrm{mol}\ /\ \mathrm{dm}^3$, and one along seven isotherms from 225 to 375 K at pressures up to 1.4 MPa.

The mixture was prepared in a $0.5\ \mathrm{dm}^3$ stainless-steel cylinder previously baked under vacuum. Starting with both the resonator and the sample cylinder under vacuum at approximately 300 K, methane was admitted to a pressure calculated to correspond to an amount-of-substance 3.61 mol. The cylinder was then cooled in liquid nitrogen so as to condense the sample and isolated from the sphere by closing a valve. Propane was then admitted to the sphere to a pressure calculated to correspond to 0.128 mol. This gas was then condensed into the sample cylinder and the process repeated four times so as to meter a total of 0.64 mol of propane. At the conclusion of this procedure, the sample cylinder contained approximately 4.25 mol of $(0.85\ CH_4 + 0.15\ C_3H_8)$, sufficient to reach a density in the entire system greater than the required, $5\ \mathrm{mol}\ /\ \mathrm{dm}^3$.

The mixture to be used in the isothermal measurements was prepared in the same manner but for an amount-of-substance corresponding to 1.5 times the amount needed to fill the sphere for each of the seven isotherms up to about 1.4 MPa.

Convective mixing was used to obtain a homogeneous sample. Large temperature gradients were established across the sample cylinder to obtain mixing of the gas. After 24 h, the resonator was filled with gas from the cylinder, up to a pressure corresponding to a density of $5\ \mathrm{mol}\ /\ \mathrm{dm}^3$ for the case of isochoric measurements, or up to the maximum pressure (here 1.4 MPa), for the case of the isothermal measurements. Additional convective mixing was then promoted by maintaining a temperature difference between the top and the bottom of the resonator of about 1 K for a further 24 h.

4.8 Experimental procedure

Isothermal and isochoric measurements were performed in this work and they are discussed separately.

(a) Isothermal measurements:

Gas from the commercial gas cylinder was transfered into a sample cylinder by condensation with liquid nitrogen. For the particular case of propane and methane-propane mixture, after the desired pressure was reached, a degasing procedure followed in order to remove any uncondensable impurities. Subsequently, the gas was passed into the sphere, already evacuated and flushed with gas several times, through a series of manual valves. After filling the resonator to the maximum pressure, the desired temperature was set and the temperature control program started. When the steady state was reached, i.e. the mean temperature of the sphere was stabilized, measurements of the resonance frequencies were taken. The pressure was then lowered in preparation for the next set of measurements. This was done either by condensing gas from the sphere into the sample cylinder, which was immersed into a liquid nitrogen bath, or by pumping the gas out through the vacuum pumps. The expansion produced a decrease in the temperature. Therefore the servo control system discussed previously was used in order to bring the temperature of the sphere back to the set value. During the measurements the vacuum reading of the thermostat was 10^{-5} Torr. The vacuum reading of the thermostat was used to test if there is any leak in the thermostated area. After the lower pressure was reached and the data taken, the system was pressurized again to the highest pressure and set for the next temperature.

For measurements below room temperature the thermostat was immersed in liquid nitrogen. The cooling procedure when the thermostat is under vacuum is very slow. Therefore a helium supply unit was constructed, which allowed helium gas to pass into the space around the resonator, to provide the medium for the heat to be transfered. However, this unit was seldom used, because it was proved difficult to control.

(b) Isochoric measurements:

Isochoric measurements were only taken for one of the methane-propane mixtures. These measurements proceeded along the isochores at amount of substance densities 5, 4, 3, 2, 1 and 0.085 mol / dm^3. Measurements were performed at temperatures of 280, 300, 325, 350 and 375 K on each isochore. The system was then returned to 280 K for a check measurement before reducing the gas density in preparation for the next isochore. Measurements were only taken with the system in full thermal equilibrium and approximately 12 h were required to traverse each isochore followed by 12 h of cooling to return to the initial temperature.

4.9 References

[1] B. E. Gammon and D. R. Douslin, J. Chem. Phys. **64**, 203 (1975).

[2] B. E. Gammon, J. Chem. Phys. **64**, 2556 (1976).

[3] M. R. Moldover, M. Waxman and M. Greenspan, High Temp. High Pressure **11**, 75 (1979).

[4] J. B. Mehl and M. R. Moldover, J. Chem. Phys. **74**, 4062 (1981).

[5] M. R. Moldover, J. B. Mehl and M. Greenspan, J. Acoust. Soc. Am. **79**, 253 (1986).

[6] J. P. M. Trusler and M. Zarari, J. Chem. Thermodyn. **24**, 973 (1992).

[7] A. R. H. Goodwin, PhD Thesis, University of London, 1984.

[8] M. B. Ewing, A. R. H. Goodwin, M. L. McGlashan and J. P. M. Trusler, J. Chem. Thermodyn. **19**, 721 (1987).

[9] M. B. Ewing, A. R. H. Goodwin, M. L. McGlashan and J. P. M. Trusler, J. Chem. Thermodyn. **20**, 243 (1988).

[10] M. B. Ewing, A. R. H. Goodwin and J. P. M. Trusler, J. Chem. Thermodyn. **21**, 867 (1989).

[11] J. P. M. Trusler, personal communication.

[12] S. J. Boyes, M. B. Ewing and A. R. H. Goodwin, J. Chem. Thermodyn. **24**, 1151

[13] M. B. Ewing and J. P. M. Trusler, J. Chem. Phys. **90**, 1106 (1989).

[14] A. R. H. Goodwin and M. R. Moldover, personal communication.

[15] M. B. Ewing, A. A. Owusu and J. P. M. Trusler, Physica A **156**, 899 (1989).

[16] M. B. Ewing and J. P. M. Trusler, Physica A **184**, 415 (1992).

(1992).

[17] M. R. Moldover, J. P. M. Trusler, T. J. Edwards, J. B. Mehl and R. S. Davis, J. Res. Natl. Bur. Stand. **93**, 85 (1988).

[18] M. R. Moldover and J. P. M. Trusler, Metrologia **25**, 165 (1988).

[19] B. A. Younglove and N. V. Frederick, Int. J. Thermodyn. **11**, 897 (1989).

[20] S. O. Colgate, A. Sivaraman and K. Reed, J. Chem. Thermodyn. **22**, 245 (1990).

[21] M. B. Ewing, J. B. Mehl, M. R. Moldover and J. P. M. Trusler, Metrologia **25**, 211 (1988).

[22] M. B. Ewing, M. L. McGlashan, and J. P. M. Trusler, Metrologia **22**, 93 (1986).

[23] J. P. M. Trusler, *Physical Acoustics and Metrology of Fluids* (Adam Hilger, Bristol, 1991), p. 76.

[24] P. M. Morse and K. U. Ingard, *Theoretical Acoustics* (McGraw-Hill, New York, 1968), p. 306.

[25] H. Preston-Thomas, Metrologia **27**, 3 (1990).

[26] D. Ambrose, R. R. Collerson and J. H. Ellender, J. Phys. **E 6**, 975 (1973).

CHAPTER 5

EXPERIMENTAL RESULTS

5.1 Introduction.

In chapter 3 an acoustic model has been developed which allows the speed of sound in a fluid to be determined from the measurements of the complex resonance frequencies $F_{0n} = f_{0n} + ig_{0n}$ of the radial modes of a spherical resonator enclosing a test fluid. Using exactly the methodology set out in that chapter the speed of sound in gaseous methane, propane and a binary mixture ($0.85\ CH_4 + 0.15\ C_3H_8$) has been determined. The present chapter presents the results for the speed of sound and various derived quantities obtained by an appropriate analysis.

5.2 Analysis of the acoustic measurements.

According to the acoustic model established in chapter 3 the speed of sound u is related to the resonance frequencies f_{0n} of the radial modes (0,n) by

$$u = 2\pi a\ (f_{0n} - \sum \Delta f_j) / \nu_{0n} \qquad (1)$$

where a is the radius of the sphere, which is a function of the pressure, ν_{0n} is an eigenvalue of the ideal spherical cavity, which results from the turning points of the spherical Bessel function of zeroth order, and $\sum \Delta f_j = \Delta f_h + \Delta f_{sh} + \Delta f_o$ is the sum of small correction terms to account for the thermal boundary layer at the resonator wall, the coupling of the fluid and the shell motion and the tubular opening on the resonator wall through which the gas was admitted. For the case of methane the above equation requires further correction for dispersion Δf_{dis} associated with vibrational relaxation in the gas [1].

At high pressures the most important correction is that arising from the coupling of the shell and the fluid motion, Δf_{sh} . For example we mention that for methane at 300 K

and 10 MPa the correction Δf_{sh} to the (0,4) mode was 225 parts per million, while the correction arising from the thermal boundary layer, Δf_h , was just 15 parts per million. The values of Young's modulus E and Poisson's ratio σ needed for the calculation of Δf_{sh} were taken from fit to data given by Ledbetter et al. [2,3].

At low pressures the most significant correction is that for the thermal boundary layer, Δf_h , which for methane at 125 K and 0.02 MPa this correction to the (0-4) mode was 90 parts per million. The correction for dispersion Δf_{dis} is equally important at low pressures for the case of methane. For the calculation of the correction for the thermal boundary layer, values of the thermal conductivity as well as the isobaric and isochoric heat capacity are required. In addition, values for the viscosity of the fluid are required for the calculation of the correction arising from the tubular opening Δf_o . The values of the thermodynamic properties as well as of the density and the speed of sound, which also appear in some of the correction terms, are presented below when each individual system is considered.

5.2.1 Calibration

Calibration measurements with argon were performed, in order to obtain the radius of the sphere at zero pressure a_0 . This value is needed for the calculation of the actual radius of the sphere a at any pressure. The calibration measurements were also utilized to derive corrections to account for imperfections in the geometry of the sphere.

For the calibration purposes the first five radial modes were measured at the temperatures and pressures of interest. The thermodynamic properties required for the calculation of the correction terms Δf_j were obtained as described in [4].

5.2.1.1 Calibration for geometric imperfections

After applying all the calculated corrections into equation (1), the right handside of the equation did not give the same result for all five modes $(0,n)$ measured. As discussed

in chapter 4, this is a consequence of the fact that the spherical resonator employed here, has suffered some distortion during the welding, as the microwave spectrum indicated. Since the welding was performed by an electron beam around the equator, the most likely effect on the resonator was to make it prolate or oblate, as a result of stresses created during the cooling (which followed the welding process). According to Mehl [5], the existence of geometric imperfections in the resonator results in a shift of the eigenvalues ν_{0n} of the perfect sphere, which for prolate or oblate spheroids, is given by:

$$\Delta\nu_{0n} / \nu_{0n} = (4 / 135)\varepsilon^2 \nu_{0n}^2 + O(\varepsilon^3) \qquad (2)$$

where ε indicates a first order perturbation of the sphere radius. If we suppose that the eigenvalues are shifted to the value $\nu_{0n}(1+\lambda_{0n})$, where $\lambda_{0n} = \Delta\nu_{0n} / \nu_{0n}$, due to the geometrical imperfections of the present resonator, then substitution of this value into equation (1) in place of the unperturbed eigenvalues ν_{0n} should yield the correct value u for the speed of sound, which would be the same for all modes $(0,n)$. The corrected form of equation (1) would then be:

$$u = 2\pi\alpha\ (f_{0n} - \Delta f_j) / [\nu_{0n}(1+\lambda_{0n})] \qquad (3)$$

By plotting the fractional deviations $\delta_{0n} = (u_{0n} - \langle u\rangle) / \langle u\rangle$, of the value for the speed of sound u_{0n} obtained from equation (1) for the $(0,n)$ modes measured in argon, from the mean value $\langle u\rangle$, against the eigenvalue ν_{0n}, the dependence shown in figure 5.1 was obtained. This dependence was found to be quite independent of temperature and pressure. Thus, equation (1) could be written as follows:

$$\langle u\rangle = 2\pi\alpha\ (f_{0n} - \Delta f_j) / [\nu_{0n}(1+\delta_{0n})] \qquad (4)$$

Comparing equations (3) and (4) we obtain

$$u\ (1+\lambda_{0n}) = \langle u\rangle(1+\delta_{0n}) \qquad (5)$$

Assuming that the correct speed of sound u equals the mean value $\langle u\rangle$, then equation (5) yields that the shift to the eigenvalues λ_{0n} is equal to δ_{0n}. Based on this assumption the mean values of δ_{0n} obtained by averaging the fractional deviations at the different

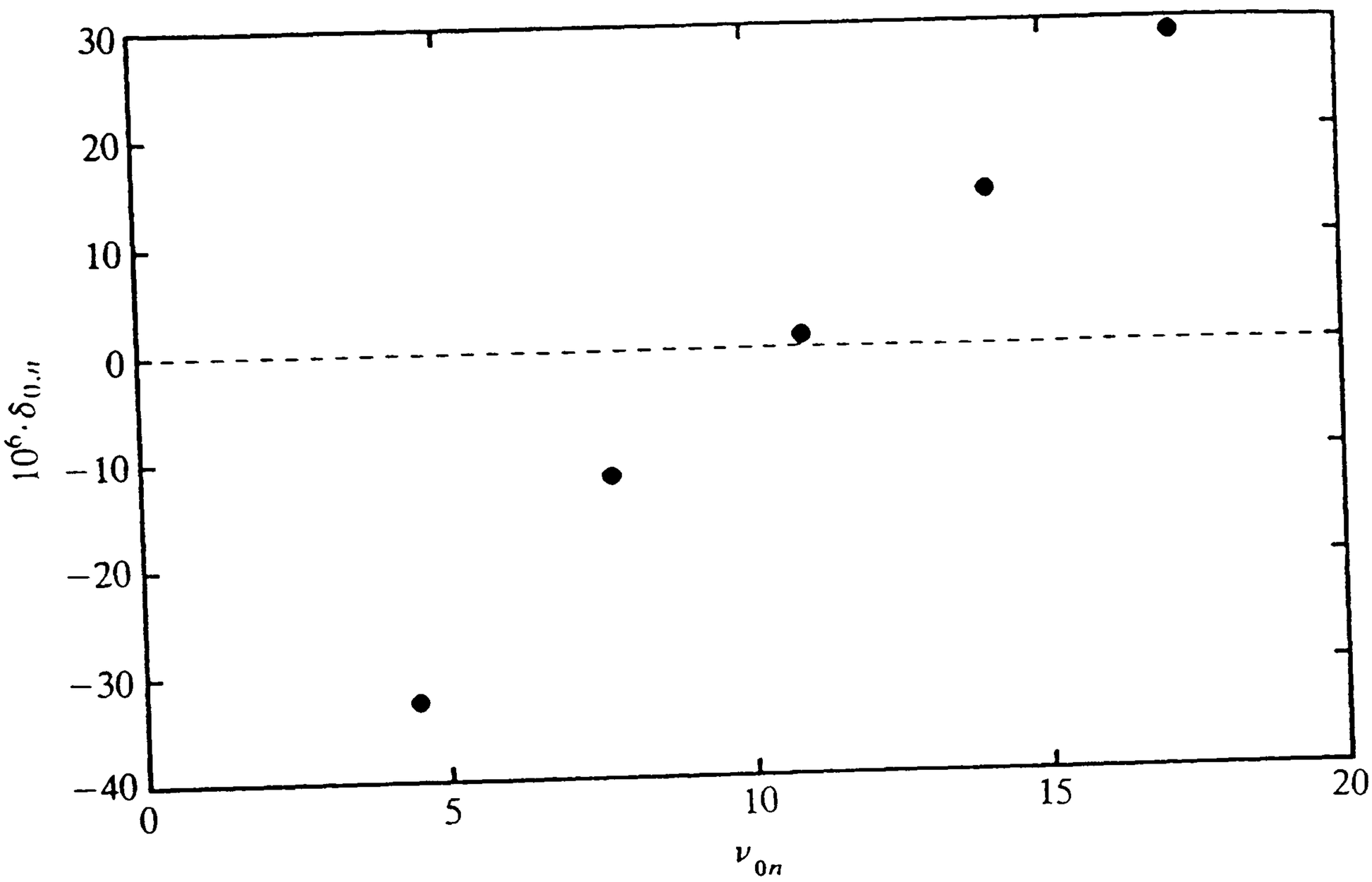

Figure 5.1. Fractional deviations $\delta_{0n} = (u_{0n} - \langle u \rangle) / \langle u \rangle$ of sound speeds u_{0n} determined from the $(0,n)$ radial modes from the mean value $\langle u \rangle$ for modes with $n = 2,3,\cdots,6$ before corrections for imperfect geometry. •, Average of 13 determinations in argon covering the pressure range 0.1 MPa to 0.5 MPa and the temperature range 275 to 375 K.

temperatures and pressures, were treated as a set of corrections to the eigenvalues $\nu_{0n}{}^{0}$ to yield the corrected eigenvalues k_{0n} given by

$$k_{0n} = (1+\delta_{0n})\,\nu_{0n} \qquad (6)$$

The eigenvalues k_{0n} were used instead of ν_{0n} in equation (1) in all subsequent measurements. The corrections δ_{0n} are presented in table 5.1. Although, according to equation (2) δ_{0n} should vary as ν_{0n}^2, which is not exactly the behaviour illustrated in figure 5.1; the correction we applied for imperfect geometry seems to work. This can be asserted because following application of this correction to the speed of sound measurements for other gases, the fractional deviations of the speeds of sound calculated from the different modes from the mean value were usually only a few part in $\cdot 10^{-6}$. Inconsistencies found in some cases between the speeds of sound obtained from the different modes in excess of this level were always attributed to causes other than geometrical imperfections and they will be discussed for each substance in the corresponding section.

5.2.1.2 Determination of the sphere radius at zero pressure.

In order to obtain the speed of sound from equation (1) after it is corrected for imperfect geometry, one needs also to calculate the sphere radius a. As will be shown in the next section the sphere radius a can be calculated from a_0, the Poisson's ratio and the Young's modulus. Fitting of the available now values of $(u / a_0)^2$ into a polynomial of the pressure or the density, yields the value of the intercept A_0 / a_0^2 (see section 5.3). For the case of argon $A_0 = RT\gamma^{pg} / M$ is known since for monatomic substances $\gamma^{pg} = 5/3$. Thus for every temperature T, at which the speed in argon is measured, one can obtain the values for a_0. Calibration measurements of the speed of sound in argon at the temperatures 275, 325 and 375 K and pressures 0.1 to 0.5 MPa, gave values for a_0 represented by the quadratic interpolation formula:

$$a_0 / \mathrm{m} = 40.152 \cdot 10^{-3}\{1 + 15.94 \cdot 10^{-6}[(T / \mathrm{K}) - 300] + 1.6 \cdot 10^{-8}[(T / \mathrm{K}) - 300]^2\} \qquad (7)$$

This equation represents the values of a_0 better than $\pm\, 0.0005$ per cent which results in a fractional error in the speed of sound of $\pm\, 5 \cdot 10^{-6}$. The above calibration equation was used in deriving the speed of sound of methane in the temperature range 275 to 375 K and pressures up to 10 MPa [6], and the speed of sound of the methane-propane mixture at temperatures 280 to 375 K and pressures up to 12 MPa. Before going to low temperatures (about 120 K) the change in the sphere radius was always less than 5 parts per million, over a period of one year. However, after going to low temperatures the sphere exhibit some hysteresis and recalibration became necessary.

Calibration in the temperature range 120 to 400 K yield the equation

$$a_0 \,/\, \mathrm{m} = 40.1718 \cdot 10^{-3}\{1 + 15.58 \cdot 10^{-6}[(T \,/\, \mathrm{K}) - 300] + 1.08 \cdot 10^{-8}[(T \,/\, \mathrm{K}) - 300]^2\} \quad (8)$$

This equation represents the values of a_0 within an error of $\pm\, 0.003$ per cent which results to a fractional error in the speed of sound of $\pm\, 30 \cdot 10^{-6}$. It was used to obtain the speed of sound of methane in the temperature range 125 to 250 K and at pressures up to 1.4 MPa, the speed of sound of propane at temperatures between 225 and 375 K and at pressures up to 0.85 MPa and the speed of sound of the methane-propane mixture at temperatures between 225 and 375 K and at pressures up to 1.4 MPa. In the derivation of equation (8) fit of α_0 data in a narrower temperature range did not improve the quality of the fit and thus the fractional error of $\pm\, 30 \cdot 10^{-6}$ could not be avoided.

5.2.2 Effect of pressure on radius

As mentioned before, calibration with argon yielded the radius of the sphere at zero pressure a_0. This value was needed for the calculation of the sphere radius a at any pressure. The radius of the sphere a is related to a_0 using the shell compliance C_o by

$$a = a_0(1 + C_o p) \quad (9)$$

The shell compliance is obtained from the equation [2,3]:

$$C_o = [(1 + \sigma) \cdot q^3 + 2(1 - 2\sigma)] \,/\, [2E(q^3 - 1)] \quad (10)$$

where q is the ratio of the outside diameter to the inside diameter of the sphere, σ is Poisson's ratio and E is the Young's modulus. Fit to the data of Ledbetter et al. [2,3] yield the equations predicting σ and E for the material of the sphere (type 321 stainless-steel):

$$\sigma = \sigma_0[1 + \sigma_t(T / \mathrm{K} - 300)] \tag{11}$$

with $\sigma_0 = 0.297$ and $\sigma_t = 1.8 \cdot 10^{-4}$,and

$$E = E_0 - \frac{E_t}{\exp(s / T) - 1} \tag{12}$$

with $E_0 = 212 \cdot 10^9$ Pa, $E_t = 2.812 \cdot 10^9$ Pa and s=37 K

5.3 Perfect-gas heat capacities and acoustic virial coefficients.

As shown in chapter 2, the square of the speed of sound can be expanded in a virial series in powers of the density as follows:

$$u^2 = A_0(1 + \beta_a \rho_n + \gamma_a \rho_n^2 + \cdots) \tag{13}$$

with

$$A_0 = \frac{RT\gamma^{pg}}{M} \tag{14}$$

Here ρ_n is the amount-of-substance density, β_a and γ_a are the second and third acoustic virial coefficients respectively, R is the gas constant, T is the temperature, M is the molar mass and γ^{pg} is the perfect-gas heat-capacity ratio.

Equation (13) can also be written as an expansion in terms of the pressure p as follows:

$$u^2 = A_0 + A_1 p + A_2 p^2 + \cdots \tag{15}$$

The coefficients of the above expansion are given by

$$A_1 = \beta_a \gamma^{pg} / M \tag{16}$$

$$A_2 = (\gamma_a - B\beta_a)\ \gamma^{pg} / RTM \tag{17}$$

where B is the second volumetric virial coefficient, defined in chapter 2.

The expressions in equations (16) and (17) can be readily derived by substituting into equation (15) the virial expansion of the pressure in terms of the density $p/(\rho_n RT) = 1 + B\rho_n + C\rho_n^2 + \cdots$ and by comparing equation (15) with equation (13).

As equations (13) and (15) imply, fitting of values obtained for u^2 into a polynomial of the density or the pressure, yields values for A_0 and the second and third acoustic virial coefficients.

5.4 Methane

Two sets of data were taken for methane; the first in the temperature range 275 to 375 K and at pressures 0.4 to 10 MPa (high temperature-pressure range), and the second in the temperature range 125 to 250 K and at pressures up to 1.4 MPa (low temperature-pressure range). The speed of sound was always obtained from the first three radial modes, (0,2), (0,3) and (0,4), which lie at frequencies 5000 to 21000 Hz, throughout the temperature and pressure range measured.

The thermal boundary layer correction Δf_h was calculated using values for the thermal conductivity obtained from the correlation of Younglove and Ely [7]. The isobaric and isochoric heat capacities, the density and the speed of sound, which were also required for the corrections, were calculated by the equation of state proposed by Setzmann and Wagner [8]. Values for the viscosity, which were needed for the calculation of the correction arising from the tubular opening on the resonator wall Δf_o, were also taken from the correlation of Younglove and Ely [7].

5.4.1 Dispersion correction

For methane, the sound speeds obtained from equation (1) after corrected for imperfect geometry, required further correction for dispersion associated with vibrational relaxation [1] in the gas. Fortunately the measurements were conducted at frequencies and

densities where the main consequence of vibrational relaxation is enhanced sound absorption and the associated dispersion is small. In the temperature range 275 to 375 K where we have worked at comparatively high pressures, the vibrational relaxation time was always less than $0.5\,\mu s$. However, at densities as low as $40\ \mathrm{mol}\ /\ \mathrm{m}^3$ and temperatures as low as 125 K, the vibrational relaxation time reached $8\,\mu s$. The value of $8\,\mu s$ for the vibrational relaxation time could also be considered small compared to the period of the sound waves which was between 45 and $200\,\mu s$. However, at densities below $100\ \mathrm{mol}\cdot\mathrm{m}^{-3}$ and at temperatures below 275 K the speeds of sound calculated from the different modes showed a considerable disagreement.

The vibrational relaxation time τ, which is needed for the calculation of the dispersion correction, was obtained by analysis of the experimental half-widths of the resonances, assuming that the product $\tau\rho$ is independent of the density ρ. For this purpose, we first subtracted the other known contributions from the half-widths g_{0n} ($g_{0n} = g_h + g_o + g_b$) measured; these arise from the thermal boundary layer g_h, the dissipation in the tubular opening g_o and the classical viscothermal sound absorption $g_{cl} = g_b - g_{rel}$. The remaining half-width arises from the contribution of vibrational relaxation g_{rel} which is given by [1]:

$$g_{rel} / f_{0n} = \frac{1}{2}(\gamma - 1)\Delta\omega\tau + \mathrm{O}(\omega^3\tau^3) \qquad (18)$$

where $\Delta = C_{rel} / C_p$ is the fraction of the constant-pressure heat capacity undergoing relaxation and $\omega = 2\pi f$ is the angular frequency (f is the source transducer frequency, which is almost equal to f_{0n} at resonance).

Equation (18) was derived assuming that the vibrational-to-vibrational energy transfer is rapid compared with the translational-to-vibrational energy exchange, so that the entire vibrational contribution to the heat capacity relaxes with a single relaxation time τ, and neglecting rotational relaxation. This assumption was already employed for the

case of pentane [9], butane [10], dimethylpropane [11] and CF_4 [12], which has a similar molecular structure to methane.

The terms of order $(\omega\tau)^3$ are found to be negligible under the conditions of our measurements and therefore we were able to analyse the residual experimental half-widths in terms of the equation

$$g_{\text{rel}} / f_{0n} = \{(\gamma - 1)\Delta\pi f_{0n} / \rho\}\ b_0 + b_b \qquad (19)$$

where $b_0 = \tau\rho$ and b_b is an empirical background term that accounts for most of the unexplained additional loss mechanisms in the resonator.

The values of τ obtained for a density of $1\,\text{kg}\cdot\text{m}^{-3}$ are given in table 5.2 for the temperature range 200 to 375 K. These values were compared with the data presented in [13] and the agreement was found very satisfactory. The vibrational relaxation times at the temperatures below 200 K were obtained by extrapolation of the values at 200 to 375 K. The extrapolation equation used is the following

$$\tau\rho = 1079\ /\ 62.5\ \exp(-T\ /\ 105.1) \qquad (\mu\text{s}\cdot\text{kg}\cdot\text{m}^{-3}) \qquad (20)$$

and represents the vibrational relaxation times at the temperatures between 200 and 375 K within their estimated error. At the temperatures 125 to 175 K the vibrational relaxation times obtained from the fit of the resonance half-widths were found to be substantially lower than the values predicted by equation (20). In fact the vibrational relaxation times were found to be decreasing as the temperature decreases, while all eight values obtained in the temperature range 200 to 375 K were found to be increasing according to the simple exponential equation (20). A logical explanation of the deviations noticed is that at the temperatures 125 to 175 K and at the densities at which the fit was performed the order of magnitude of the background term (10^{-6}) mentioned above, is the same with that of g_{rel} / f_{0n}, fact which causes large uncertainty in the fitting coefficient b_0 which provides the vibrational relaxation time.

The dispersion correction Δf_{dis} at an angular frequency ω was calculated from the relation [1]:

$$\Delta f_{\mathrm{dis}} / f_{0\mathrm{n}} = \frac{1}{2}(\gamma - 1)\Delta\,(\omega\tau)^2\{1 - \Delta(1 + 3\gamma\,) / 4\} + \mathrm{O}(\omega^3\tau^3) \qquad (21)$$

using the derived values for the relaxation times.

5.4.2 Error analysis

Having obtained corrected values of the sound speed for each of the first three radial modes of the spherical resonator, we next consider the level of agreement between them as well as the effect of all the other possible sources of error in the speed of sound.

(a) High temperature-pressure range:

In the temperature range 275 to 375 K the agreement between the three modes is generally within $\pm\, 5 \cdot 10^{-6}$ over the whole pressure range. For the isotherm at 300 K the situation is slightly less satisfactory. The agreement at low pressures remains good but, at higher pressures, the sound speed determined by the (0,4) mode departs systematically from the mean of (0,2) and (0,3) modes by an amount that reaches about $20 \cdot 10^{-6}$ at $p = 10$ MPa . This is far too large to arise from errors in the elastic constants within the estimated bounds for such errors [2]. Indeed a change in the elastic constants greater than these bounds would destroy the good agreement still observed between the results of the (0,2) and (0,3) modes. This deviation of the (0,4) mode was therefore interpreted as coupling between the (0,4) mode and a relatively nearby resonance of the shell and thus the (0,4) mode at 300 K was rejected. Similar deviations at high pressures were observed for the (0,4) mode at 350 K and 375 K where it was also rejected.

The fractional uncertainty in the above speed of sound data, resulting from small inconsistencies between the modes, including uncertainties propagated from the calibration measurements, is estimated to be $\pm\, 7 \cdot 10^{-6}$ at low pressures. The maximum uncertainty of $\pm\, 1$ kPa in the pressure gives rise to an additional fractional uncertainty which never exceeds $\pm\, 10 \cdot 10^{-6}$. All the possible impurities listed in table 5.3, heavier than methane, would cause a decrease in the sound speed, since, as equation (13) indicates, $u^2 \propto M^{-1}$.

Although there is no evidence that the actual impurity levels approach the upper bounds given in table 5.3, the greatest possible depression of the speed of sound at 300 K from this substances would be $29 \cdot 10^{-6}$. The main effect of the plausible impurity levels would be the introduction of small errors into the derived perfect-gas properties, as it will be shown later for the case of propane. Finally there is an uncertainty, significant at the higher pressures, which arises from possible errors of up to 5 per cent in Young's modulus. Since the net effect of the fractional uncertainty along the isobar at 10 MPa is approximately constant and equal to $14 \cdot 10^{-6}$ the overall fractional error bound is estimated to be

$$|\varepsilon| \leq \{7^2 + 10^2 + 29^2 + 2(p / \text{MPa})^2\}^{1/2} \cdot 10^{-6} \qquad (22)$$

The estimated error bound for the highest pressure of 10 MPa does not exceed $35 \cdot 10^{-6}$.

(b) Low temperature-pressure range:

In the temperature range 125 to 250 K the agreement of the three modes was better than $\pm 7 \cdot 10^{-6}$ over the whole pressure range, except at pressures corresponding to densities lower than $100 \text{ mol} \cdot \text{m}^{-3}$, where the deviation could become as large as $\pm 25 \cdot 10^{-6}$. At those very low densities the dispersion correction and the correction for the thermal boundary layer become very important. The relative contributions of Δf_h and Δf_{dis} to the resonance frequencies of the (0,4) mode, varied from $93 \cdot 10^{-6}$ and $-88 \cdot 10^{-6}$ at 125 K and 0.020 MPa, to $50 \cdot 10^{-6}$ and $-67 \cdot 10^{-6}$ at 250 K and 0.198 MPa, respectively. Both correction contributions being of order $100 \cdot 10^{-6}$ at the lower pressures, small errors in them could produce quite considerable error in the speed of sound. However, the model for the thermal boundary correction has been well tested [9-12,14], a further test being the very good agreement between the modes of propane at the very low densities as shown in the following, a fact which leaves the dispersion responsible for the observed deviations. When the vibrational relaxation time is comparable with the period of the sound waves then the assumption made in deriving the acoustic model (chapter 3) employed in present measurements, about local equilibrium is no longer valid and thus neither is the model.

Accordingly, for the speed of sound data obtained at the temperatures between 125 and 250 K the fractional estimated error is given by:

$$|\varepsilon| \leq [7^2 + 30^2 + 10^2 + 29^2 + (5.3T/\rho)^2]^{1/2} \cdot 10^{-6} \qquad (23)$$

where the five values in the parenthesis account for the small disagreements between the modes, the error arising from the quality of the fit of the α_0 data obtained from the calibration, the uncertainty in the pressure measurements, the uncertainty in the purity of the methane sample and finally the uncertainty caused by the vibrational relaxation at the very low densities. The net effect of the disagreement between the modes caused by vibrational relaxation at 125 K and 0.040 MPa, which corresponds to a density of $39\ \mathrm{mol/m^3}$ is a fractional uncertainty of $\pm\ 17 \cdot 10^{-6}$ in the sound speed. Based on the observation that the uncertainty increases as the density decreases and the temperature increases, we calculated the term $\{17 \cdot (T/125)/(\rho/39)\} = (5.3T/\rho)$, which was found to be consistent for the other temperatures and densities measured (corresponding to the pressures measured). The maximum fractional estimated error according to equation (23) is then, that occuring at 250 K and 0.099 MPa ($\rho = 47.6\ \mathrm{mol/m^3}$),which is $50 \cdot 10^{-6}$.

5.4.3 Internal consistency of the results

With the exception of the situation at the very low densities at the temperatures below 275 K, where the assumption of local equilibrium is questionable, the agreement at low pressures confirms that the corrections for dispersion, imperfect geometry and the thermal boundary layer have been applied with adequate accuracy, while the agreement at high pressures suggests that the model of shell motion and the values used for the elastic constants are adequate.

The mean speeds of sound determined from the average of the selected modes at each temperature and pressure are presented in table 5.4. The pressures given here include small corrections for the hydrostatic head between the mid-point of the resonator and the pressure transducer.

As a further test of internal consistency of the results, u^2 was fitted along each isotherm to polynomials in the pressure or the density. The data of u^2 obtained in the temperature range of 275 to 375 K which reach up to a pressure of 10 MPa were fitted to a polynomial in the pressure. It was found that 5 to 7 terms were needed to accommodate all the results, but fractional deviations of less than $\pm 6 \cdot 10^{-6}$ were then obtained. The data of u^2 obtained in the temperature range of 125 to 250 K and at pressures up to 1.4 MPa were fitted to a polynomial of the density. In this case 3 terms were enough to accommodate the data within the fractional deviations shown in table 5.5.

5.4.4 Comparison of the results

The speed of sound results in the temperature range 275 to 375 K are illustrated in figure 5.2 together with those obtained earlier by Goodwin [15] at 300 K and 350 K using a spherical resonator at $p \leq 7$ MPa [8]. At 300 K where a reliable value of the radius of Goodwin's resonator was available, the two sets of results differ by less than 0.003 per cent from above 1 MPa. The agreement at 350 K is slightly less good; here Goodwin's results are lower than the present ones by 0.022 per cent at 1.3 MPa and by 0.007 per cent at 7.2 MPa. Gammon and Douslin [16] have also reported speeds of sound in methane, which at 298.15 K, overlap the pressure range of the present work. Despite the need for dispersion corrections much greater than in the present work, their value at 2.4 MPa lies only 0.020 per cent below that interpolated from our results, while at 5.6 and 10.5 MPa the differences are just 0.003 per cent.

The results in the present range of temperatures and pressures (275 to 375 K and up to 10 MPa) are also in good agreement with most recent equations of state for methane . In particular, the wide ranging equation of Setzmann and Wagner [8] predicts results that deviate only very slightly from these measurements. The worst deviation, just -0.03 per cent, occurs at 275 K and 10 MPa, while for the three isotherm above 300 K the deviations are all better than ± 0.01 per cent. The GRI [17] equation of state applied to

pure methane also predicts sound speeds which agree with experiment to within ± 0.03 per cent on the isotherm of 275 K and to better than 0.01 per cent above 300 K. The data obtained at 275 to 375 K and at pressures up to 10 MPa were also compared with the values predicted by GERG [18] equation of state and Friend's [19] equation of state. The predictions of GERG were found very poor, showing deviations on the 10 MPa isobar of +2 per cent at 275 K and -2.2 per cent at 325 K. The equation of Friend et al agrees to within ± 0.04 per cent at 275 K but gives values at higher temperatures which lie up to 0.08 per cent below experiment.

The low pressure data obtained at temperatures between 125 and 250 K were compared with the values predicted by GRI equation of state [17]. The agreement was found to be excellent throughout the temperature and pressure range. At 125 K the deviation was always less than 0.02 per cent, at 175 and 200 K the deviation was always less than ± 0.01 and 0.01 per cent respectively, while at 225 and 250 K the maximum deviation was 0.005 per cent occuring at the highest pressure. However, at the temperature of 150 K the deviation was 0.01 per cent at the six lowest pressures, while it varied from -0.01per cent at 0.6 MPa to -0.11 per cent at 0.92 MPa. In that case either the equation of state employed is not very accurate close to saturation, or precondensation effects, which were decreasing as the pressure was lowered, perturbed our values for the speed of sound.

5.4.5 Regression analysis

The speed of sound data obtained in the temperature range 275 to 375 K and at pressures truncated up to 2.8 MPa were fitted in terms of equation (15) (pressure series) to yield the perfect-gas heat capacities and the second and third acoustic virial coefficients. Even in this truncated pressure range, four terms were required for every case, except at 375 K were three- and four-term fit gave almost identical results. The second virial

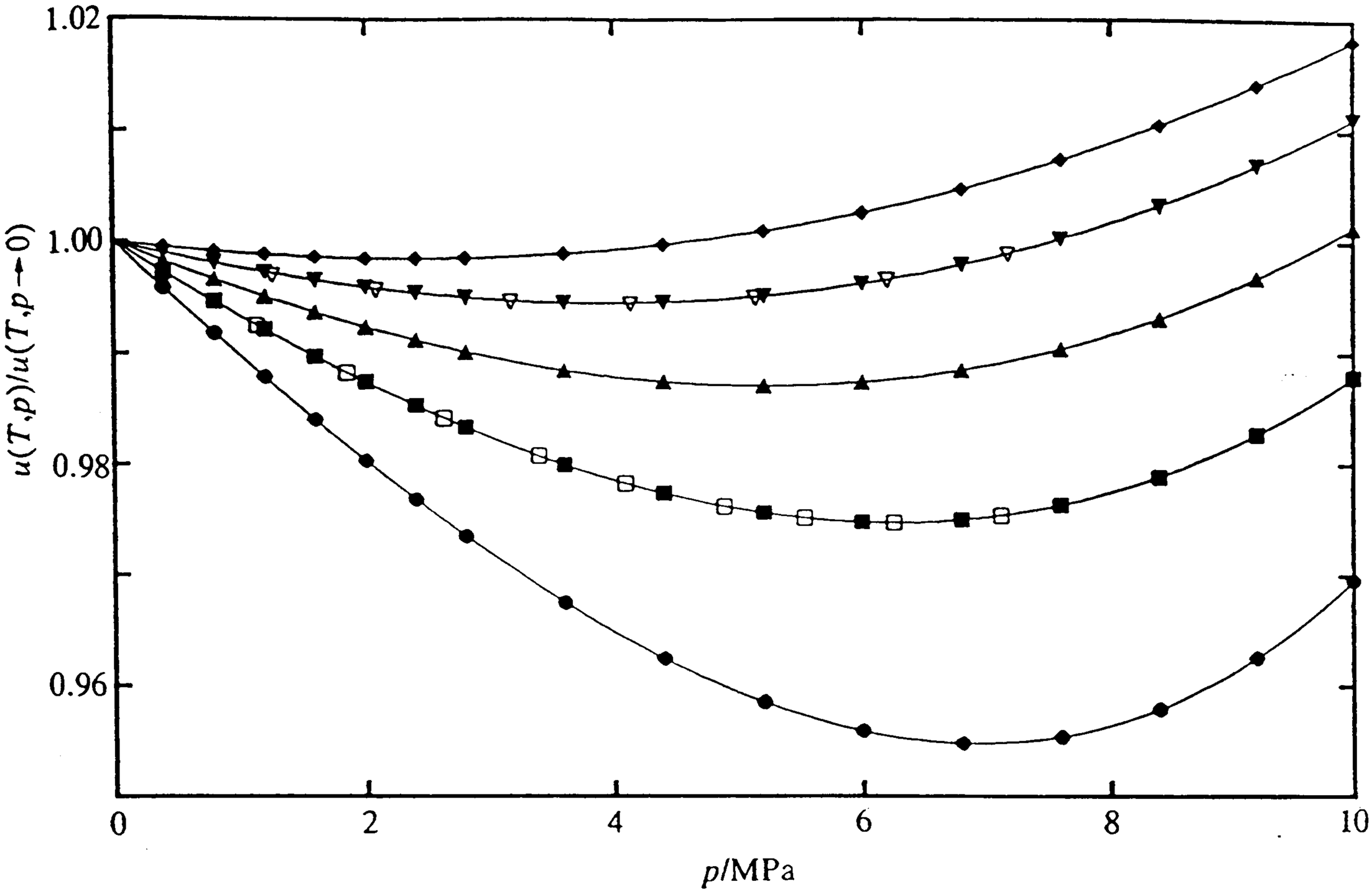

Figure 5.2. Speeds of sound in methane along the five isotherms. The results are plotted as $u(T,p)/u(T,p\to 0)$ where values of $u^2(T,p\to 0)=A_0$ are given in table 5.5. T =: •, 275 K; ■ 300 K; Δ, 325 K; ∇, 350 K; ♦, 375 K. Open symbols are Goodwin's results [15].

coefficients B used for the calculation of the third acoustic virial coefficients from equation (17), were obtained from the data of Douslin et al. [20].

The speed of sound data obtained at the temperatures between 125 and 250 K were fitted in terms of equation (13) (density series). The perfect-gas heat capacities and the acoustic virial coefficients obtained from the two fits are tabulated in table 5.5 together with their uncertainties and the fractional deviations of u^2 from the fit. In figure 5.3 the fractional deviations of u^2 from the fit are plotted against the density for the isotherm of 250 K. The perfect-gas heat capacities were compared with the values proposed by Setzmann and Wagner [8], which are based on spectroscopic data. The deviations were found always less than $\pm 0.002\ R$.

In the following chapter, the second and third acoustic virial coefficients obtained by the regression analysis of the speeds of sound are simultaneously fitted to spherical potentials to yield values for the second and third volumetric virial coefficients as well as for the viscosity.

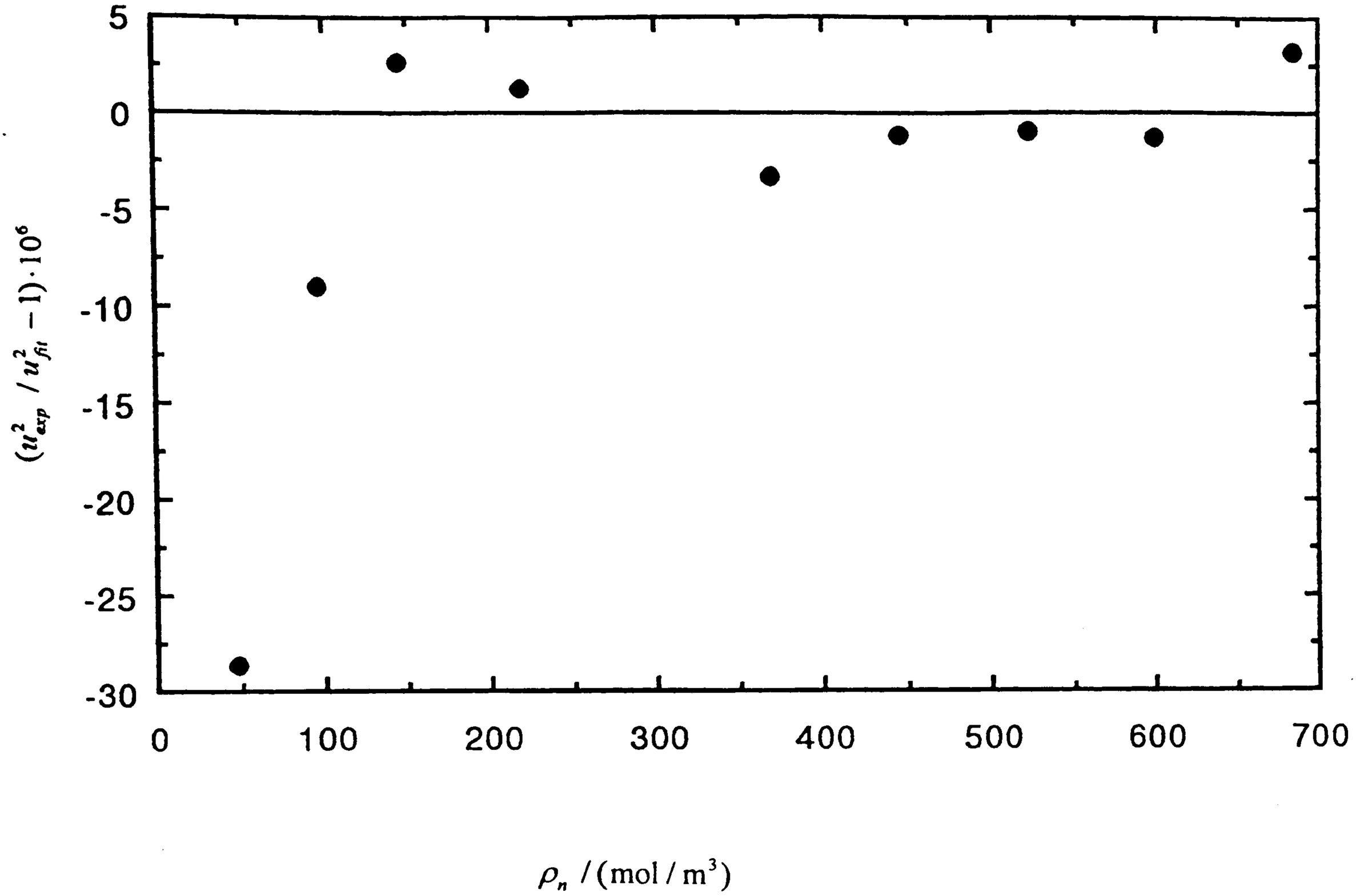

Figure 5.3. Fractional deviations of u^2 from values obtained from the three term fit against the density at 250 K, for methane.

5.5 Propane

Measurements were performed in propane gas along seven isotherms between 225 and 375 K and at pressures 0.010 to 0.850 MPa. At each point the resonance frequencies and halfwidths of the lowest five radial modes of the gas-filled resonator were measured. Under the conditions of the measurements, the resonance frequencies fell between 4000 and 19000 Hz.

The pressure was always kept below 85 per cent of the saturation pressure in order to avoid precondensation phenomena [1]. The variation of temperature and pressure during the acoustic cycle at conditions close to the saturation could cause condensation on the surface of the resonator. The thin liquid film formed on the surface perturbs the specific acoustic admittance of the surface. It was found that the specific acoustic admittance could increase by an order of magnitude above the corresponding value without precondensation [21].

The thermal boundary layer correction was calculated using values for the thermal conductivity taken from the correlation of Younglove and Ely [7]. The isobaric and isochoric heat capacity, the density and the speed of sound, required for the calculation corrections, were calculated from the Lee-Kessler equation of state [22]. This equation, which was derived on the corresponding-states principal, operates using values of the critical pressure, critical temperature and of the acentric factor. Although not as accurate as the equation employed for the case of methane, the accuracy of this equation is adequate for the calculation of the correction terms in equation (1). The viscosity values required for the calculation of the correction for the tubular opening in the resonator wall, were obtained also from the correlation of Younglove and Ely [7].

5.5.1 Error analysis

Generally, the agreement between all five modes was excellent throughout the temperature and pressure range of the measurements. At the temperatures of 225, 300 and

325 K, all five modes agreed better than $\pm 5 \cdot 10^{-6}$. At 250 and 275 K the four modes (0,2) to (0,5) agreed better than $\pm 5 \cdot 10^{-6}$, while mode (0,6) showed a systematic deviation from the average of the other four and has been excluded. The most probable explanation for this systematic deviation is the coupling of the (0,6) mode with a nearby shell resonance. At the temperature of 350 K the mode (0,2) and at 375 K the modes (0,2) and (0,3) were not measured because of a strong noise signal picked up by the receiver transducer at the corresponding frequencies. The agreement between the remaining modes at 350 and 375 K was better than $\pm 7 \cdot 10^{-6}$ and $\pm 5 \cdot 10^{-6}$ respectively.

The very good agreement between the modes measured in this low pressure range verifies the accuracy of the thermal boundary layer correction Δf_h, which for the (0,2) mode reached up to $75 \cdot 10^{-6} f$ at 225 K and 0.020 MPa. A dispersion correction was not taken into account since, as the results from the excess half-widths indicate, the vibrational relaxation time is too small to produce considerable dispersion. The relative contribution of the correction arising from the coupling of the fluid and the shell motion Δf_{sh} to the resonance frequencies was always less than $10 \cdot 10^{-6}$.

5.5.2 Regression analysis

Fitting of the values u^2 obtained, (shown in table 5.6) in terms of equation (13) yield the values for the perfect gas heat capacities and the second and third acoustic virial coefficients. In all cases a good fit was obtained using the first three terms of the density series expansion. This behaviour was expected, since the data lie at very low densities, which however, were high enough to yield significant values for the third acoustic virial coefficients. The perfect-gas heat capacities as well as the acoustic virial coefficients derived by the regression analysis are presented in table 5.7, together with the estimated uncertainties obtained from the fit.

5.5.3 Discussion of the results

The speeds of sound obtained from the average of the modes selected are presented in table 5.6. The present data were compared with the values predicted by the GRI equation of state [17] applied to pure propane. Systematic positive deviations were found, which at 300 K varied from 0.01 per cent at 0.02 MPa to 0.30 per cent at 0.8 MPa whereas at 375 K varied from 0.00 per cent at 0.02 MPa to 0.07 per cent at 0.8 MPa. These errors are much larger (by a factor of 10 at the largest pressure) than the estimated uncertainty of our speed of sound data, as is shown in the following.

The isochoric perfect-gas heat capacities obtained here were compared with the values predicted by the correlation of Younglove and Ely [7], based on spectroscopic data and were found systematically negative, from -0.25 up to a maximum of -0.70 per cent occuring at 300 K. At 300 K our value was found also to deviate from the spectroscopic value of Chao et al. [23] by -0.40 per cent. It is worth noticing here that the value of Younglove and Ely [7] and that of Chao et al. [23], both based on spectroscopic data which are considered to be the best source of information, differ by 0.30 per cent, which implies that the spectroscopic data available for propane show inconsistencies of the same order as our deviations. Our isochoric perfect-gas heat capacity values were also compared with the values at 250 and 300 K obtained by Malik [24] also from fit to speed of sound data. The agreement was found to be better than -0.10 per cent for both temperatures, which is of the same order as that found for the values of methane compared to the data of Setzmann and Wagner [8] ($\pm$ 0.05 per cent).

Deviations of the experimental perfect-gas heat capacity values from those predicted by spectroscopic data were expected as the natural consequence of the impurity of the propane gas sample. The mole fraction purity of propane was of the order 0.9995. Gas chromatography indicated that the main impurity was methane. Making thus the assumption that the impurity is only methane, we calculated the effect that could have on the perfect-gas heat capacities. At 300 K it was calculated a value for the isochoric

perfect-gas heat capacity of 0.31 per cent higher than the value obtained assuming pure propane, which explained indeed the negative deviations found in the experimental perfect-gas heat capacities. The corresponding effect of the methane impurity on the speed of sound at 300 K was found to be a fractional increase of $180 \cdot 10^{-6}$.

Finally the total fractional error ε in the speed of sound data is estimated to be

$$|\varepsilon| \leq [10^2 + 7^2 + 30^2 + 180^2]^{1/2} \cdot 10^{-6} \qquad (24)$$

where the four values in the parenthesis account for uncertainties in the pressure, disagreement between the different modes in the calculation of the speed of sound, uncertainty in the sphere radius and finally effects of impurities which were found to be quite independent of the temperature. According to equation (24) the maximum fractional uncertainty in the speed of sound is about $180 \cdot 10^{-6}$.

5.6 0.85 Methane-0.15 propane

Two sets of speed of sound measurements have been performed in a binary gaseous mixture of 85 per cent methane and 15 per cent propane. In the first set, the measurements proceeded along the isochores at amount-of-substance densities of 5, 4, 3, 2, 1 and 0.085 mol / dm^3 at temperatures 280 to 375 K and pressures up to 12 MPa. In the second set the speed of sound was measured along the isotherms of 225 to 375 K and at pressures up to 1.4 MPa.

Thermodynamic properties required for the calculation of the corrections appearing in equation (1) were obtained from the Lee-Kessler corresponding states equation of state [22] with interaction parameters from Plocker et al. [25]. The values for the perfect gas heat capacities of the mixture used for this calculation were obtained from the values we derived for the pure substances. Thermal conductivity and viscosity were obtained from the suitably-modified rigid sphere model of Vesovic and Wakeham [26,27].

5.6.1 First set of measurements

During the first set of the measurements an error occured in the temperature control of the system which caused a partial condensation of the gas. After that accident, the sample inside the resonator was remixed for two days through convection. However, some parts of the apparatus, such as the inlet tube through which the gas was introduced into the resonator, never recovered after the condensation, as a result of the very slow diffusion mechanism in these parts. This lead to an unstable composition of the mixture throughout the isochoric measurements. As obtained from the following analysis, the composition calculated from the average of the values derived at each temperature, was $x = 0.15089 \pm 0.0005$. This deviation can perturb the speed of sound by ± 0.04 per cent which is still very small.

The speed of sound has been calculated here for the (0,2), (0,3) and (0,4) frequency modes. The agreement between the speeds of sound obtained from the three modes was always of the order $10 \cdot 10^{-6}$ in the whole pressure range. Since the effect of the condensation is by far the most significant source of error in the speed of sound, the maximum fractional error in the speed of sound is estimated to be ± 0.04 per cent.

The speed of sound data obtained from the average of the selected modes are presented in table 5.8. These results were compared with the GRI equation of state [17] which was developed especially for natural gas systems. This equation of state predicts $p\ (T, \rho_n)$ values for methane-rich gas mixtures such as ours that agree with experimental results to better than ± 0.1 per cent under the conditions of the present measurements. The deviations of the present speed of sound data from those calculated from the GRI equation of state are illustrated in figure 5.4. We see that the agreement is within ± 0.1 per cent only up to densities of around $2\ \text{mol}/\text{dm}^3$ and that the deviations increase to nearly 0.50 per cent at $5\ \text{mol}/\text{dm}^3$. It would appear therefore that the GRI equation predicts sound speeds with considerably less accuracy than is achieved for the pressure.

We expect that significant improvements in the reliability of equations of state will follow from the inclusion of more extensive speed of sound data in the fitting process.

The speed of sound data obtained were initially fitted to equation (13) in order to yield perfect-gas heat capacities, and second and third acoustic virial coefficients. However, the limiting slope analysis was proved more successful in fitting the data. The limiting slope analysis has been used before by Douslin et al. [28] for deriving the second and higher volumetric virial coefficients from his compressibility data. According to this method the coefficients of a virial series are determined based on their definition, which for the second acoustic virial coefficient is:

$$\beta_a = \lim_{\rho_n \to 0} (u^2 / A_0 - 1) / \rho_n \qquad (25)$$

Thus the speed of sound data were analysed in terms of the equation:

$$(u^2 / A_0 - 1) / \rho_n = \beta_a + \gamma_a \rho_n + \cdots \qquad (26)$$

For the purpose of the regression analysis in terms of equation (26), the density has been calculated from the GRI equation of state [17]. The fitting coefficients obtained are presented in table 5.9. In order to check the sensitivity of the fit to the density values used, the fit was again performed having the density calculated from the less accurate Lee-Kessler equation of state. The deviations between the two sets of fitting coefficients obtained were found to be within their estimated uncertainty.

The constants A_0 determined from the fit, w ere used for deriving the composition using equation (14), which for the mixture is written:

$$A_0 = \frac{RT\,(x_M C_{pM}^{pg} + x_P C_{pP}^{pg})}{(x_M C_{pM}^{pg} + x_P C_{pP}^{pg} - R)(x_M M_M + x_P M_P)} \qquad (27)$$

In the above equation the notations M and P stand for methane and propane respectively. The perfect-gas heat capacities C_{pi}^{pg} of the pure substances were taken from our experimental values. The compositions derived are given in table 5.9 resulting in an average value of $x = 0.15089 \pm 0.0005$. This relatively large deviation (compared to the deviation obtained in the second set of measurements) is a consequence of the

condensation occured during the measurements in some part of the apparatus as mentioned above.

5.6.2 Second set of measurements

The speed of sound data in this set of measurements were obtained from the measurements of the resonance frequencies of the modes (0,2) to (0,5). The agreement between the speeds of sound determined from the different modes was always better than $\pm 8 \cdot 10^{-6}$. The data were compared with values predicted by the GRI equation of state [17]. At 225 K the experimental data were found by 0.01 per cent more positive than those predicted by GRI [16]. At 250 K the experimental data for the speed of sound were found to be systematically more negative than the calculated by 0.01 per cent. Negative deviations up to 0.01 per cent were generally noticed at the other temperatures, the only exception being a deviation of -0.02 per cent at 1.2 and 1.4 MPa at the temperatures of 325, 350 and 375 K.

The speed of sound data obtained (shown in table 5.10) were fitted to equation (13) in order to yield perfect-gas heat capacities, and second and third acoustic virial coefficients. For the purpose of the regression analysis in terms of equation (13), the density has been calculated from the GRI equation of state [16]. The fitting coefficients obtained are presented in table 5.11. In order to check the sensitivity of the fit to the density values used, the fit was again performed having the density calculated from the less accurate Lee-Kessler equation of state. The deviations between the two sets of fitting coefficients obtained were found to be within their estimated uncertainty.

The composition derived from equation (27) are given in table 5.11. As it can be seen the agreement between the compositions calculated at each isotherm for the second set of measurements is excellent ($x = 0.14908 \pm 0.0001$). This fact implies that the mixture was kept well mixed so that no composition changes took place throughout the measurements. It is also a test for internal consistency, meaning that the values of the

perfect-gas heat capacities of the pure components employed and the constant A_0, determined from fit the speed of sound data of the mixture, converge yielding a constant composition throughout the temperature range. However, the success of this internal consistency test does not necessarily mean that the values employed are the correct ones. In fact, by employing the values for the heat capacity suggested by Younglove and Ely [7] instead of the experimental ones, in equation (27) we obtain values for the composition at each temperature which are also in excellent agreement between them ($x = 0.14887 \pm 0.0001$). The fractional error for the speeds of sound calculated for this mixture is therefore estimated from

$$|\varepsilon| \leq [8^2 + 10^2 + 30^2 + 80^2]^{1/2} \cdot 10^{-6} \qquad (28)$$

where the four terms in the parenthesis account for the small disagreement between the modes, the uncertainty in the pressure measurements, the uncertainty in the sphere radius and the error in the composition (a change by -0.0001 in the composition results in a fractional increase in the speed of sound $80 \cdot 10^{-6}$) respectively. In fact, at 225 K the composition calculated differs by -0.0001 from the average value which was used for the speed of sound calculation by GRI equation of state [17]. According to the above scheme that could lead to values of the speed of sound by $80 \cdot 10^{-6}$ higher than those obtained for the average value. This explains the positive deviations of order 0.01 per cent of our experimental data at 225 K from the values calculated by GRI. On the other hand, at 250 K the composition calculated differs by 0.0001 from the average value. This difference should accordingly lead to speed of sound values by about $80 \cdot 10^{-6}$ lower than those obtained by employing the average value. Indeed at 250 K the deviations of the experimental values from those predicted by GRI were found of the order -0.01 per cent. After this analysis it is made clear that the deviations observed comparing our data with the calculated from GRI values, are attributed to the incorrect composition specification when comparing with the GRI values. Thus, the estimated fractional error of the speed of sound data in table 5.10 is given by:

$$|\varepsilon| \leq [8^2 + 10^2 + 30^2]^{1/2} \cdot 10^{-6} \qquad (29)$$

if at each temperature we employ the corresponding value derived for the composition (presented in table 11). According to equation (29) the maximum estimated fractional error is only $\pm 32 \cdot 10^{-6}$.

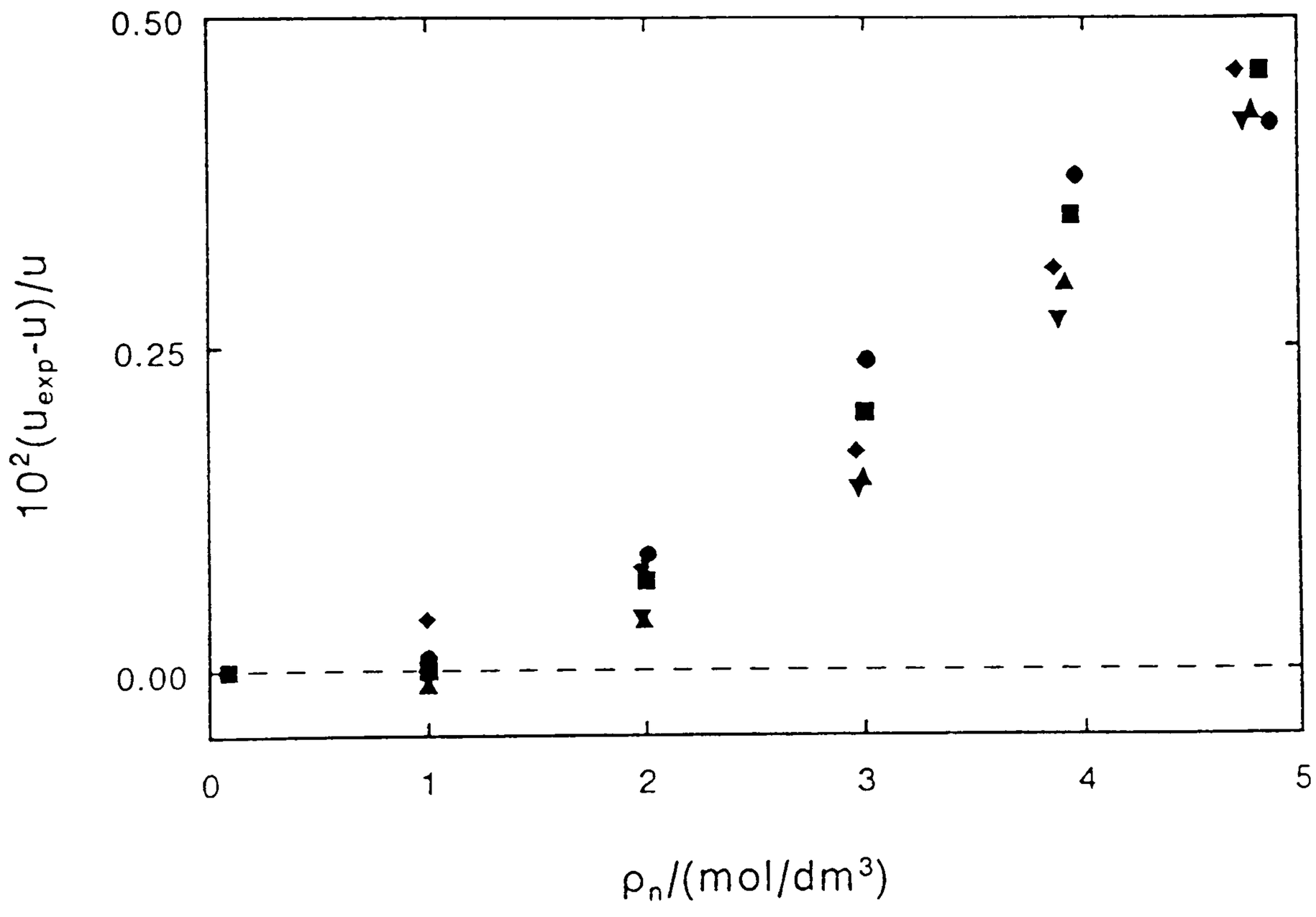

Figure 5.4. Percentage deviations of the experimental speed of sound values from values calculated from the GRI equation of state for the methane-propane mixture. • 280 K, ■ 300 K, ▲ 325 K, ▼ 350 K, ♦ 375 K. The gas densities were also obtained from this equation of state.

Table 5.1. Fractional deviations of the sound speeds $\delta_{0n} = (u_{0n} - \langle u \rangle) / \langle u \rangle$ of sound speeds u_{0n} determined from the (0,n) radial modes from the mean value $\langle u \rangle$ for modes 2-6 before correction for imperfect geometry. The values of δ_{0n} tabulated are the average of 13 determinations in argon covering the pressure range 0.1 to 0.5 MPa and the temperature range 275 to 375 K.

n	2	3	4	5	6
$10^6 \cdot \delta_{0n}$	-45.9	-18.0	-1.6	19.4	43.2

Table 5.2. Vibrational relaxation times τ in methane at density $\rho = 1\,\mathrm{kg \cdot m^{-3}}$.

T/K	τ / μs	T/K	τ / μs	T/K	τ / μs
200	2.56± 0.045	275	1.273± 0.015	350	0.614± 0.009
225	2.160± 0.016	300	0.997± 0.006	375	0.494± 0.006
250	1.632± 0.024	325	0.783± 0.007		

Table 5.3.Upper bounds for the mole fractions x_B of possible impurities in methane gas sample.

B:	N_2	O_2	CO_2	H_2O	C_2H_6	Other hydrocarbons
$10^6 \cdot x_B$:	<4	<4	<6	<6	<5	<7
$(1/u)(\partial u / \partial x_B)$:	-0.1	-0.3	-0.9	0.0	-1.1	-2.3

Table 5.4. The speeds of sound u in methane at temperatures T and pressures p.

p/MPa	u/(m·s^{-1})	p/MPa	u/(m·s^{-1})	p/MPa	u/(m·s^{-1})	p/MPa	u/(m·s^{-1})
			T=125.000 K				
0.21092	283.9857	0.15022	286.9818	0.08989	289.8259	0.03988	292.0970
0.18037	285.5093	0.12030	288.4056	0.06002	291.1923	0.02022	292.9637
			T=150.000 K				
0.91895	291.4732	0.70155	299.7986	0.39966	310.0220	0.09928	319.0897
0.85288	294.1095	0.60015	303.3809	0.30039	313.1236	0.04954	320.5030
0.79899	296.1873	0.50077	306.7409	0.19962	316.1635		
			T=175.000 K				
1.39933	317.8105	0.95249	328.2269	0.49901	337.8398	0.19439	343.8687
1.25666	321.2568	0.79890	331.5768	0.40036	339.8263	0.09861	345.7038
1.10382	324.8183	0.65038	334.7220	0.29880	341.8367		
			T=200.000 K				
1.38887	352.3081	0.95056	358.5078	0.49934	364.6808	0.20026	368.6625
1.24945	354.3035	0.79787	360.6193	0.40082	366.0016	0.09762	370.0137
1.10081	356.4061	0.64501	362.7099	0.29974	367.3473		
			T=225.000 K				
1.38915	380.4423	0.99716	384.0758	0.59939	387.7564	0.19953	391.4444
1.30093	381.2603	0.90091	384.9672	0.50091	388.6663	0.09937	392.3679
1.20278	382.1699	0.79838	385.9164	0.40059	389.5907		
1.09881	383.1334	0.69882	386.8374	0.30009	390.5178		
			T=250.000 K				
1.36099	404.9890	0.89916	407.8788	0.44925	410.7454	0.09866	413.0000
1.19790	406.0023	0.74892	408.8304	0.29880	411.7130		
1.04960	406.9310	0.59800	409.7928	0.19891	412.3553		

Table 5.4. continue

				T=275.000 K			
10.03660	419.4693	6.79170	412.9209	3.59523	418.4386	1.59567	425.5683
9.28123	416.5507	5.99172	413.4119	2.78223	421.0833	1.20231	427.1919
8.48529	414.4408	5.17575	414.5824	2.39056	422.4883	0.81522	428.8466
7.55257	413.1386	4.38058	416.2865	1.99285	423.9925	0.38910	430.7198
				T=300.000 K			
9.96690	444.5084	6.80724	438.8416	3.59759	441.0621	1.60162	445.4003
9.23575	442.3876	6.00990	438.7382	2.79741	442.5757	1.20625	446.4657
8.38280	440.5471	5.20812	439.0979	2.40724	443.4274	0.80836	447.5973
7.61667	439.4563	4.40630	439.8821	2.00355	444.3816	0.40237	448.8030
				T=325.000 K			
10.00958	467.1599	6.79616	461.1911	3.60018	461.1382	1.60087	463.5166
9.19295	465.0207	5.98937	460.6722	2.80071	461.8932	1.18571	464.2038
8.42680	463.4061	5.19704	460.5084	2.39559	462.3782	0.79938	464.8981
7.64200	462.1393	4.39606	460.6707	1.99953	462.9154	0.39338	465.6774
				T=350 K			
9.99178	487.2842	6.78365	481.0220	3.62073	479.3302	1.57626	480.2834
9.22309	485.3390	6.00128	480.2127	2.75485	479.5542	1.20488	480.6084
8.38278	483.5357	5.18819	479.6527	2.37593	479.7369	0.80234	481.0094
7.59459	482.1499	4.39378	479.3682	1.99204	479.9721	0.40123	481.4545
				T=375 K			
10.13942	506.0105	6.80446	499.0455	3.62002	496.0944	1.60248	495.9161
9.17623	503.5756	6.00088	497.9725	2.84282	495.8799	1.22021	496.0175
8.40282	501.8701	5.20716	497.1360	2.43474	495.8413	0.79453	496.1778
7.24325	499.7280	4.34932	496.4693	1.97507	495.8591	0.40305	496.3696

Table 5.5. Perfect-gas heat capacities $C_{p,m}^{pg}$ and second β_a and third γ_a acoustic virial coefficients of methane.

T/K	A_0 / $m^2 \cdot s^{-2}$	$C_{p,m}^{pg} / R$	β_a / (cm^3 / mol)	γ_a / (cm^6 / mol^2)	$10^6 \cdot \Delta$
125	86348± 1	4.0041	-307.41± 0.32	-244± 1350	13
150	103615± 1	4.0044	-215.64± 0.04	10535± 38	8
175	120801± 1	4.0127	-156.80± 0.01	10188± 8	3
200	137852± 1	4.0308	-116.8± 0.02	8965± 23	5
225	154667± 1	4.0640	-87.30± 0.02	7939± 17	3
250	171103± 1	4.1193	-65.28± 0.03	6967± 40	4
275	187034± 2	4.2021	-48.16± 0.05	5766± 90	5
300	202544± 2	4.3037	-34.94± 0.07	5510± 124	5
325	217606± 2	4.4258	-24.36± 0.06	5440± 108	5
350	232272± 3	4.5653	-15.44± 0.07	5104± 146	5
375	246621± 4	4.7182	-8.15± 0.12	5345± 250	5

Table 5.6. Speeds of sound u in propane at temperatures T and pressures p.

p/MPa	u / (m·s^{-1})	p/MPa	u / (m·s^{-1})	p/MPa	u / (m·s^{-1})	p/MPa	u / (m·s^{-1})
			T=225.000 K				
0.06978	217.4059	0.05011	218.7241	0.03003	220.0304	0.01011	221.2981
0.05921	218.1212	0.04008	219.3807	0.02017	220.6613		
			T=250.000 K				
0.20032	222.3661	0.10981	227.2341	0.03987	230.7526		
0.17019	224.0320	0.07920	228.7961	0.01989	231.7263		
0.14017	225.6444	0.06012	229.7524	0.01008	232.2013		
			T=275.000 K				
0.45021	223.6321	0.30043	230.6135	0.14921	237.0187	0.02488	241.8957
0.40080	226.0171	0.24872	232.8673	0.10024	238.9743		
0.35038	228.3649	0.19999	234.9281	0.05018	240.9264		
			T=300.000 K				
0.79099	224.3083	0.49887	235.9146	0.19909	246.2697	0.02426	251.7741
0.70190	228.0445	0.39752	239.5636	0.09917	249.4564		
0.60117	232.0512	0.29828	242.9846	0.04923	251.0071		
			T=325.000 K				
0.83543	238.5395	0.59859	245.7250	0.29722	254.1324	0.04960	260.5389
0.80091	239.6234	0.50015	248.5538	0.19829	256.7408	0.02363	261.1893
0.69981	242.7236	0.39727	251.4222	0.09985	259.2707		
			T=350.000 K				
0.85130	251.7667	0.59873	257.7199	0.29849	264.4079	0.04924	269.6813
0.79928	253.0195	0.49909	259.9834	0.19949	266.5306	0.02446	270.1944
0.69739	255.4324	0.39858	262.2217	0.09916	268.6435		
			T=375.000 K				
0.83358	264.2474	0.59885	268.6638	0.29797	274.1239	0.04960	278.4757
0.80077	264.8735	0.50008	270.4805	0.19894	275.8749	0.02510	278.8986
0.69987	266.7808	0.39983	272.2996	0.09896	277.6208		

Table 5.7. Perfect-gas heat capacities $C_{p,m}^{pg}$ and second β_a and third γ_a acoustic virial coefficients of propane.

T/K	A_0 / $m^2 \cdot s^{-2}$	$C_{p,m}^{pg} / R$	β_a / (cm^3 / mol)	γ_a / (cm^6 / mol^2)	$10^6 \cdot \Delta$
225	49252± 1	7.2112	-1044.64± 2.41	-130760± 54500	15
250	54140± 1	7.7295	-850.50± 0.80	55641± 7358	19
275	58968± 0.7	8.2838	-706.25± 0.26	68928± 1130	14
300	63760± 0.8	8.8604	-597.27± 0.16	73072± 440	17
325	68526± 0.3	9.4538	-511.41± 0.05	70312± 130	5
350	73277± 0.2	10.0572	-441.22± 0.04	63748± 113	3
375	78025± 0.2	10.6590	-382.90± 0.04	57109± 120	3

Table 5.8. Speeds of sound u in $\{(1-x)\,CH_4 + x\,C_3H_8\}$ with x=0.15089.

p/MPa	u / (m · s^{-1})	p/MPa	u / (m · s^{-1})	p/MPa	u / (m · s^{-1})
		T=280 K			
7.80470	337.408	5.49900	342.449	2.14965	363.859
6.74970	338.105	3.96000	351.123	0.20070	378.833
		T=300 K			
8.92730	362.152	6.12920	362.339	2.32815	378.434
7.62490	360.468	4.34974	368.361	0.21489	390.977
		T=325 K			
10.29350	389.500	6.89650	384.885	2.54861	395.415
8.68895	385.552	4.82600	388.166	0.23221	405.332
		T=350 K			
11.62970	414.122	7.64565	405.499	2.76536	411.286
9.72940	408.262	5.29408	406.451	0.24030	418.889
		T=375 K			
12.93435	436.680	8.38160	424.632	2.98023	426.253
10.74525	429.189	5.75285	423.544	0.26625	431.720

Table 5.9. Isotherm parameters determined in the analysis of $\{(1-x)\,CH_4 + x\,C_3H_8\}$ with x=0.15089.

T/K	A_0 / $m^2 \cdot s^{-2}$	x	β_a / (cm^3 / mol)	γ_a / (cm^6 / mol^2)
280	144710		-96.14	10941± 68
300	153900	0.15065	-78.57	9514± 101
325	165180	0.15066	-62.90	9123± 15
350	176194	0.15086	-48.61	8224± 15
375	186946	0.15139	-35.84	7206± 54

Table 5.10. Speeds of sound u in $\{(1-x)\,CH_4 + x\,C_3H_8\}$ with x=0.14908.

p/MPa	u / (m · s^{-1})	p/MPa	u / (m · s^{-1})	p/MPa	u / (m · s^{-1})	p/MPa	u / (m · s^{-1})
			T=225.000 K				
0.44812	337.7642	0.30065	340.0230	0.14954	342.3026		
0.40024	338.5015	0.24996	340.7912	0.09981	343.0414		
0.34926	339.2825	0.19976	341.5478	0.04933	343.7866		
			T=250.000 K				
1.36430	346.3807	0.80106	352.8212	0.34588	357.8798	0.04949	361.1903
1.20087	348.2635	0.65114	354.5127	0.20059	359.5325		
1.00244	350.5338	0.50073	356.1995	0.09984	360.6411		
			T=275.000 K				
1.36553	366.5639	0.80050	371.1944	0.35035	374.9012	0.04977	377.3722
1.20123	367.9067	0.65067	372.4273	0.20017	376.1383		
1.00346	369.5266	0.50057	373.6637	0.09979	376.9639		
			T=300.000 K				
1.40275	384.2685	0.80094	387.8688	0.35010	390.6278	0.04940	392.4818
1.20009	385.4689	0.65019	388.7860	0.19981	391.5557		
0.99964	386.6682	0.49906	389.7112	0.09953	392.1753		
			T=325.000 K				
1.41436	400.5680	0.80011	403.2625	0.34980	405.3113		
1.20053	401.4912	0.64998	403.9396	0.19975	406.0068		
1.00047	402.3698	0.50013	404.6212	0.09996	406.4704		
			T=350.000 K				
1.39956	415.7214	0.80052	417.6322	0.35044	419.1434	0.05011	420.1765
1.20061	416.3423	0.65026	418.1297	0.19967	419.6617		
0.99992	416.9825	0.50023	418.6336	0.10003	420.0058		
			T=375.000 K				
1.36317	429.9377	0.80039	431.2160	0.34962	432.3079	0.04837	433.0637
1.20093	430.2954	0.65054	431.5733	0.20029	432.6818		
1.00106	430.7483	0.49977	431.5733	0.09989	432.9364		

Table 5.11. Results of the regression analysis for $\{(1-x)\,CH_4 + x\,C_3H_8\}$ with x=0.14908.

T/K	A_0 / $m^2 \cdot s^{-2}$	x	β_a / (cm^3 / mol)	γ_a / (cm^6 / mol^2)	$10^6 \cdot \Delta$
225	118690± 1	0.14900	-159.49± 0.17	10099± 610	8
250	130852± 1	0.14918	-125.76± 0.05	11286± 65	9
275	142722± 1	0.14906	-99.68± 0.06	10521± 85	9
300	154286± 1	0.14910	-79.03± 0.08	9561± 125	12
325	165600± 1	0.14909	-62.45± 0.03	8893± 52	4
350	176699± 1	0.14909	-48.62± 0.07	8137± 131	9
375	187655± 1	0.14904	-37.07± 0.06	7596± 122	6

5.7 References

[1] J. P. M. Trusler, *Physical Acoustics and Metrology of Fluids* (Adam Hilger, Bristol, 1991), p. 76, 98.

[2] H. M. Ledbetter, Cryogenics **22**, 653 (1982).

[3] H. M. Ledbetter, W. F. Weston and E. R. Naimon, J. Appl. Phys. **46**, 3855 (1975).

[4] M. B. Ewing, A. A. Owusu and J. P. M. Trusler, Physica A **156**, 899 (1989).

[5] J. B. Mehl, J. Acoust. Soc. Am. **71**, 1109 (1982).

[6] J. P. M. Trusler and M. Zarari, J. Chem. Thermodyn. **24**, 973 (1992).

[7] B. A. Younglove and J. F. Ely, J. Phys. Chem. Ref. Data **16**, 577 (1987).

[8] U. Setzmann and W. Wagner, J. Phys. Chem. Ref. Data **20**, 1061 (1991).

[9] M. B. Ewing, A. R. H. Goodwin and J. P. M. Trusler, J. Chem. Thermodyn. **21**, 867 (1989).

[10] M. B. Ewing, A. R. H. Goodwin, M. L. McGlashan and J. P. M. Trusler, J. Chem. Thermodyn. **20**, 243 (1988).

[11] M. B. Ewing, A. R. H. Goodwin, M. L. McGlashan and J. P. M. Trusler, J. Chem. Thermodyn. **19**, 721 (1987).

[12] M. B. Ewing and J. P. M. Trusler, J. Chem. Phys. **90**, 1106 (1989).

[13] J. D. Lambert, *Vibrational and rotational relaxation in gases*, (Clarendon Press, Oxford, 1977), p. 65.

[14] M. B. Ewing, M. L. McGlashan and J. P. M. Trusler, Metrologia **22**, 93 (1986).

[15] A. R. H. Goodwin, PhD thesis, University of London, 1988.

[16] B. E. Gammon and D. R. Douslin, J. Chem. Phys. **64**, 103 (1976).

[17] K. E. Starling, M. Mannan, J. L. Savidge, S. Sadasivan, T. B. Jr. Reid, K. Gangadhar and M. A. Drass, *Development of an equation of state for computation of supercompressibility factors, critical flow factor and other properties of wet sour natural gases, synthetic gas and admixtures* (Final Report 1987, Gas Research Institute (GRI), Chicago, U.S.A. 1987).

[18] M. Jaeschke, S. Audibert, P.van Caneghem, A. E. Humphreys, R. Janssen-Van Rosmalen, Q. Pellei, J. A. Schouten and J. P. J. Michels, S.P.E. Prod. Engng, 350 (1991).

[19] D. G. Friend, J. F. Ely and J. Ingham, J. Phys. Chem. Ref. Data **18**, 583 (1989).

[20] D. R. Douslin, R. H. Harrison, R. T. Moore and J. P. McCullough, J. Chem. Engng Data **9**, 358 (1964).

[21] J. B. Mehl and M. R. Moldover, J. Chem. Phys. 77, 455 (1982).

[22] B. I. Lee and M. G. Kessler, AIChE Journal **21**, 510 (1975).

[23] J. Chao, R. C. Wilhoit and B. J. Zwolinski, J. Phys. Chem. Ref. Data **2**, 427 (1973).

[24] K. Malik, MSc thesis, University of London, 1991.

[25] U. Ploecker, H. Knapp and J. M. Prausnitz, Ind. Chem. Process Des. Dev. **17**, 324 (1978).

[26] V. Vesovic and W. A. Wakeham, Chem. Eng. Sci. **44**, 2181 (1989).

[27] V. Vesovic and W. A. Wakeham, High Temp. High Pres. **23**, 179 (1991).

[28] D. R. Douslin, R. H. Harrison, R. T. Moore and J. P. McCullough, J. Chem. Phys. **35**, 1357 (1961).

CHAPTER 6

NUMERICAL INTEGRATION OF THE SPEED OF SOUND

6.1 Introduction.

A method is presented in this chapter by which the speed of sound data can be integrated to yield the compressibility factor.

A substance is completely characterized from the thermodynamic point of view when a functional relationship exists between its pressure (p), temperature (T) and density (ρ) in addition to the knowledge of its heat capacity at zero density. The $p\rho T$ properties (usually known as pVT, where $V = 1 / \rho$ is the volume) are therefore of great importance for scientific as well as industrial purposes. Most equilibrium properties such as the compression factor, the internal energy, the enthalpy, the entropy, the free energy, the isobaric and isochoric heat capacity, etc., which find large demand in the industry are obtained from the $p\rho T$ surface. Second and third volumetric virial coefficient may also be derived from $p\rho T$ data by regression analysis.

It takes great efforts to derive accurate $p\rho T$ data. For the purpose of measuring accurate $p\rho T$ data several experimental techniques have been developed, many of them very sophisticated. For example we can refer to the simple Amagat's methods [1], the several Burnett's methods [2-5], pycnometer methods [6] and the more sophisticated methods developed recently such as those based on the buoyancy principle [7-9] or refractive-index measurements [10].

Some properties which relate to the derivatives of the $p\rho T$ properties, such as the speed of sound u ($u^2 = (\partial p / \partial \rho)_s$ where s is the entropy) are particularly sensitive to the accuracy of $p\rho T$ data. In fact such properties are so sensitive to the accuracy of the latter

that are used to test equations of state (usually functional relationships between the $p\rho T$ data).

It will be shown that the proposed method for the determination of the compression factor $z = p / \rho RT$ by integration of the speed of sound data is very accurate and moreover its accuracy is increasing when the temperature increases.

The method is applied to pure methane and the compression factor is obtained in the temperature range 275 to 375 K and at pressures up to 10 MPa. This numerical procedure yield simultaneously values for the isobaric and isochoric heat capacity, for which experimental data are not available in the literature.

6.2 Method of analysis

The fundamental equation for the speed of sound u is

$$u^2 = (\partial p / \partial \rho)_s \qquad (1)$$

where p is the pressure, ρ is the density and s indicates entropy. After some algebra employing standard thermodynamic relations [11], equation (1) may be written in terms of the compression factor z and its partial derivatives with respect to the temperature T and the pressure p as follows:

$$u^2 = (RTz^2 / M)\{[z - p(\partial z / \partial p)_T] - (R / C_{p,m})[z + T(\partial z / \partial T)_p]^2\}^{-1} \qquad (2)$$

with

$$(\partial C_{p,m} / \partial p)_T = -(R / p)[2T(\partial z / \partial T)_p + T^2(\partial^2 z / \partial T^2)_p] \qquad (3)$$

where $C_{p,m}$ is the isobaric molar heat capacity and $C_{p,m}^{pg}$ is the perfect gas (zero density) isobaric molar heat capacity.

Equations (2) and (3) may be solved simultaneously to yield the compressibility factor, the isobaric molar heat capacity and, employing the equation

$$C_{V,m} / R = C_{p,m} / R - [z + T(\partial z / \partial T)_p]^2 / [z - p(\partial z / \partial p)_T] \qquad (4)$$

the isochoric molar heat capacity $C_{V,m}$ inside the region in which $u(T, p)$ is known.

For this purpose two initial values are required, selected from z, $(\partial z / \partial T)_p$, $(\partial^2 z / \partial T^2)_p$, $C_{p,m}$, and $C_{V,m}$ at the starting temperature of the integration and at all pressures. The choice of the initial values is based entirely on the available data. From the above set of the data which can be used as initial values, most likely to be available in the literature are z and $(\partial z / \partial T)_p$. Thus, for example, let us choose the initial values, z and $(\partial z / \partial T)_p$, at the starting temperature, T_0. From the initial values of z along the starting isotherm T_0, it is possible to calculate $(\partial z / \partial p)_T$ and then, using the experimental values for the speed of sound, obtain from (2) the values for $C_{p,m}$ and from (4) those of $C_{V,m}$. By differentiating $C_{p,m}$ with respect to the pressure, $(\partial^2 z / \partial T^2)_p$ is obtained from equation (3). The values of z and $(\partial z / \partial T)_P$ along the new isotherm $T_1 = T_0 + \delta T$ can be readily obtained by means of a Taylor expansion about T_0.

If instead of (2) and (3), equation (1) was employed for performing the integration, then initial values of the density would be required at the lowest temperature. This can be justified as follows:

Equation (1) is rewritten

$$[d\rho = u^{-2} dp]_s \qquad (5)$$

In order to obtain the density from equation (5) we perform integration starting from the point where initial values of the density are available. In a (p,T) diagram such as that of figure 6.1 this point will be called (p_0, T_0). At this point the corresponding speed of sound and density are u_0 and ρ_0 respectively and the isentrope passing through that point s_0. The integration proceeds by calculating the density $(\rho_0 + d\rho)$ at the new point $(p_0 + dp,\ T_0 + dT)$ as follows:

$$\rho_0 + d\rho = \rho_0 + u_0^{-2}[(p_0 + dp) - p_0] \qquad \text{along the isentrope } s_0 \qquad (6)$$

Since the integration takes place along isentropes, it is obvious that in order to obtain the density throughout the (p,T) region where the speed of sound is known, initial values of the density ρ_0 are needed along a path which crosses all isentropes passing through that region. If this path is chosen to be an isotherm, the only isotherm satisfying this

requirement is, as shown in figure 6.1, the one of the lowest temperature. However, when the integration is performed using equations (2) and (3) such restriction is not required and the initial values can essentially be chosen at any temperature.

In a following section it will be shown that the proposed integration method is of increasing accuracy when the integration proceeds in the direction of increasing temperature.

6.3 Error propagation

Since the initial values discussed in the previous section are not exactly known it is important to examine the propagation of error in the solution obtained. This can be done either numerically, applying known perturbations in the initial values or an analytical method, in which case approximations are essential. In this section we derive the analytical solution of the homogeneous equation relating the speed of sound to the compressibility factor and its derivatives, for the simplified case of the monatomic argon, for which the perfect-gas heat-capacity is temperature independent.

If instead of pressure and temperature, as independent variables are selected the density and the temperature, equation (2) results in:

$$u^2 = (RT / M)\{[z + \rho_n(\partial z / \partial \rho_n)_T] - (R / C_{V,m})[z + T(\partial z / \partial T)_\rho]^2\} \quad (7)$$

where

$$C_{V,m} = C_{V,m}^{pg} + \int_0^{\rho_n} (\partial C_{V,m} / \partial \rho_n)_T \, d\rho_n \quad (8)$$

with

$$(\partial C_{V,m} / \partial \rho_n)_T = -(R / \rho_n)[2T(\partial z / \partial T)_\rho + T^2(\partial^2 z / \partial T^2)_\rho] \quad (9)$$

where ρ_n is the amount of substance density.

We define the function $F(z)$ as follows:

$$F(z) = (RT / M)\{[z + \rho_n(\partial z / \partial \rho_n)_T] - (R / C_{V,m})[z + T(\partial z / \partial T)_\rho]^2\} \quad (10)$$

Equations (7) to (9) are coupled and can be combined into a single 'integro-differential' non-linear equation by substituting (9) into (8) and (8) into (7). The resulting equation has the particular solution z_p obtained by specific initial values. If the initial values are perturbed by a small amount, then another solution z is obtained which can be written as follows:

$$z = z_p + z_1 \tag{11}$$

where z_p is the particular solution and z_1 would be the solution of the homogeneous version of equation (7), if equation (7) were linear. Here z_1 is the perturbation in the particular solution arising from perturbation in the initial values.

Since z_p is a solution of (7) one can write using (10)

$$F(z_p) = u^2 \tag{12}$$

Also since $z_p + z_1$ is a solution of (7) as well then:

$$F(z_p + z_1) = u^2 \tag{13}$$

From the definition of the function in equation (10) we have:

$$\begin{aligned} F(z_p + z_1) = (RT/M)\,\{&[(z_p + z_1) + \rho_n\, \partial(z_p + z_1)/\partial\rho_n] \\ &-[R/C_{V,m}(z_p + z_1)]\,[(z_p + z_1) + T\,\partial(z_p + z_1)/\partial T]^2\} \end{aligned} \tag{14}$$

where, using equations (8) and (9):

$$C_{V,m}(z_p + z_1) = C_{V,m}^{pg} - R\int_0^{\rho} [2T\,\partial(z_p + z_1)/\partial T + T^2\partial^2(z_p + z_1)/\partial T^2]\,d\rho_n/\rho_n \tag{15}$$

Also from equations (8-10) we obtain

$$F(z_p) = (RT/M)\,\{[z_p + \rho_n\, \partial z_p/\partial\rho_n] - [R/C_{V,m}(z_p)]\,[z_p + T\,\partial z_p/\partial T]^2\} \tag{16}$$

and

$$C_{V,m}(z_p) = C_{V,m}^{pg} - R\int_0^{\rho} [2T\,\partial z_p/\partial T + T^2\partial^2 z_p/\partial T^2]\,d\rho_n/\rho_n \tag{17}$$

Since from equations (12) and (13) we have

$$F(z_p + z_1) = F(z_p) \tag{18}$$

equations (15) and (17) imply that

$$1/C_{V,m}(z_p + z_1) = 1/[C_{V,m}(z_p) - R\int_0^{\rho_n} (2T\partial z_1/\partial T + T^2\partial^2 z_1/\partial T^2)d\rho_n/\rho_n] \tag{19}$$

Since in this analysis the quantity z_1 is treated as the error accompanying the particular solution z_p, elimination of second- and higher-order terms in z_1, results in negligible error. Thus eliminating second order terms equation (19) is reduced to the simplest form:

$$1/C_{V,m}(z_p + z_1) = [C_{V,m}(z_p) + R\int_0^{\rho_n} (2T\partial z_1/\partial T + T^2\partial^2 z_1/\partial T^2)d\rho_n/\rho_n]/C^2_{V,m}(z_p) \tag{20}$$

Equations (14), (16), (18) and (20) yield after elimination of second- and higher-order terms the following relation

$$\begin{aligned}&\left(z_1 + \rho_n\frac{\partial z_1}{\partial \rho_n}\right) + \frac{2R}{C_{V,m}(z_p)}\left(z_p + T\frac{\partial z_p}{\partial T}\right)\left(z_1 + T\frac{\partial z_1}{\partial T}\right)\\ &+ \frac{R^2}{C^2_{V,m}(z_p)}\left(z_p + T\frac{\partial z_p}{\partial T}\right)^2\int_0^{\rho_n}\left(2T\frac{\partial z_1}{\partial T} + T^2\frac{\partial^2 z_1}{\partial T^2}\right)\frac{d\rho_n}{\rho_n} = 0\end{aligned} \tag{21}$$

For the case of the perfect monatomic gas, $z_p = 1$ and $C^{pg}_{V,m} = 3/2R$ so that equation (21) and (17) give

$$\left(z_1 + \rho_n\frac{\partial z_1}{\partial \rho_n}\right) + \frac{4}{3}\left(z_1 + T\frac{\partial z_1}{\partial T}\right) + \frac{4}{9}\int_0^{\rho_n}\left(2T\frac{\partial z_1}{\partial T} + T^2\frac{\partial^2 z_1}{\partial T^2}\right)\frac{d\rho_n}{\rho_n} = 0 \tag{22}$$

which when differentiated with respect to the density, yields:

$$2\rho_n \frac{\partial z_1}{\partial \rho_n} + \rho_n^2 \frac{\partial^2 z_1}{\partial \rho_n^2} + \frac{4}{3}\left(\rho_n \frac{\partial z_1}{\partial \rho_n} + T\rho_n \frac{\partial^2 z_1}{\partial T\, \partial \rho_n}\right) + \frac{4}{9}\left(2T\frac{\partial z_1}{\partial T} + T^2 \frac{\partial^2 z_1}{\partial T^2}\right) = 0 \qquad (23)$$

Equation (23) can be readily expressed in the form

$$4\frac{\partial^2 z_1}{\partial x^2} + 12\frac{\partial^2 z_1}{\partial x \partial y} + 9\frac{\partial^2 z_1}{\partial y^2} + 4\frac{\partial z_1}{\partial x} + 21\frac{\partial z_1}{\partial y} = 0 \qquad (24)$$

where $x = \ln T$ and $y = \ln \rho_n$. The solution of the above equation z_1 is given [12] by the sum of terms:

$$z_1 = \sum_i [c \exp(\alpha x + \beta y)]_i \qquad (25)$$

where c is an arbitrary constant and α and β are related through the equation

$$4\alpha^2 + 12\,\alpha\beta + 9\beta^2 + 4\alpha + 21\beta = 0 \qquad (26)$$

or

$$\alpha = \frac{-(1+3\beta) \pm \sqrt{1-15\beta}}{2} \qquad (27)$$

When $\beta > 1/15$ one can write

$$\exp(\alpha x + \beta y) = \exp[-(1+3\beta)x/2 + \beta y \pm i\sqrt{15\beta - 1}\,x/2] \qquad (28)$$

which after substitution of x and y by their equals yields:

$$c\exp(\alpha x + \beta y) = T^{-(1+3\beta)/2}\rho_n^{\beta}\,[c_1 \cos(\sqrt{15\beta-1}\ln T/2) + c_2 \sin(\sqrt{15\beta-1}\ln T/2)] \qquad (29)$$

When $\beta < 1/15$ the exponential term is given by:

$$c\exp(\alpha x + \beta y) = c_1 T^{-(1+3\beta)/2+\sqrt{1-15\beta}/2}\rho_n^{\beta} + c_2 T^{-(1+3\beta)/2-\sqrt{1-15\beta}/2}\rho_n^{\beta} \qquad (30)$$

The number of terms in the summation of equation (25) as well as the values of the coefficients c_1 and c_2 are specified by the initial conditions. For example, at the starting temperature T_0 let the error in the compressibility factor be

$$z_1(\rho_n, T_0)=k\rho_n^{\beta} \tag{31}$$

and the error in the first derivative of the compressibility factor with respect to the density

$$\partial z_1(\rho_n, T_0)/\partial T=0 \tag{32}$$

Equation (31), since it is valid for every density ρ_n, restricts the number of terms in the summation of equation (25) to the two terms varying as ρ_n^{β}, as given by equation (29) or (30). In addition equation (31) provides a first relation between the coefficients c_1 and c_2. A second relation between the two coefficients is obtained by equation (32). The two relations suffice for the two coefficients to be calculated. Thus the quantity z_1 and through it the propagation of error in the quantities z, $\partial z / \partial T$, $\partial^2 z / \partial T^2$, $\partial z / \partial \rho$ and $c_{V,m}$ are completely defined.

The characteristic of the solution obtained for z_1 is that for all positive values of β the quantity z_1 is ultimately decreasing when the temperature increases. In the case of a polyatomic gas $C_{V,m}^{pg}>3/2R$ which results in much faster decrease of z_1 when the temperature increases. In this way the monatomic perfect-gas case sets the upper error bound. This can be illustrated in figures 6.2 and 6.3. In figure 6.2 the error in the initial values of the compression factor is taken to be proportional to the density, while the error in the initial values of its derivative with respect to the temperature is taken to be zero. In figure 6.3 the error in the initial values of the compression factor was taken to be zero, while the error in the initial values of its derivative with respect to the temperature was taken proportional to the density. In both figures it is shown, that the same initial error for both substances decreases more rapidly for methane than it does for argon as the temperature increases. The numerical simulation for methane was based on the GRI equation of state [13]. For monatomic perfect gas the analytical form of the error was employed as derived in equation (29).

For $\beta = 1$, which means that the error is proportional to the density, we obtain for z_1 the solution:

$$z_1=\rho_n T^{-2}[c_1 \cos(\sqrt{3.5}\ln T)+c_2 \cos(\sqrt{3.5}\ln T)] \tag{33}$$

In this case there is $z_1=B_1\rho_n$ and the above equation yields the expression of the homogeneous solution B_1 of the linear differential equation relating the second acoustic virial coefficient β_a to the second volumetric virial coefficient B (see chapter 2) for the case of a monatomic gas.

The argument that $z_1=B_1\rho_n$ is justified as follows:

The particular solution z_p can be written

$$z_p = 1 + B_p\rho_n + C_p\rho_n^2 + \cdots \tag{34}$$

where for the present case of the perfect gas $B_p = C_p = \cdots = 0$ .If a perturbation z_1 in the initial value of the compressibility factor z_p is applied which is proportional to the density, then z_p is perturbed to the value z given by:

$$z=z_p+z_1=z_p+\varepsilon\rho_n =1+(B_p+\varepsilon)\rho_n+C_p\rho_n^2+\cdots \tag{35}$$

where ε is the proportionality factor (independent of density). The new solution z can be also expanded in virial series as follows:

$$z = 1 + B\rho_n + C\rho_n^2 + \cdots \tag{36}$$

As derived in chapter 2 the differential equation which relates the second acoustic virial coefficients β_a to the second volumetric virial coefficients B is

$$\beta_a=2B+2(\gamma^{pg}-1)T\frac{dB}{dT}+\frac{(\gamma^{pg}-1)^2}{\gamma^{pg}}T^2\frac{d^2B}{dT^2} \tag{37}$$

where $B=B_p+\varepsilon$. The above equation is satisfied for $B=B_p$ for the case $z=z_p$. Any other solution of equation (37) is given by

$$B = B_p + B_1 \tag{38}$$

where B_1 is the homogeneous solution of (37). Thus, $\varepsilon=B_1$ and accordingly

$$B_1\rho_n=\varepsilon\rho_n=z_1 \tag{39}$$

As derived above for the simplified case of the monatomic perfect gas the numerical integration of speed of sound data is a method which for certain kinds of density dependence of the error, is of increasing accuracy as the temperature increases. Of course, it is never possible to know which exactly is the density dependence of the error in the initial values used. As it results from equation (30) if the error varies as ρ_n^{β} where $\beta < 0$, it could be increasing in a catastrophic manner as the temperature increases. However, this error dependence can be easily avoided if the initial values z and $(\partial z / \partial T)_\rho$ are smoothened by fitting z in a virial series of the density with the boundary condition $z \to 1$ as $\rho_n \to 0$. Then since the particular solution z_p is by definition a virial series of the density (in which for this case of perfect gas the coefficients are zero) the error z_1, according to the above proof for B_1, is forced to be a linear combination of the homogeneous solutions $B_1\rho_n$, $C_1\rho_n^2$, etc., which all decrease as the temperature increases. Here C_1 is the homogeneous solution of the linear part of the differential equation relating the third acoustic virial coefficient γ_a with the third volumetric virial coefficient C (see chapter 2). The proof of the above argument is as follows:

If $z_1 = \varepsilon_1\rho_n + \varepsilon_2\rho_n^2 + \cdots$ then according to equations (54) and (55) of chapter 2 we may write for the perfect gas case ($z_p = 1$, so that $z = 1 + \varepsilon_1\rho_n + \varepsilon_2\rho^2 + \cdots$, and $u^2 = A_0$):

$$0 = 2\varepsilon_1 + 2(\gamma^{pg} - 1)T\frac{d\varepsilon_1}{dT} + \frac{(\gamma^{pg} - 1)^2}{\gamma^{pg}}T^2\frac{d^2\varepsilon_1}{dT^2} \tag{40}$$

$$0 = \frac{(\gamma^{pg} - 1)}{\gamma^{pg}}\left[\varepsilon_1 + (2\gamma^{pg} - 1)T\frac{d\varepsilon_1}{dT} + (\gamma^{pg} - 1)T^2\frac{d^2\varepsilon_1}{dT^2}\right]^2 + \frac{(1 + 2\gamma^{pg})}{\gamma^{pg}}\varepsilon_2 + \frac{(\gamma^{pg})^2 - 1}{\gamma^{pg}}T\frac{d\varepsilon_2}{dT} + \frac{(\gamma^{pg} - 1)^2}{2\gamma^{pg}}T^2\frac{d^2\varepsilon_2}{dT^2} \tag{41}$$

In (40) ε_1 is by definition the homogeneous solution B_1 which for the monatomic case has the temperature dependence predicted for $\beta = 1$. Since ε_1 is an error term, it is considered to be small enough so that second order terms can be neglected in (41).

Consequently, ε_2 is equal to C_1 as defined above, which for the monatomic case has the temperature dependence predicted for $\beta = 2$.

6.4 Application of the method to methane

The compression factor of methane was calculated using equations (2) to (4) exactly as described in section 6.2. The initial values for this integration were chosen to be z and $(\partial z / \partial T)_p$ at 275 K, which was the lowest temperature measured. From the initial values of z along the isotherm of $T_0 = 275$ K, $(\partial z / \partial p)_T$ was calculated and then, using the experimental values of the speed of sound, $C_{p,m}$ was obtained from (2) and subsequently $C_{V,m}$ .from (4). By differentiating $C_{p,m}$ with respect to the pressure, $(\partial^2 z / \partial T^2)_p$ was obtained from equation (3).

The values of z and $(\partial z / \partial T)_p$ along the new isotherm $T_1 = T_0 + \delta T$ were initially obtained by means of a Taylor expansion about T_0 (Euler method [14]). It was found that there is some advantage in using the predictor-corrector algorithm in place of the simple Euler method. In the predictor-corrector method, one seeks to estimate $(\partial^2 z / \partial T^2)_p$, not at T_0, but midway from T_0 and T_1 before evaluating the new starting values at T_1 required for the next step. Use of this mid-point value of the second derivative reduces the truncation error of the Taylor expansion from $O(\delta T^3)$ to $O(\delta T^4)$ [14]. The method is to "predict" z and $(\partial z / \partial T)_p$ on the new isotherm at T_1 by using the simple Euler method described above, and to proceed through the next step until $(\partial^2 z / \partial T^2)_p$ has been obtained. One then estimates the mid-point second derivative as the mean of the values at T_0 and T_1 and obtains "corrected" values of z and $(\partial z / \partial T)_p$ at T_1. The method was found to be very efficient and in a numerical simulation, where all quantities (speed of sound and initial values) were calculated by the GRI equation of state for reasons of internal consistency, a step size of $10^{-3} T_c$ (here T_c is the critical temperature) was small enough for a numerical accuracy of 10^{-5} in z.

In order to implement the integration with equations (2) to (4), a table of the slow varying function $(T_0 / T)u^2(T,p)$ was compiled at the five temperatures and at 25 round values of the pressure 0.4 MPa apart. For this purpose, 3-point interpolation was used where the required value of the pressure were nominally coincident with an experimental one; otherwise the 4-point Lagrangian formula [14] was used. The numerical integration was performed along these isobars so that no further interpolation was required. For interpolation of $(T_0 / T)u^2(T,p)$ between isotherms 5-point Lagrangian formula was used. Temperature increments of 0.05 K and 0.1 K both gave identical results [15].

6.4.1 Initial values

The initial values z and $(\partial z / \partial T)_p$ were taken from the very accurate equation of Pieperbeck et al. [7]. This equation was based on IPTS-68, while the speeds of sound of the present work were measured on ITS-90. Therefore, values of $(\partial z / \partial T_{68})_p$ computed by the equation were adjust to the 1990 scale by use of the factor (dT_{90} / dT_{68}), where T_{68} and T_{90} denote temperatures measured on the 1968 and 1990 temperature scales respectively. At 275 K that correction factor is 1.00024 [16]. The difference $(T_{90} - T_{68})$ at 275 K is so small that z itself required no correction.

6.4.2 Derived properties

The results of the numerical integration of the speed of sound data, for the compressibility factor, the molar isobaric heat capacity and the molar isochoric heat capacity are presented in tables 6.1, 6.2 and 6.3 respectively.

Since the effects of changes in the speed of sound within its estimated uncertainty $\pm 0.00002\ u$, were negligible compared with the uncertainty in the initial values, the propagation of errors is attributed to the effects of the latter. The estimated largest error in the initial values of z calculated from Pieperbeck et al. is $\pm 0.00015\ z$ [7]. The corresponding largest error in $(\partial z / \partial T)_p$ is taken to be 10 times that in z itself. If the

assumption is made that the errors in the initial values increase linearly with pressure, reaching their estimated largest values at p=10 MPa, then the resulting fractional errors in the solutions of z and $C_{p,m}$ behave along the isobars of 2, 6 and 10 MPa as illustrated in figures 6.4 and 6.5 respectively.

In figure 6.6, the results derived for z are compared with the values obtained from the $p\rho T$ measurements of Pieperbeck et al. [7] and Kleinrahm et al. [8]. Those measurements were made in the same laboratory using two different magnetically coupled buoyancy balances operating at temperatures up to 323.15 K. Not surprisingly, since the initial conditions were based on fit to these results, the deviations are very small at 283.15 K (the lowest isotherm shown in figure 6.4). At higher temperatures, the direct measurements tend to be slightly greater than those obtained by the integration, but to an extent less than the estimated uncertainties.

In figure 6.7 the integration results are compared with those of Douslin et al. [6]. Except at the highest temperature, these results tend to lie somewhat below those of the present work, but in no case are the deviations worse than $\pm 0.00015\ z$; very small compared with the estimated accuracy of $\pm 0.0003\ z$ given by Douslin et al. [6].

Table 6.1. Compressibility factor $z(T,p)$ for methane

T/K	275.0	287.5	300.0	312.5	325.0	337.5	350.0	362.5	375.0
p/MPa					z				
1	0.97703	0.98038	0.98322	0.98564	0.98771	0.98949	0.99104	0.99239	0.99356
2	0.95408	0.96094	0.96670	0.97158	0.97574	0.97932	0.98240	0.98508	0.98742
3	0.93125	0.94175	0.95051	0.95789	0.96416	0.96953	0.97415	0.97815	0.98163
4	0.90868	0.92293	0.93475	0.94465	0.95303	0.96018	0.96631	0.97161	0.97620
5	0.88651	0.90461	0.91951	0.93194	0.94241	0.95131	0.95893	0.96549	0.97118
6	0.86496	0.88693	0.90491	0.91983	0.93236	0.94298	0.95204	0.95984	0.96658
7	0.84428	0.87008	0.89108	0.90843	0.92295	0.93522	0.94569	0.95466	0.96242
8	0.82476	0.85425	0.87815	0.89783	0.91425	0.92811	0.93990	0.95001	0.95872
9	0.80673	0.83965	0.86625	0.88811	0.90633	0.92167	0.93472	0.94588	0.95551
10	0.79054	0.82648	0.85553	0.87939	0.89924	0.91596	0.93016	0.94232	0.95279

Table 6.2. Molar heat capacity at constant pressure $C_{p,m}(T, p)$ for methane

T/K	275.0	287.5	300.0	312.5	325.0	337.5	350.0	362.5	375.0
p/MPa					$C_{p,m} / R$				
1.0	4.343	4.375	4.415	4.463	4.517	4.577	4.641	4.710	4.783
2.0	4.502	4.512	4.536	4.569	4.612	4.662	4.719	4.781	4.848
3.0	4.680	4.664	4.666	4.683	4.752	4.752	4.799	4.854	4.914
4.0	4.878	4.829	4.806	4.804	4.818	4.844	4.882	4.927	4.981
5.0	5.097	5.007	4.954	4.930	4.927	4.940	4.966	5.002	5.049
6.0	5.338	5.198	5.112	5.062	5.040	5.039	5.052	5.080	5.117
7.0	5.597	5.401	5.276	5.198	5.156	5.138	5.141	5.156	5.187
8.0	5.871	5.613	5.445	5.338	5.273	5.240	5.228	5.235	5.254
9.0	6.151	5.829	5.618	5.479	5.392	5.340	5.316	5.311	5.324
10.0	6.427	6.046	5.790	5.620	5.509	5.441	5.403	5.388	5.392

Table 6.3. Molar heat capacity at constant volume $C_{V,m}(T, p)$ for methane.

T/K	275.0	287.5	300.0	312.5	325.0	337.5	350.0	362.5	375.0
p/MPa	$C_{V,m} / R$								
1.0	3.225	3.269	3.321	3.378	3.440	3.507	3.577	3.651	3.729
2.0	3.250	3.291	3.339	3.394	3.454	3.519	3.589	3.662	3.738
3.0	3.276	3.313	3.358	3.410	3.468	3.531	3.600	3.672	3.748
4.0	3.303	3.335	3.376	3.426	3.482	3.544	3.610	3.681	3.757 *
5.0	3.330	3.358	3.395	3.442	3.496	3.556	3.621	3.691	3.765
6.0	3.357	3.380	3.414	3.458	3.510	3.568	3.632	3.701	3.774
7.0	3.385	3.402	3.432	3.473	3.523	3.580	3.643	3.710	3.783
8.0	3.411	3.424	3.450	3.489	3.536	3.592	3.653	3.720	3.790
9.0	3.435	3.445	3.468	3.503	3.549	3.602	3.663	3.728	3.799
10.0	3.456	3.464	3.485	3.518	3.561	3.613	3.672	3.737	3.806

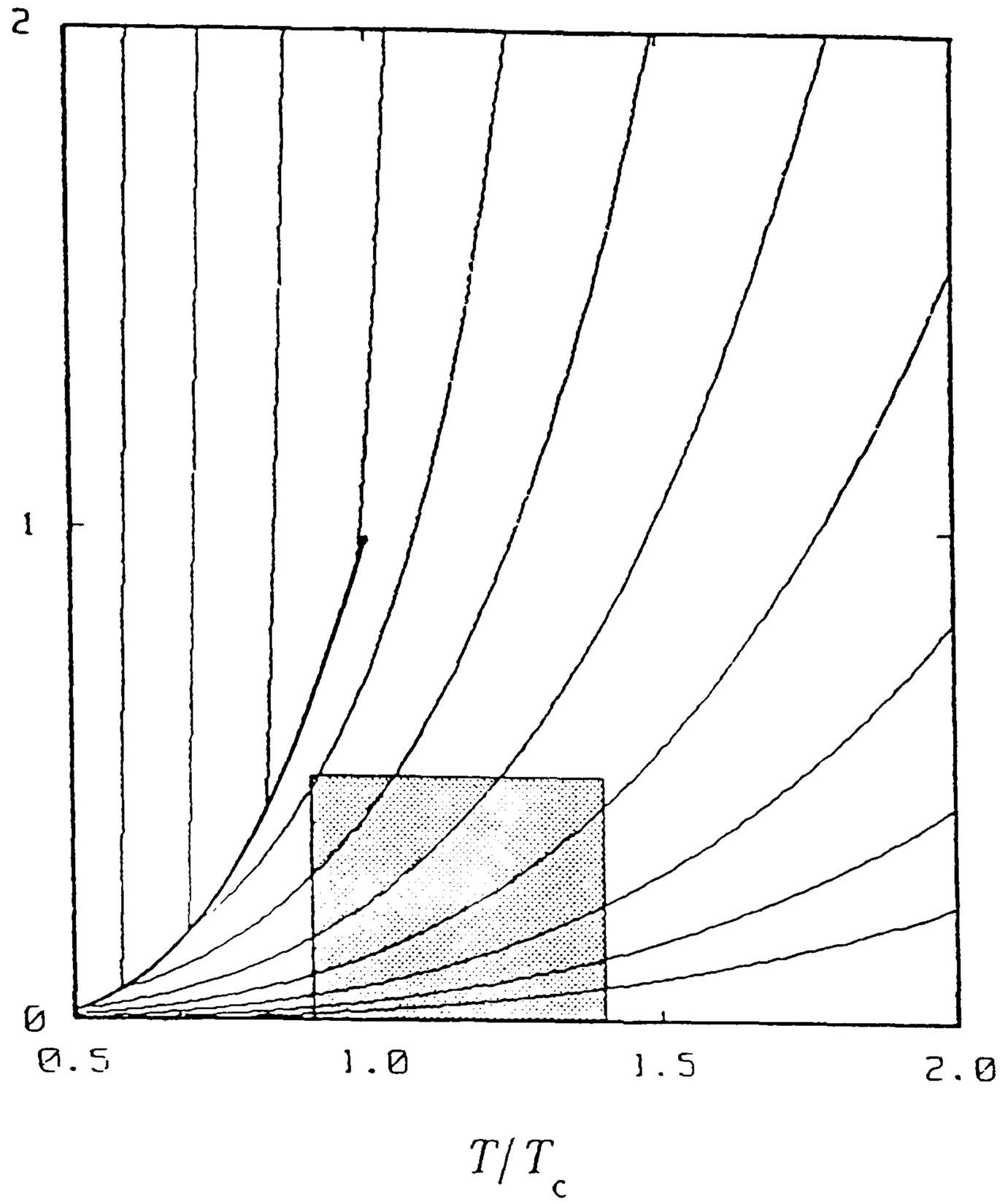

Figure 6.1. Isentropic lines calculated from van der Waals equation of state for a diatomic fluid with $\gamma^{pg} = 1.4$ and plotted as function of reduced temperature T/T_c and reduced pressure p/p_c .

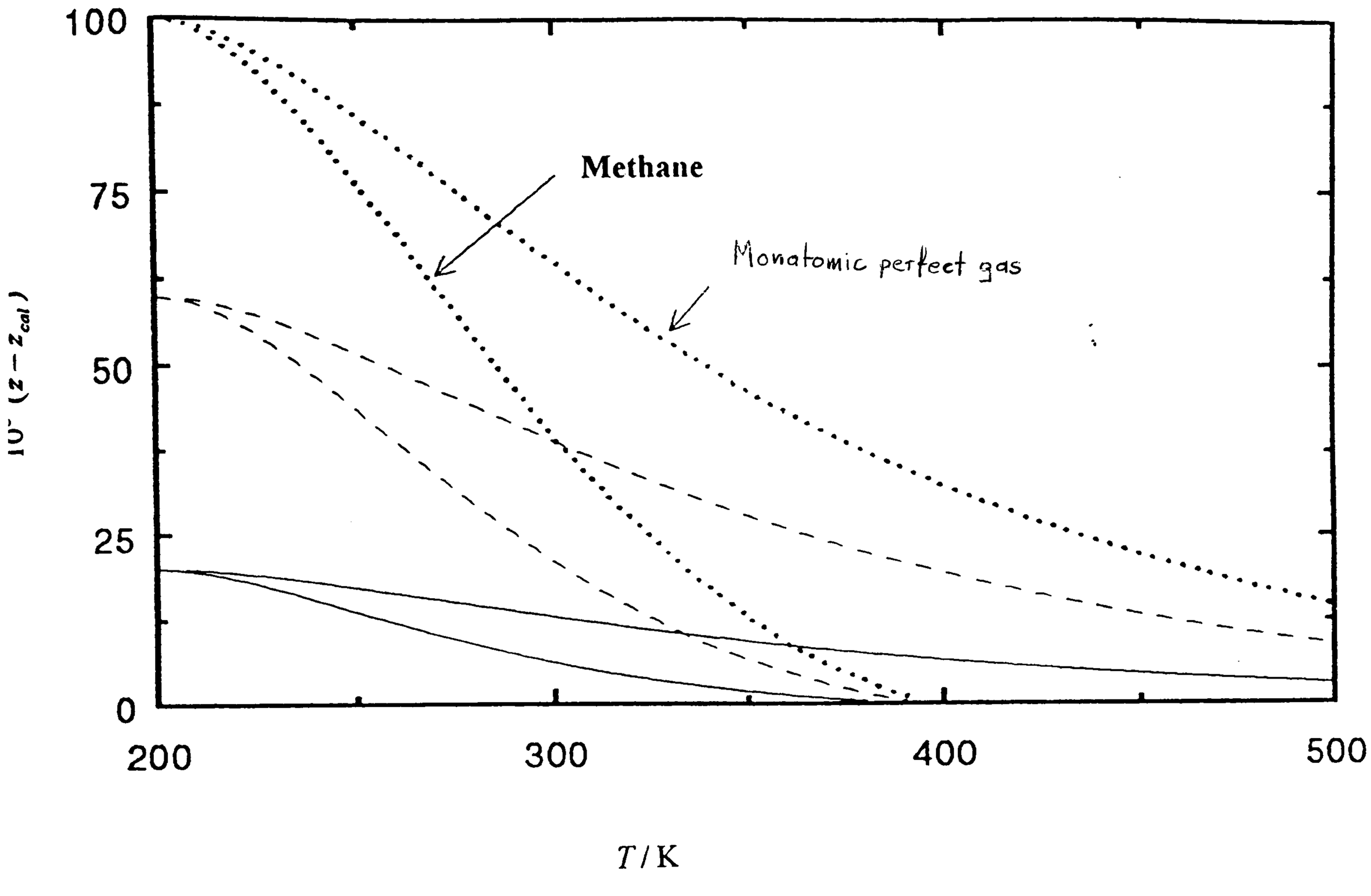

Figure 6.2. Error propagation in the compression factor $(z - z_{cal})$ when the error in the initial values of z is proportional to ρ_n, for a monatomic perfect gas and methane. ρ_n =: – , 1 mol / dm^3; ---, 3 mol / dm^3; ⋯, 5 mol / dm^3 . The numerical simulation is based on the GRI equation of state [13].

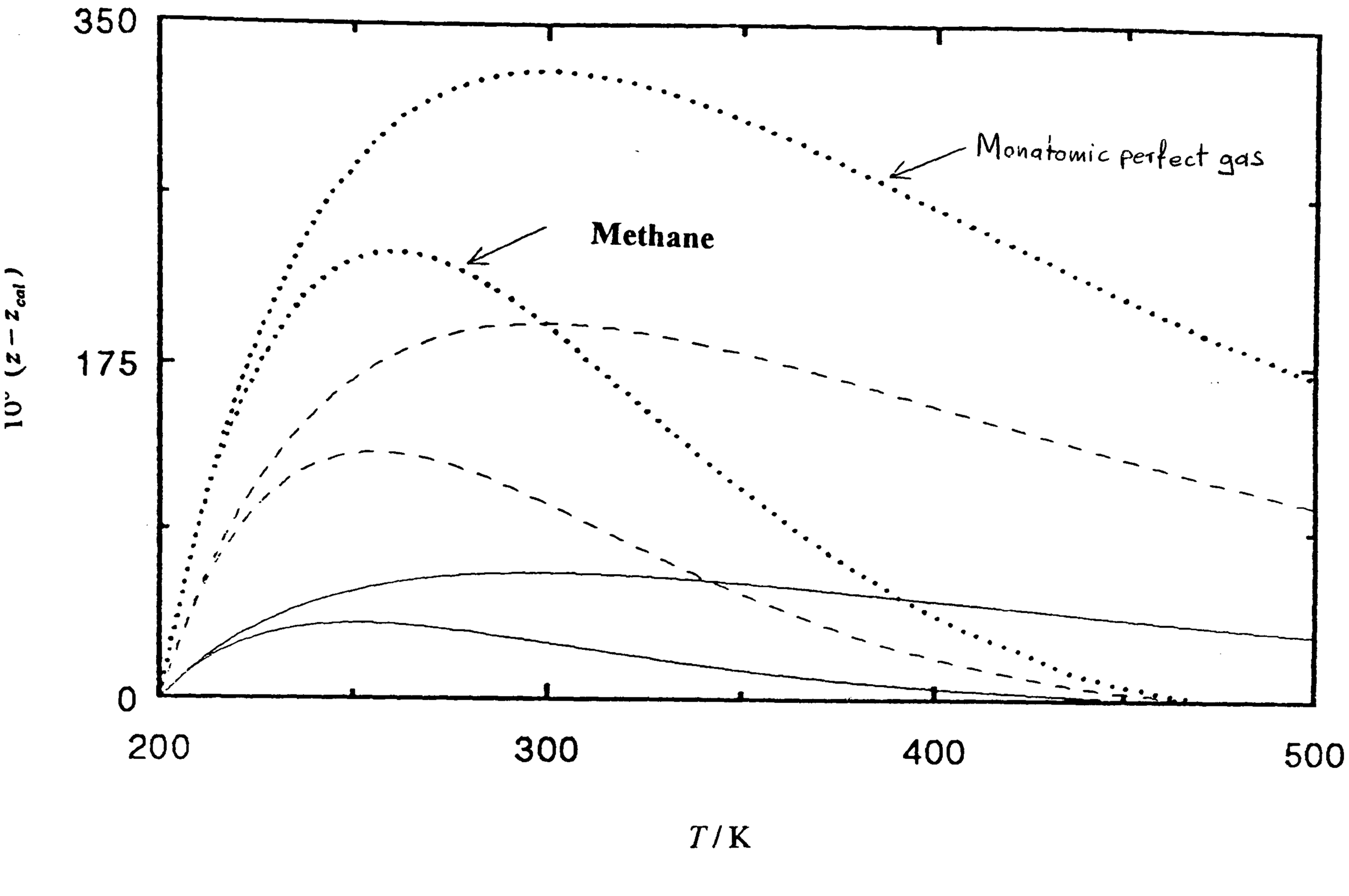

Figure 6.3. Error propagation in the compression factor $(z - z_{cal})$ when the error in the initial values of $\partial z / \partial T$ is proportional to ρ_n, for a monatomic perfect gas and methane. ρ_n =: –, 1 mol / dm^3; ---, 3 mol / dm^3; ···, 5 mol / dm^3. The numerical simulation is based on the GRI equation of state [13].

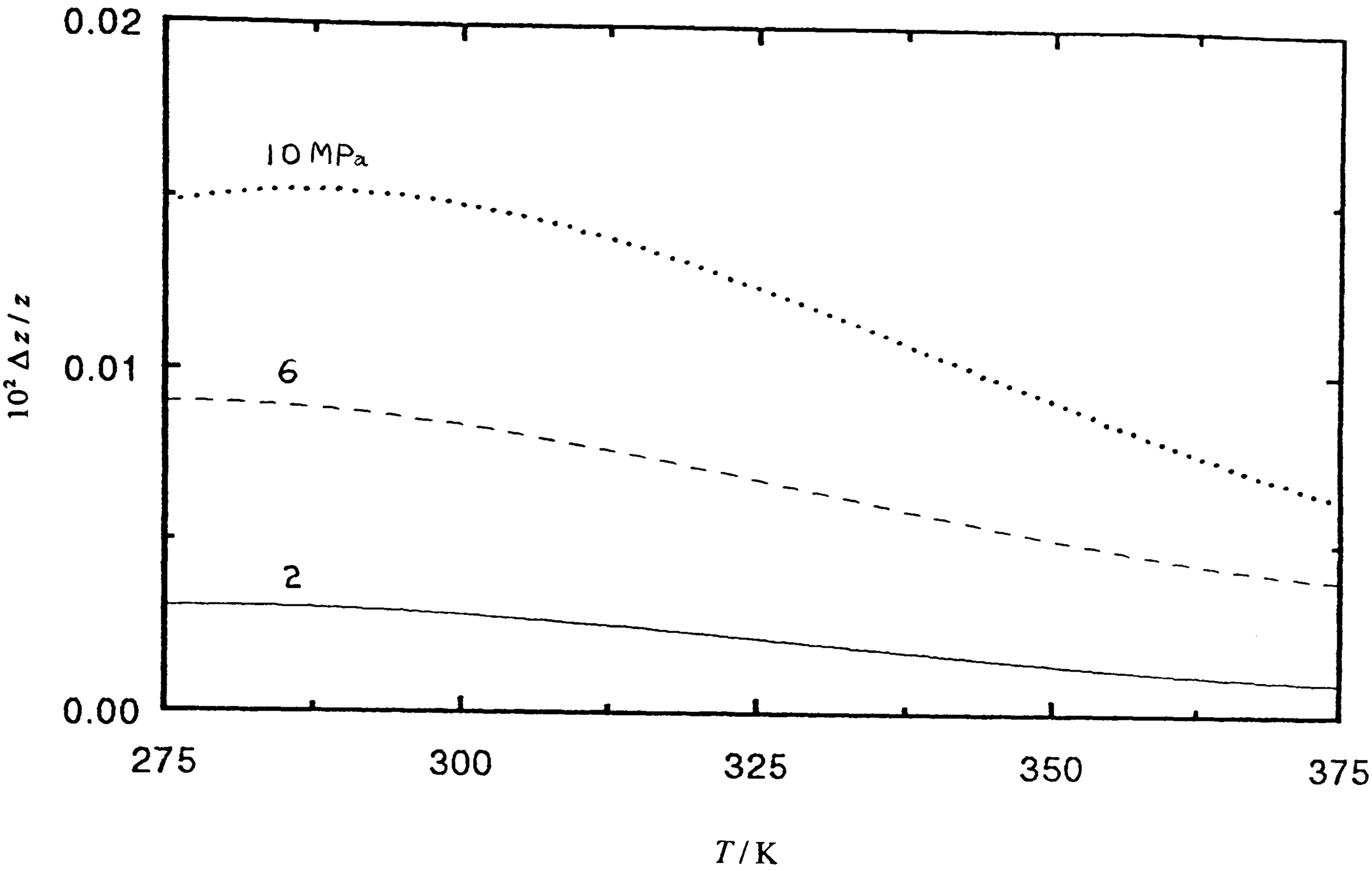

Figure 6.4. Fractional deviations $\Delta z / z$ of the compression factors z obtained by perturbation in the initial values equal to their estimated accuracy, (0.015 per cent in z and 0.15 per cent in $\partial z / \partial T$), from the unperturbed values. The numerical simulation is based on the equation of Pieperbeck et al. [7].

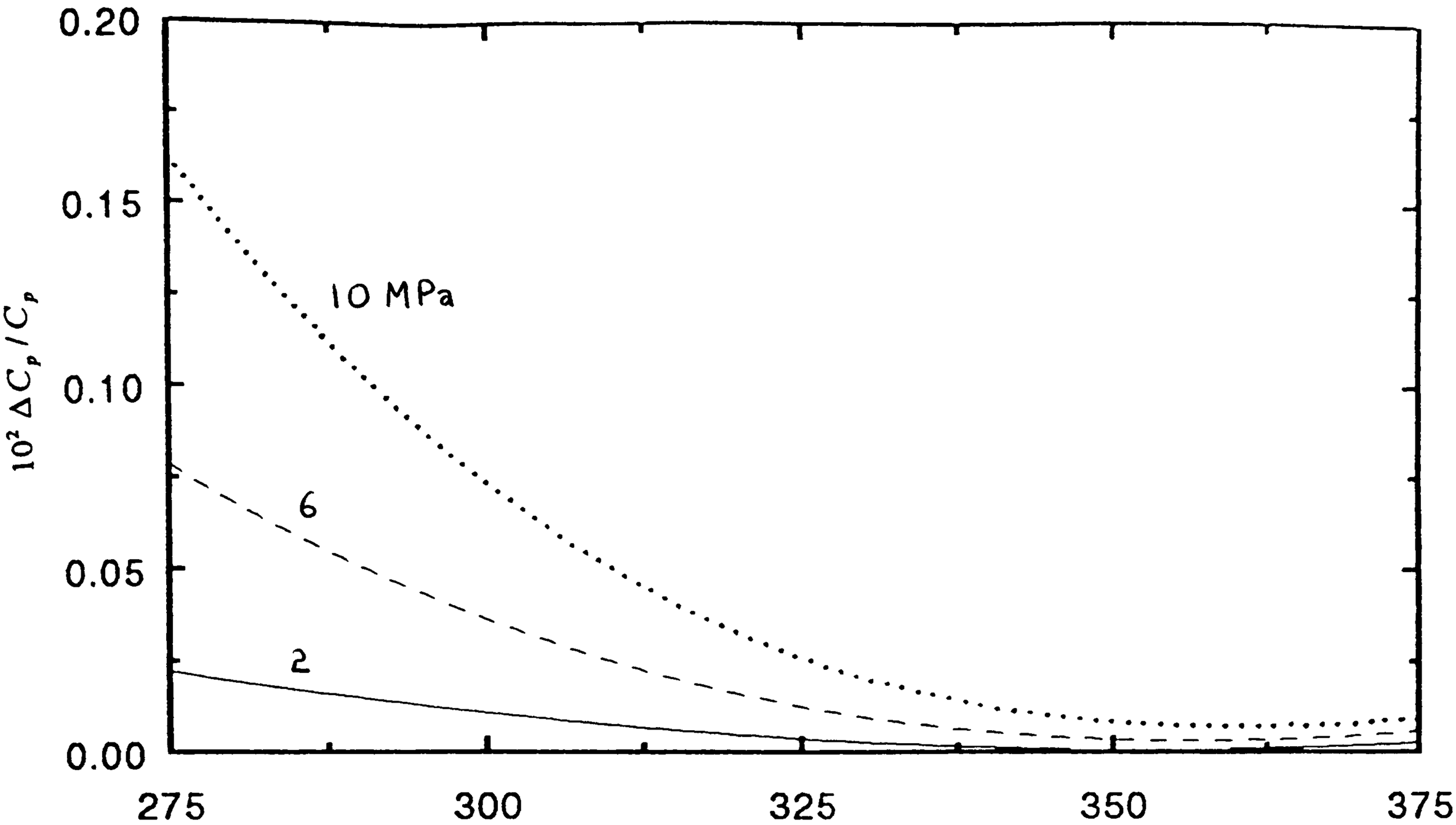

Figure 6.5. Fractional deviations $\Delta C_p / C_p$ of the isobaric heat capacity C_p obtained by perturbation in the initial values equal to their estimated accuracy, (0.015 per cent in z and 0.15 per cent in $\partial z / \partial T$), from the unperturbed values. The numerical simulation is based on the equation of Pieperbeck et al. [7].

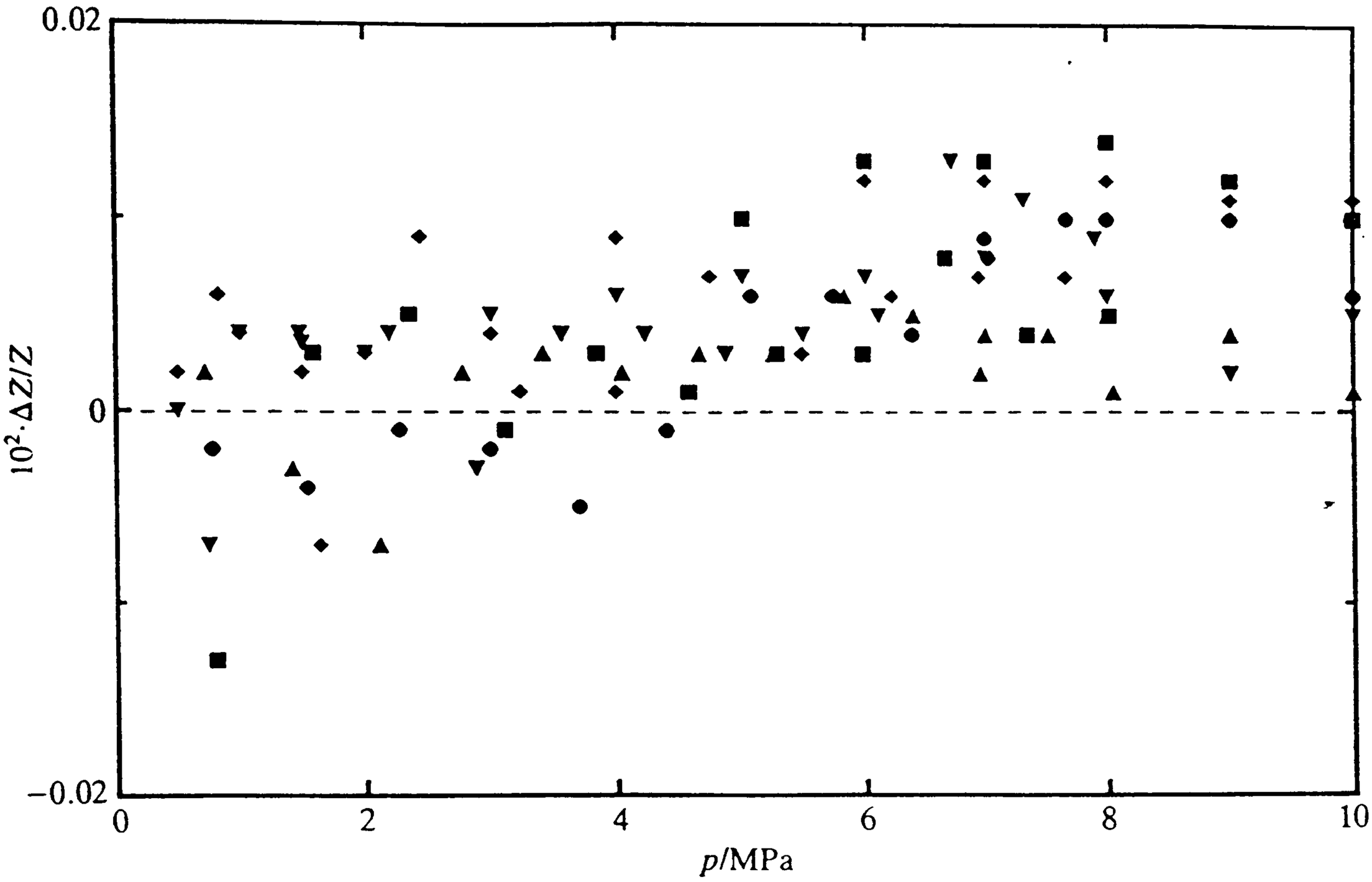

Figure 6.6. Fractional deviations $\Delta z / z$ of the compression factors z reported by Pieperbeck et al. [7] and Kleinrahm et al [8] from the present results.

$T =$: ▲, 283 K; ▼, 293 K; ●, 303 K; ■, 313 K; ◆, 323 K.

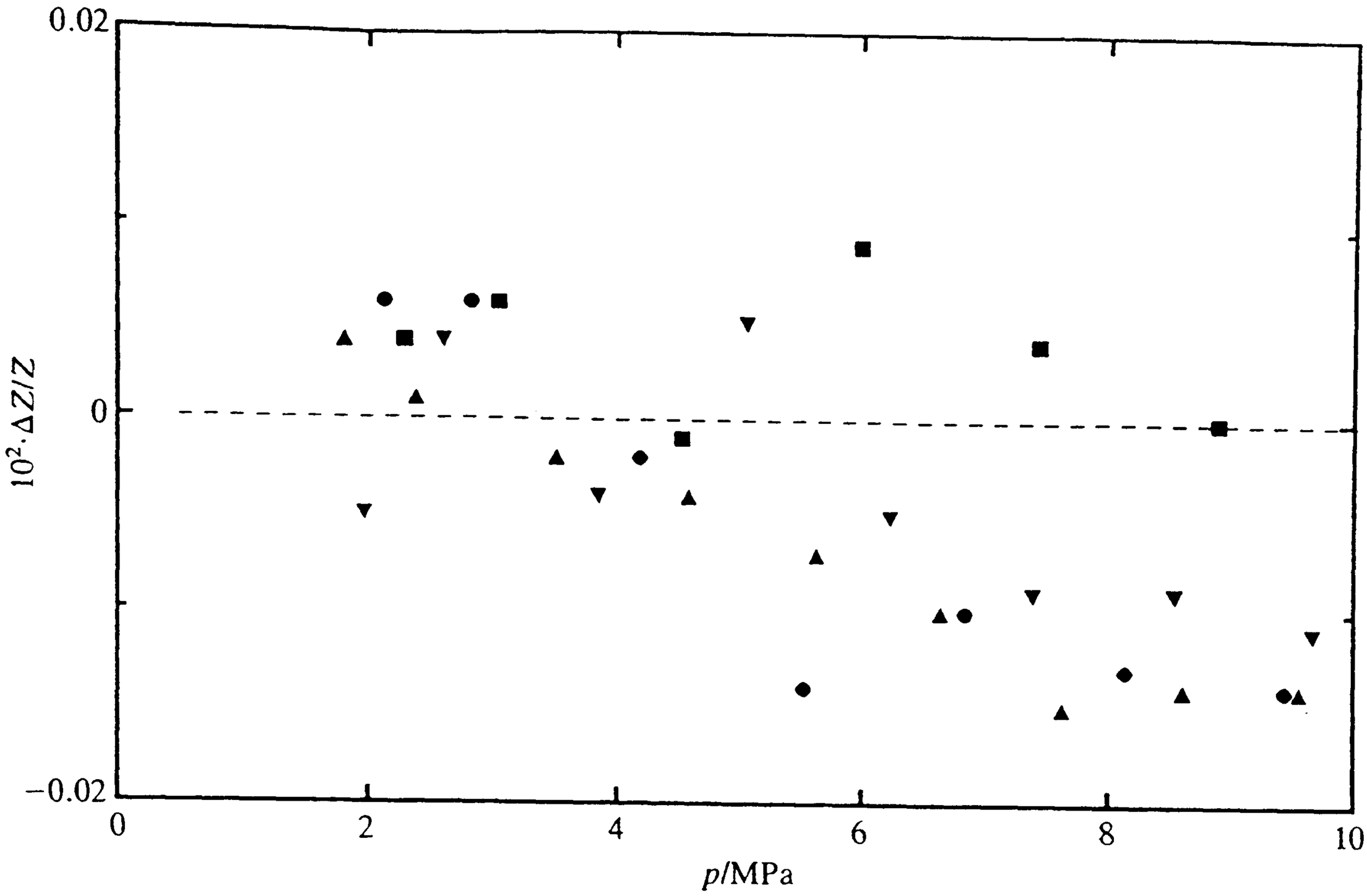

Figure 6.7. Fractional deviations $\Delta z / z$ of the compression factors z reported by Douslin et al. [6] from the present results. $T =$: ▲, 298 K; ▼, 323 K; ●, 348 K; ■, 373 K.

6.5 References

[1] E. H. Amagat, C. R. Acad. Sci. Paris **103**, 429 (1886).

[2] E. S. J. Burnett, J. Appl. Mech. A **136**, 3 (1936).

[3] W. Warowny, P. Wiepolski and J. Stecki, Physica A **91**, 73 (1978).

[4] J. Mollerup, J. Chem. Thermodyn. **17**, 489 (1985).

[5] A. E. Hoover, I. Nagata, T. W. Leland Jr., and R. Kobayashi, J. Chem. Phys. **48**, 2633 (1968).

[6] D. R. Douslin, R. H. Harrison, R. T. Moore and J. P. McCullough, J. Chem. Engng Data **9**, 358 (1964).

[7] N. Pieperbeck, R. Kleinrahm, R. Wagner and M. Jaeschke, J. Chem. Thermodyn. **23**, 175 (1991).

[8] R. Kleinrahm, W. Duschek, W. Wagner and M. Jaeschke, J. Chem. Thermodyn. **20**, 621 (1988).

[9] R. Kleinrahm and W. Wagner, J. Chem. Thermodyn. **18**, 739 (1986).

[10] T. K. Bose and J. M. St-Arnaud, H. J. Achtermann and R. Scharf, Rev. Sci. Instrum. **57**, 26 (1986).

[11] J. P. M. Trusler, *Physical Acoustics and Metrology of Fluids* (Adam Hilger, Bristol, 1991), p. 76.

[12] R. Aris and N. R. Amundson, *Mathematical Methods in Chemical Engineering* (Prentice-Hall, New Jersey, 1973).

[13] K. E. Starling, M. Mannan, J. L. Savidge, S. Sadasivan, T. B. Jr. Reid, K. Gangadhar and M. A. Drass, *Development of an equation of state for computation of supercompressibility factors, critical flow factor and other properties of wet sour natural gases, synthetic gas and admixtures* (Final Report 1987, Gas Research Institute (GRI), Chicago, U.S.A. 1987).

[14] C. F. Gerald and P. O. Wheatley, *Applied Numerical Analysis* (Addison-Wesley, New York, 1989).

[15] J. P. M. Trusler and M. Zarari, J. Chem. Thermodyn. **24**, 973 (1992).

[16] C. A. ten Seldam and S. N. Biswas, J. Chem. Phys. **94**, 2130 (1991).

CHAPTER 7

INTERMOLECULAR FORCES FROM THE SPEED OF SOUND

7.1 Introduction.

In this chapter we present, for first time, a new method by means of which very good approximations to the true intermolecular pair-potential can be obtained. It is shown that the potentials of spherical substances can be derived using only accurate values of the second and third acoustic virial coefficients of a gas such as these reported in chapter 5. This method is based on fitting simultaneously the second and third acoustic virial coefficients to a chosen potential model such as that of Maitland-Smith [1]. It is found that the potential which best represents both the second and third acoustic virial coefficients, also represents very satisfactorily the second and third volumetric virial coefficients and independently, the viscosity of the dilute gas.

An essential step in the implementation of this method is the calculation of the third acoustic virial coefficients. These coefficients, as shown in chapter 2, are related to the second and third volumetric virial coefficients through ordinary differential equations, with temperature as the independent variable. The expressions given in chapter 2 for the third volumetric or acoustic virial coefficients make it clear that these quantities depend not only upon the pair-potential but also upon a non-additive three-body potential. The calculation of the third virial coefficients therefore involves two steps. First, an assumption must be made about the non-pairwise-additive term of the potential when three molecules interact. Secondly, multiple (three-fold) integration, over all possible separations between the three interacting molecules must be performed.

The problem generated by the requirement for multiple integration was solved by using Gaussian quadrature [2], in place of the more commonly employed Simpson's rule

[3,4-6]. The technique adopted proved very much faster than the use of Simpson's rule and rendered routine evaluations of the third virial coefficients tractable. The most important step was the assumption about the non-additive term of the three-body potential. It is known for the case of argon [7] that the dominant contribution to the non-pairwise additive part of the three-body potential is the Axilrod-Teller triple-dipole term, presented in chapter 2. The conclusion about the dominance of this particular term in the three-body energy has relied upon measurements of third volumetric virial coefficients [7]. New experimental data [8] on the third acoustic virial coefficients provide a means of conducting a very much more severe test of the adequacy of the Axilrod-Teller triple-dipole term in repredicting the non-additivity of three-body potentials. It will be shown that the Axilrod-Teller term does indeed provide an excellent description of the third acoustic virial coefficients of argon when used in conjunction with the best available pair-potential for the same substance. The success of the Axilrod-Teller triple-dipole term for argon encourages the belief that the same term will be adequate for the description of non-additive three-body forces in other molecular systems. Adoption of this hypothesis allows us to develop the method by which second and third acoustic virial coefficients for a number of gases and gas mixtures can be used to elucidate the pair-potentials for a number of systems.

In order to demonstrate the viability of the proposed technique it has been first applied to argon. That is, simply from the experimental measurements of the second and third acoustic virial coefficients of argon we have derived an intermolecular pair-potential over a limited range of separations. The potential derived is consistent with the best available pair-potential for argon. Subsequently, the same technique has been applied to pure methane, which can be quite realistically treated as a spherical molecule.

For interactions that are not spherically symmetric it is strictly necessary to consider the orientation dependence of the potential as discussed in chapter 2. In this work, which is mainly concerned with the development of methodology, we consider

instead the elucidation of effective spherical potentials for moderately anisotropic systems. However, the basis will be laid for future work making use of non-spherical potential models and, importantly, it will be demonstrated that effective potentials can be found from acoustic measurements, which enable the accurate calculation of several gaseous properties such as the second and third volumetric virial coefficients and the dilute gas viscosity. The latter point is significant because it permits evaluation of quantities not always accessible to direct measurement.

Included in the systems studied by this technique are nitrogen-nitrogen and argon-nitrogen. By an appropriate adaptation of the method developed to the latter case it has been possible for the first time to derive interaction third volumetric virial coefficients over a wide range of temperatures.

In the following sections the development of the methodology is presented together with the treatment and results for each individual system.

7.2 Method of analysis

In this analysis the pure substances argon, methane and nitrogen and the mixture of argon-nitrogen were studied.

The potential model chosen for the analysis is that of Maitland and Smith [1]

$$U(r) = \frac{\varepsilon}{n-6}[6(r_m / r)^n - n\,(r_m / r)^6] \qquad (1)$$

with

$$n = m + \gamma\,(r / r_m - 1) \qquad (2)$$

where ε is the potential well depth, r_m is the separation at which the potential attains its minimum value, $-\varepsilon$, and m and γ are two shape parameters. This potential was chosen for its simplicity and simultaneously for its flexibility (by having four disposable parameters). As the test with argon shows this potential model is capable of reproducing very satisfactorily the well region of the potential on which the second and third acoustic

virial coefficients are found to depend. The simpler Lennard-Jones $(n,6)$ potential model [9], to which the Maitland-Smith potential is reduced for $\gamma = 0$, was found inappropriate for the analysis of argon.

The method begins by fitting the second acoustic virial coefficients β_a to several M-S potential models, with different values for the shape parameters γ and m. The fit yields the values of the scaling parameters of each potential model, ε and r_m .

Next, the third acoustic virial coefficients γ_a are calculated for each of the M-S $(\gamma - m)$ potentials that β_a were fitted to and then the calculated values are compared with the experimental ones. It is found for all substances studied that there is a certain set of $(\gamma - m)$ values for which both second and third acoustic virial coefficients are best represented. It is also found that this minimum coincides with the overall minimum of the standard deviations for each acoustic virial coefficient.

The M-S $(\gamma - m)$ potential which corresponds to the minimum standard deviation was employed for the calculation of other properties, those being the second B and third C volumetric virial coefficients and the viscosity.

The excellent agreement of the calculated properties with the experimental ones is a strong argument in support of the statement that the simultaneous fit of the second and third acoustic virial coefficients yields a good effective spherical potential.

7.2.1 Fitting of the second acoustic virial coefficients

As it is shown in chapter 2 the second acoustic virial coefficient β_a is given by:

$$\beta_a = 2B + 2(\gamma^{pg} - 1)T\frac{dB}{dT} + \frac{(\gamma^{pg} - 1)^2}{\gamma^{pg}}T^2\frac{d^2B}{dT^2} \qquad (3)$$

where T is the temperature and γ^{pg} is the perfect gas heat capacity ratio. The second volumetric virial coefficient B is given in terms of a spherical intermolecular pair-potential as follows:

$$B = 2\pi N_0 \int_0^\infty [1 - \exp(-U_{12}/kT)] r_{12}^2 dr_{12} \qquad (4)$$

where N_0 is the Avogadro constant and, U_{12} and r_{12} are the intermolecular pair-potential and the distance between molecules 1 and 2.

The derivatives dB / dT and d^2B / dT^2 were calculated by differentiating equation (4) with respect to the temperature, in order to obtain from (3) the expression of β_a in terms of the potential U_{12} :

$$\beta_a = 2\pi N_0 \int_0^\infty \{1-[1+(P_a-2Q_a)(U_{12}/kT)+Q_a(U_{12}/kT)^2]\exp(-U_{12}/kT)\} r_{12}^2 dr_{12} \quad (5)$$

where $P_a = (\gamma^{pg}-1)$ and $Q_a = (\gamma^{pg}-1)^2 / 2\gamma^{pg}$. The integral in equation (5) was being evaluated using a simple Simpson method [9]. The integration region $0 \le r_{12} \le \infty$ was reduced to $r_{min} \le r_{12} \le r_{max}$. The contribution to the integral for $r_{12} < r_{min}$, was calculated analytically assuming $U_{12}(r_{12}) = \infty$ and found to be $2\pi N_0 r_{min}^3 / 3$. For $r_{12} > r_{max}$ the potential $U_{12}(r_{12})$ is given approximately by the dispersion contribution, $-C_6 / r_{12}^6$, where C_6 is the two-body dispersion energy coefficient. Since C_6 is not known, in the general case, it has been approximated by a Taylor expansion about $C_{6,1} = -r_1^6 U(r_1)$:

$$C_6(r_{12}) = C_{6,1} + (r_{12}-r_1)\frac{C_{6,2}-C_{6,1}}{r_2-r_1} \quad (6)$$

where $r_1 = r_{max}$, $r_2 = 1.1 r_1$ and $C_{6,2} = -r_2^6 U(r_2)$. The integration limits were held constant for all substances studied to the values $r_{min} = 0.5\sigma$ and $r_{max} = 15\sigma$. Larger values for r_{min} and smaller values for r_{max} which were also tested yield the same results.

The experimental values of β_a were fitted (non-linear regression analysis [9]) in terms of equation (5) using potentials from the Maitland-Smith [1] family with different values of γ and m (these values were kept fixed for each fit) and values of the scaling parameters ε and r_m were obtained for each potential of the M-S family.

The M-S $(\gamma - m)$ potential functions obtained in this manner, were employed for the calculation of the third acoustic virial coefficients as is described in the following.

7.2.2 Calculation of the third acoustic virial coefficients

In this section, the integration method is presented which was used in the calculation of the third virial coefficient C and its derivatives with respect to the temperature, dC/dT and d^2C/dT^2, from a spherical potential function, in order to obtain the third acoustic virial coefficient γ_a.

As already discussed in chapter 2, the expression which yields the third volumetric virial coefficient in terms of a spherical intermolecular pair-potential is:

$$C = C^{add} + \Delta C \tag{7}$$

with

$$C^{add} = -\frac{8\pi^2 N_0^{\,2}}{3}\iiint[1-\exp(-U_{12}/kT)][1-\exp(-U_{13}/kT)] \times[1-\exp(-U_{23}/kT)]r_{12}r_{13}r_{23}dr_{12}dr_{13}dr_{23} \tag{8}$$

and

$$\Delta C = -\frac{8\pi^2 N_0^{\,2}}{3}\iiint\exp[-(U_{12}+U_{13}+U_{23})/kT] \times[\exp(-\Delta U/kT)-1]r_{12}r_{13}r_{23}dr_{12}dr_{13}dr_{23} \tag{9}$$

where U_{ij} and r_{ij} are the pair potential and the separation between molecules i and j respectively and ΔU is the non additive term of the potential discussed previously in chapter 2. The formula for ΔU employed for these calculations is presented in the next section.

The third volumetric virial coefficient C was differentiated analytically with respect to the temperature, to yield dC/dT and d^2C/dT^2, which were required for the calculation of the third acoustic virial coefficient γ_a from the following expression (see chapter 2):

$$\gamma_a = \frac{(\gamma^{pg}-1)}{\gamma^{pg}}\left[B+(2\gamma^{pg}-1)T\frac{dB}{dT}+(\gamma^{pg}-1)T^2\frac{d^2B}{dT^2}\right]^2 + \frac{(1+2\gamma^{pg})}{\gamma^{pg}}C+\frac{(\gamma^{pg})^2-1}{\gamma^{pg}}T\frac{dC}{dT}+\frac{(\gamma^{pg}-1)^2}{2\gamma^{pg}}T^2\frac{d^2C}{dT^2} \tag{10}$$

The region of integration in equations (8) and (9) includes all the values of the r_{ij} which form a triangle, and thus the three-fold integral appearing in (8) and (9) is equivalent to:

$$\int_0^{\infty}\int_0^{\infty}\int_{|r_{12}-r_{13}|}^{r_{12}+r_{13}} \tag{11}$$

By holding $r_{23} \geq r_{13} \geq r_{12}$ we can reduce the integration region to one sixth. The new integration limits may be understood by inspection of figure 7.1 [3], where the variables of the integration r_{ij} have been changed to:

$$r_1 = r_{23}$$

$$y = r_{13} / r_{23} \tag{12}$$

$$x = r_{12} / r_{23}$$

with $x \leq y \leq 1$.

Employing this new set variables the integral in equations (8) and (9) can be thus written as

$$\int_0^{\infty}\int_0^{\infty}\int_{|r_{12}-r_{13}|}^{r_{12}+r_{13}} = 6\int_0^{\infty}\int_{0.5}^{1}\int_{1-y}^{y} \tag{13}$$

For the numerical implementation of the integration, we kept $r_{\text{core}} \leq r_1 \leq r_{\max}$ and calculated analytically the contribution of the core (i.e. for $r_1 < r_{\text{core}}$) by taking $U_{23}(r_1) = U_{13}(yr_1) = U_{12}(xr_1) = \infty$. Thus the integral in the right part of equation (13) was substituted by:

$$6\int_0^{\infty}\int_{0.5}^{1}\int_{1-y}^{y} = 6\int_{r_{core}}^{r_{max}}\int_{0.5}^{1}\int_{1-y}^{y} + (\text{core contribution}) \tag{14}$$

For C_{add} this contribution was found:

$$C_{core} = 6\frac{8\pi^2 N_0^2}{3}\int_0^{r_{core}}\int_{0.5}^{1}\int_{1-y}^{y} r_{12}r_{13}r_{23}dr_{12}dr_{13}dr_{23} = 6\frac{8\pi^2 N_0^2}{3}\frac{(r_{core})^6}{6}\frac{5}{48} \tag{15}$$

while for ΔC and for the derivatives of C_{add} or ΔC with respect to the temperature the 'core contribution' was found to be zero.

The three-fold integration involved in the calculation of C and its derivatives with respect to the temperature, was performed using Gaussian quadrature [2]. In the

integration, r_{core} and r_{max} were chosen from $0.5\sigma < r_{core} < 0.9\sigma$ and $3\sigma < r_{max} < 5\sigma$, depending each time on the substance under study. The adequacy of the particular values chosen was checked by repeating the integration employing a smaller value for r_{core} and a larger value for r_{max},, and independently, more Gaussian quadrature points. The convergence of the integration, was checked by performing the integration in the same integration limit but with a larger (or smaller) number of quadrature points. For example for methane r_{core} was chosen 0.3 nm ($\approx 0.8\sigma$) and r_{max} 1.4 nm ($\approx 4\sigma$). For this integration range a grid of 100-10-10 points quadrature yield the same result with a grid of less points, 80-10-10, or more points, 120-20-20, a fact which verified the convergence. For the same number of quadrature points integration in the range 0.25 nm to 1.65 nm yield exactly the same result, a fact which verified the adequacy of the integration range. For all substances a quadrature of 100-10-10 points was found more than adequate. The integration time for the calculation of the additive and non-additive part of C, dC / dT and d^2C / dT^2, for 100-10-10 points was less than 10 seconds per isotherm. The same integration using Simpson's rule required about 30 minutes per isotherm to achieve the same accuracy.

As mentioned before, the values of C, dC / dT and d^2C / dT^2 were used to obtain γ_a from equation (10). These values of γ_a were compared with the experimental ones, and that M-S $(\gamma - m)$ potential was chosen which simultaneously represents best the experimental β_a and γ_a data.

7.2.3 Approximations to ΔU

In the present calculations the non-additive part of the potential of three interacting molecules ΔU, was approximated by the Axilrod-teller triple-dipole term. This term, previously discussed in chapter 2, constitutes the leading correction term to the dispersion

energy arising from the three atom interaction. In the present case this term was applied to three molecule spherically symmetric interaction:

$$\Delta U = \nu_{123}(r_{12}r_{13}r_{23})^{-3}(1 + 3\cos\theta_1\cos\theta_2\cos\theta_3) \quad (16)$$

using for ν_{123} the Midzuno-Kihara formula [10],

$$\nu_{123} = \frac{3}{4}\alpha C_6 \quad (17)$$

where r_{ij} is the distance between molecules i and j, θ_i are the interior angles of the three body triangle, α is the zero frequency polarizability of the molecule assumed to be spherically symmetric, and C_6 is the two-body dispersion energy coefficient. For the case of non-alike interactions ν_{123} was approximated by [11]:

$$\nu_{123} = 2S_1S_2S_3\frac{S_1 + S_2 + S_3}{(S_1 + S_2)(S_1 + S_3)(S_2 + S_3)} \quad (18)$$

with $S_1 = C_{6,11}\alpha_2\alpha_3 / \alpha_1$ and similar expressions for S_2 and S_3, where α_i and $C_{6,ii}$ are the zero frequency polarizability and the two-body dispersion energy coefficient of substance i respectively. This formula has been tested for the case of neon-helium interactions and was found very accurate [12]. However, for the case of polyatomic molecules (our case), it remains an approximation.

The two-body dispersion energy coefficient C_6 appearing in equations (17) and (18) is not generally known. In the present calculations this coefficient was approximated by the ratio $-U_{a,ij}(r_{ij}) / r_{ij}^{-6}$, where $U_{a,ij}$ is the part of the potential model which represents molecular attraction. The same approximation has been used by Sherwood and Prausnitz [8], in their calculation of third volumetric virial coefficients. In the following chapter the above approximations are tested with argon.

7.2.4 Test of the Axilrod-Teller term using third acoustic virial coefficients

Third acoustic virial coefficients determined from extremely accurate speed of sound measurements provide the means of more severe test of the adequacy of the

Axilrod-Teller term in describing the three-body interactions, provided they are used in conjunction with an equivalently accurate pair-potential.

This test is performed here for argon using the very accurate third acoustic virial coefficient data [8] and the best available intermolecular pair-potential [13]. The zero frequency polarizability α was taken from [7].

The calculated values for this potential employing the Axilrod-Teller triple-dipole term to represent the non-additive part of the three body potential are shown in table 7.1. Figure 7.2 illustrates how successfully the experimental values of γ_a were represented. In figure 7.3 the third volumetric virial coefficients are presented together with experimental values taken from Dymond and Smith [14]. In both cases the agreement is well within experimental accuracy.

The dashed lines in figures 7.2 and 7.3 are the values for γ_a and C respectively, calculated using the approximation for the two-body dispersion energy coefficient, C_6. It can be seen that the agreement at the higher temperatures is well within experimental accuracy, while at lower temperatures it tends to deviate from the experimental values. The reason for this is that at the very low temperatures the contribution of the non-pairwise additive term of the potential to the third volumetric virial coefficient and accordingly to the third acoustic virial coefficient becomes enormous. Thus, small errors in the calculation of this term arising from the approximation to C_6 result in a significant error in C and hence γ_a. For example, at 90.06 K the non-additive contribution to C, $\Delta C = C - C_{add}$, is 4000 cm^6 / mol^2 when C is -6000 cm^6 / mol^2, while at 189.98 K it is 400 cm^6 / mol^2, C being 1700 cm^6 / mol^2. We see that even at the higher temperatures the contribution of the non-additive contribution is very significant, a fact which leads to the conclusion that the non-additive term of the potential cannot be ignored. Because of the error occuring from the approximation of C_6 at the very low temperatures, in the application of the proposed method of analysis, the experimental values of γ_a at the

lowest temperatures are given a larger uncertainty which results in a smaller weight in the fitting procedure.

7.3 Application of the method to pure substances

7.3.1 Argon

In this section the proposed method of analysis is applied to argon in order to obtain the $(\gamma - m)$ M-S potential which best represents its second and third acoustic virial coefficients. The second and third acoustic virial coefficients used for the potential analysis were taken from the data of Ewing and Trusler [8].

Based on the proposed method, the experimental β_a values were fitted in terms of M-S $(\gamma - m)$ potentials, to yield the scaling parameters ε and r_m for each potential. Subsequently, the third acoustic virial coefficients were calculated for each of these M-S $(\gamma - m)$ potentials. The standard deviations of β_a and γ_a values calculated for M - S potentials with different values of m and γ are illustrated in figures 7.4 and 7.5 respectively. It can be easily seen that both standard deviations of β_a and γ_a have a minimum for the M-S potential with $m = 14.5$ and $\gamma = 5$. At this minimum the standard deviation of β_a is only 0.20 cm^3 / mol and that of γ_a, 500 cm^6 / mol^2, which for both cases is very close to the average reported uncertainty of the coefficients, 0.10 and 300 respectively [8]. Because of the error arising from the C_6 approximation at the very low temperatures, when fitting γ_a the experimental values at the two lower temperatures were given an uncertainty of 3000 and 1500 cm^6 / mol^2, for the values of -15800 and -5400 cm^6 / mol^2 respectively, which resulted in a significant reduction of their weight, weight $= 1 / (\text{uncertainty})^2$, in the fitting.

Next, the chosen potential, M-S (5-14.5) was employed for the calculation of the second and third volumetric virial coefficients and, independently, the viscosity of the

dilute gas, η. The scaling parameters of the potential M-S (5-14.5) were found $r_m = 0.3683$ nm and $\varepsilon / k = 145.37$ K.

Figure 7.6 illustrates the deviations of the calculated values of B from those proposed by Dymond and Smith [14]. At the low temperatures the calculated values are found to be a little more positive than the reported experimental ones by an amount of about twice the uncertainty of the latter. At the temperatures 150 to 1000 K the agreement was excellent.

In figure 7.7 the calculated values of the third volumetric virial coefficients are presented together with experimental points over a wide range of temperatures. In the temperature range 140 to 400 K the agreement of the calculated with the experimental values was well within the estimated uncertainty of the latter. The calculated B and C are shown in tables 7.2 and 7.3 respectively.

Finally, the percentage deviation of the viscosity calculated from M-S (5-14.5) from accurate experimental values is plotted in figure 7.8. Throughout the temperature range 120 to 1600 K the viscosity was represented within an error of less than ± 1 per cent, except at the very low temperatures where the error reached up to 2.3 per cent. In the temperature range 400 to 1600 K the error in the viscosity calculation was always less than ± 0.5 per cent. Since, as discussed in chapter 2, the viscosity and the second volumetric virial coefficients depend on different parts of the potential for the same temperature range, the so good representation of the viscosity obtained by the potential chosen is a strong indication that our potential is close to the true one.

7.3.2 Methane

In the following, the method was applied to methane. In the analysis of methane the experimental acoustic virial coefficients were taken from the values reported in chapter 5. Accordingly, the experimental β_a values were fitted in terms of M-S $(\gamma - m)$ potentials, to yield the scaling parameters ε and r_m for each potential. Subsequently, the

third acoustic virial coefficients were calculated for each potential. The standard deviations of the second and third acoustic virial coefficients calculated for these potentials from the corresponding experimental values are plotted in figures 7.9 and 7.10. The standard deviations of β_a and γ_a are both minimized for $m = 19$ and $\gamma = 0$. The minimum corresponds to a standard deviation of β_a of only $0.11\ \mathrm{cm}^3/\mathrm{mol}$ and a standard deviation of γ_a of just $150\ \mathrm{cm}^6/\mathrm{mol}^2$. Both standard deviations are very small compared with the reported uncertainty of the acoustic virial coefficients. For this potential which has scaling parameters $r_m = 0.3953$ and $\varepsilon/k = 204.50\ \mathrm{K}$, we calculated the second and third volumetric virial coefficients and the viscosity.

Figure 7.11 illustrates the deviation of the calculated values of B from the values proposed in [14]. The agreement is excellent throughout the temperature range. In fact at all temperatures the deviations of the calculated B from the experimental ones were less than half the uncertainty of the latter.

In figure 7.12 the values of the third volumetric virial coefficients calculated are presented together with experimental data. The agreement is very satisfactory at all temperatures. Especially at temperatures higher than 273.15 the agreement with Douslin's data [23] is excellent. In tables 7.4 and 7.5 we present the values of B and C calculated from the potential M-S (0-19).

In figure 7.13 the percentage deviation of the calculated viscosity is plotted against the temperature. The error was found to vary from -1 per cent at 120 K to -2.5 per cent at 500 K. The potential obtained from the fit to second and third acoustic virial coefficients is very close to the potential M-S (0-20) which was found to represent the potential obtained by inversion of viscosity data, with $\varepsilon/k = 217\ \mathrm{K}$ and $r_m = 0.3879\ \mathrm{nm}$ [9,16], the error in the viscosity being ± 0.80 per cent. This simply means that by an appropriate adjustment of the potential parameters one can obtain a potential which lies very close to that already obtained, which fits simultaneously very well all the properties mentioned above.

7.3.3 Nitrogen

In the following the proposed method is applied to the moderately anisotropic nitrogen-nitrogen system. A successful implementation of the method for this system would mean that a similar analysis which takes into account the orientation dependence is very likely to provide very close approximations to the true potential.

The second and third acoustic virial coefficients employed for the analysis of nitrogen were taken from [8]. Based on the proposed method the second acoustic virial coefficients β_a were fitted to M-S potentials with different values for γ and m. Subsequently, the third acoustic virial coefficients were calculated for these potentials. Figures 7.14 and 7.15 show the standard deviations of the calculated values of β_a and γ_a from the experimental values [8] for the different M-S $(\gamma - m)$ potentials. A common minimum in the standard deviations is obtained for $m = 19$ and $\gamma = 10$. This corresponds to a standard deviation for β_a of 0.30 cm^3 / mol and a standard deviation for γ_a of 600 cm^6 / mol^2 which are about twice the estimated uncertainty of the latter, still very small. The M-S (10-19) potential, with parameters $r_m = 0.3862$ and $\varepsilon = 136.59$, was employed for the calculation of the second and third acoustic virial coefficients and the viscosity.

In figure 7.16 the deviations of the calculated second volumetric virial coefficients from the experimental values quoted in [14] are plotted against the temperature. The agreement of the calculated with the experimental values of B was found excellent throughout the temperature range 75 to 400 K, the deviations being always less than half of the uncertainties of the quoted experimental values.

In figure 7.17 the calculated third virial coefficients are illustrated together with reliable experimental results. The M-S (10-19) potential was found to represent the experimental data within their uncertainty. The calculated values for B and C are listed in tables 7.6 and 7.7 respectively.

The percentage deviation of the calculated viscosity is plotted in figure 7.18 over the temperature range 100 to 1500 K. In the temperature range 300 to 1500 K the error was found less than -2.5 per cent while at temperatures below 300 K the error was less than -3.5 per cent.

In general the non-spherically symmetric nitrogen is well represented by the very simple potential model M-S (10-19), which was solely obtained based on second and third acoustic virial coefficient data. The values calculated for B with the non-spherical potential of van der Avoird based on 'ab initio' calculations [17] are found systematically more negative from those proposed by Dymond and Smith [14], while our values are found to be almost in exact agreement. This proposed method sets the groundwork for potential calculations based on simple models which also take into account the orientation dependence. After the success of the method at least in predicting accurately second and third volumetric virial coefficients, we applied it to the also moderately anisotropic argon-nitrogen system.

7.4 Application of the method to mixtures

The acoustic virial coefficients for a mixture are given as the acoustic virial coefficients of a pure substance, by equation (3), where the perfect gas heat capacity ratio, γ^{pg}, is that for the mixture, γ_M^{pg} [18]. As discussed in chapter 2, the second volumetric virial coefficients of a mixture are given by:

$$B_M = x_1^2 B_{11} + 2x_1 x_2 B_{12} + x_2^2 B_{22} \qquad (19)$$

where B_{ii} are the second volumetric virial coefficients for the pure substances, and B_{ij} are the second interaction volumetric virial coefficients. An analogous expression we may write for the acoustic second virial coefficient of the mixture:

$$\beta_M = x_1^2 \beta_{11}^* + 2x_1 x_2 \beta_{12} + x_2^2 \beta_{22}^* \qquad (20)$$

where according to (3) the coefficients β_{ii}^{*} (the superscript * indicates that these are not the acoustic virial coefficients of the pure components) are obtained by:

$$\beta_{ii}^{*} = 2B_{ii} + 2(\gamma_M^{pg} - 1)T\frac{dB_{ii}}{dT} + \frac{(\gamma_M^{pg} - 1)^2}{\gamma_M^{pg}}T^2\frac{d^2B_{ii}}{dT^2} \quad (21)$$

and β_{12} by:

$$\beta_{12} = 2B_{12} + 2(\gamma_M^{pg} - 1)T\frac{dB_{12}}{dT} + \frac{(\gamma_M^{pg} - 1)^2}{\gamma_M^{pg}}T^2\frac{d^2B_{12}}{dT^2} \quad (22)$$

The interaction second virial coefficients B_{12} are obtained from equation (4), in which the potential between molecules 1 and 2, U_{12}, stands this time for non-alike molecules. The coefficients β_{ii}^{*} can be calculated from the second volumetric virial coefficients of the pure components, B_{ii}, and their derivatives with respect to the temperature, using the potentials derived for the pure components, as shown previously. Thus, from equation (20), we may obtain the coefficients β_{12}. Substituting into (22) the expression of B_{12} in terms of the potential U_{12}, we get the expression of β_{12} in terms of the potential U_{12}. In the following, using the Maitland-Smith potential model we fit the β_{12} values, to obtain the fitting parameters of U_{12}. The U_{12} potentials obtained from the fit are employed next for the calculation of the third acoustic virial coefficients of the mixture.

The third acoustic virial coefficients of a mixture are given from the same relation as those of the pure substances, equation (10), where all properties referring to the pure substances are substituted with those for the mixture. As discussed in chapter 2, the third volumetric virial coefficient of a mixture is given by:

$$C_M = x_1^3 C_{111} + 3x_1^2 x_2 C_{112} + 3x_1 x_2^2 C_{122} + x_2^3 C_{222} \quad (23)$$

where the coefficients C_{iii} are the third volumetric virial coefficients of the pure substances, while C_{112} and C_{122} are the third interaction volumetric virial coefficients. The third interaction volumetric virial coefficients may be obtained from equation (7), using in equations (8) and (9), the appropriate interaction potentials. For example, for evaluating the coefficient C_{112} for A-A-B interactions we correspond the set (U_{12}, U_{13}, U_{23}) in (8) and (9), to (U_{AA}, U_{AA}, U_{AB}), where U_{AA} is the intermolecular

potential between two molecules of the substance A and U_{AB} is the intermolecular potential between a molecule of the substance A and a molecule of the substance B. Since the intermolecular potential of the pure substances can be derived as shown previously, and the potential U_{AB} can be obtained from fit of the β_{12} values, we may proceed to the calculation of the acoustic third virial coefficients for the mixture of interest.

7.4.1 Argon-nitrogen

In the analysis of the argon-nitrogen interactions we employed the values for the second and third acoustic virial coefficients reported in [18] for a (0.50 argon-0.50 nitrogen) mixture. According to the method outlined above, we calculated the coefficients β_{12} from the second acoustic virial coefficients of the mixture β_M and the values of β_{ii}^* for argon and nitrogen using equation (20). The values β_{ii}^* for argon and nitrogen were calculated from the potentials obtained for the pure substances, M-S $(5-14.5)$ and M-S (10-19) respectively. The values of β_{12} obtained were fitted to Maitland-Smith potentials with different values of γ and m. Subsequently, the third interaction volumetric virial coefficients were calculated using for the alike interactions the potentials derived for the pure substances and for the non-alike interactions the M-S $(\gamma - m)$ potentials derived from the fit of β_{12}. From the third interaction volumetric virial coefficients and the third volumetric virial coefficients of the pure substances we calculated the third volumetric virial coefficients of the mixture and hence using equation (10) the third acoustic virial coefficients of the mixture.

Figures 7.19 and 7.20 illustrate the standard deviations of β_{12} and γ_M calculated from the interaction potentials for different values of γ and m, from the experimental ones. It can be readily seen that for the M-S potential with $m = 16$ and $\gamma = 10$ the standard deviation for both acoustic virial coefficients attains its minimum value. At this minimum the standard deviation of β_{12} is 0.35 cm^3 / mol, while the standard deviation of γ_M is 580 cm^6 / mol^2. These standard deviations are very satisfactory compared with

the uncertainties of β_{12} and γ_M, about 0.30 cm^3/mol and 400 cm^6/mol^2 respectively. As for the treatment of argon, for the purposes of the fit, the experimental γ_M value at the lowest temperature (90.06 K) was given an uncertainty double that quoted in [18]. Subsequently, the potential M-S (10-16) with scaling parameters $r_m = 0.3785$ and $\varepsilon / k = 140.26$ K was used for the calculation of the second and third interaction volumetric virial coefficients.

In figure 7.21 the calculated second interaction virial coefficients B_{12} are presented together with available experimental data. Our potential was found to represent the experimental values reported well within their estimated uncertainties, about ± 4 cm^3/mol. By analogy with the deviations in B values obtained for the pure substances, we can claim for temperatures higher than 120 K, an uncertainty of ± 1 cm^3/mol in B_{12}. The calculated values of B_{12} are listed in table 7.8.

The third interaction volumetric virial coefficients calculated are presented in table 7.9. It is the first time that third interaction volumetric virial coefficients have been reported over a wide range of temperatures. These coefficients are believed to be as accurate as the third volumetric virial coefficients of the pure substances, at least at temperatures higher than 120 K where the non-additive contribution to the third interaction virial coefficients becomes less important.

The potential obtained for the argon-nitrogen interactions has the scaling parameter r_m almost equal to the arithmetic mean (0.3772 nm) and the scaling parameter ε / k almost equal to the geometric mean (140.9 K) of the corresponding parameters of the pure substances.

Table 7.1. Third acoustic virial coefficients γ_a for argon calculated from HFDID1 potential for argon [13], together with experimental values taken from [8].

T K	γ_a^{calc} cm^6 / mol^2	γ_a^{exp} cm^6 / mol^2
90.06	-15716	-15800
99.58	-5539	-5400
118.88	1131	1800
149.88	2931	3100
189.98	2966	3300
240.28	2748	2600
300.61	2564	3000
373.15	2431	3000

Table 7.2. Second volumetric virial coefficients B of argon calculated from potential M-S (5 – 14.5).

T / K	B / cm^3 / mol
70	-358.45
75	-318.19
81	-268.73
85	-245.10
90	-220.08
95	-199.01
100	-181.03
110	-152.03
125	-120.32
150	-85.64
200	-48.78
250	-27.67
300	-15.29
400	-0.98
500	6.92
600	11.85
700	15.17
800	17.53
900	19.26
1000	20.58

Table 7.3. Third volumetric virial coefficients C of argon calculated from potential M-S $(5-14.5)$.

T K	C cm ^{6} / mol ^{2}
81	-13890
90	-4257
100	-3
110	1640
125	2350
150	2254
200	1634
250	1268
300	1071
400	913
500	821
600	780
700	747
800	755
900	722
1000	709

Table 7.4. Second volumetric virial coefficients B of methane calculated from potential M-S (0 – 19).

T / K	B / cm^3 / mol
110	-325.16
120	-274.79
130	-236.01
140	-205.28
150	-180.38
160	-159.79
180	-127.80
200	-104.11
225	-82.61
250	-65.35
275	-52.38
300	-42.00
350	-26.45
400	-15.39
500	-0.77
600	8.39

Table 7.5. Third volumetric virial coefficients C of methane calculated from potential M-S (0 – 19).

T / K	C / cm ^{6} / mol ^{2}
110	-16177
120	-5106
130	42
140	2465
150	3566
160	4007
180	4047
200	3721
225	3254
250	2853
275	2536
300	2293
350	1959
400	1757
500	1547
600	1453

Table 7.6. Second volumetric virial coefficients B of nitrogen calculated from potential M-S (10–19).

T / K	B / cm^3 / mol
75	-277.12
80	-244.21
90	-194.62
100	-159.16
110	-132.59
125	-103.34
150	-71.05
200	-35.43
250	-16.36
300	-4.57
400	9.09

Table 7.7. Third volumetric virial coefficients C of nitrogen calculated from potential M-S (10–19).

T / K	C / cm^6 / mol^2
80.05	-4970
90.06	683
99.99	2506
119.81	3034
149.85	2479
189.99	1867
240.28	1484
300.62	1283
373.16	1184

Table 7.8. Second interaction volumetric virial coefficients B_{12} for argon-nitrogen interactions calculated from potential M-S (10 – 16).

T K	B_{12} cm ^{3} / mol
75	-294.62
80	-259.73
90	-207.43
100	-170.21
110	-142.45
125	-112.01
150	-78.57
200	-41.91
250	-22.39
300	-10.35
400	3.54

Table 7.9. Third interaction volumetric virial coefficients C_{112} and C_{122} for argon-argon-nitrogen and for argon-nitrogen-nitrogen interactions respectively, calculated from potential M-S (10 – 16).

T K	C_{112} cm ^{6} / mol ^{2}	C_{122} cm ^{6} / mol ^{2}
90.06	-2452	-746
100.00	547	2260
119.83	2013	3512
149.90	1869	3070
189.99	1400	2362
240.31	1064	1859
300.62	880	1562
373.15	786	1389

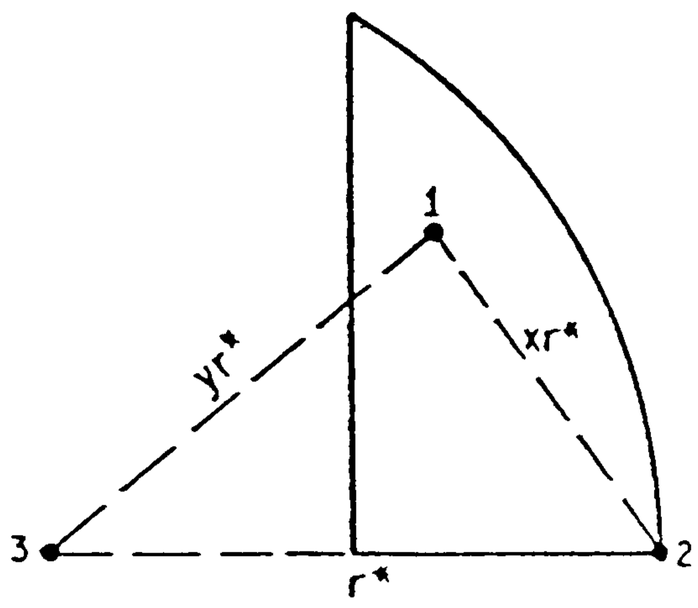

Figure 7.1. Range of integration

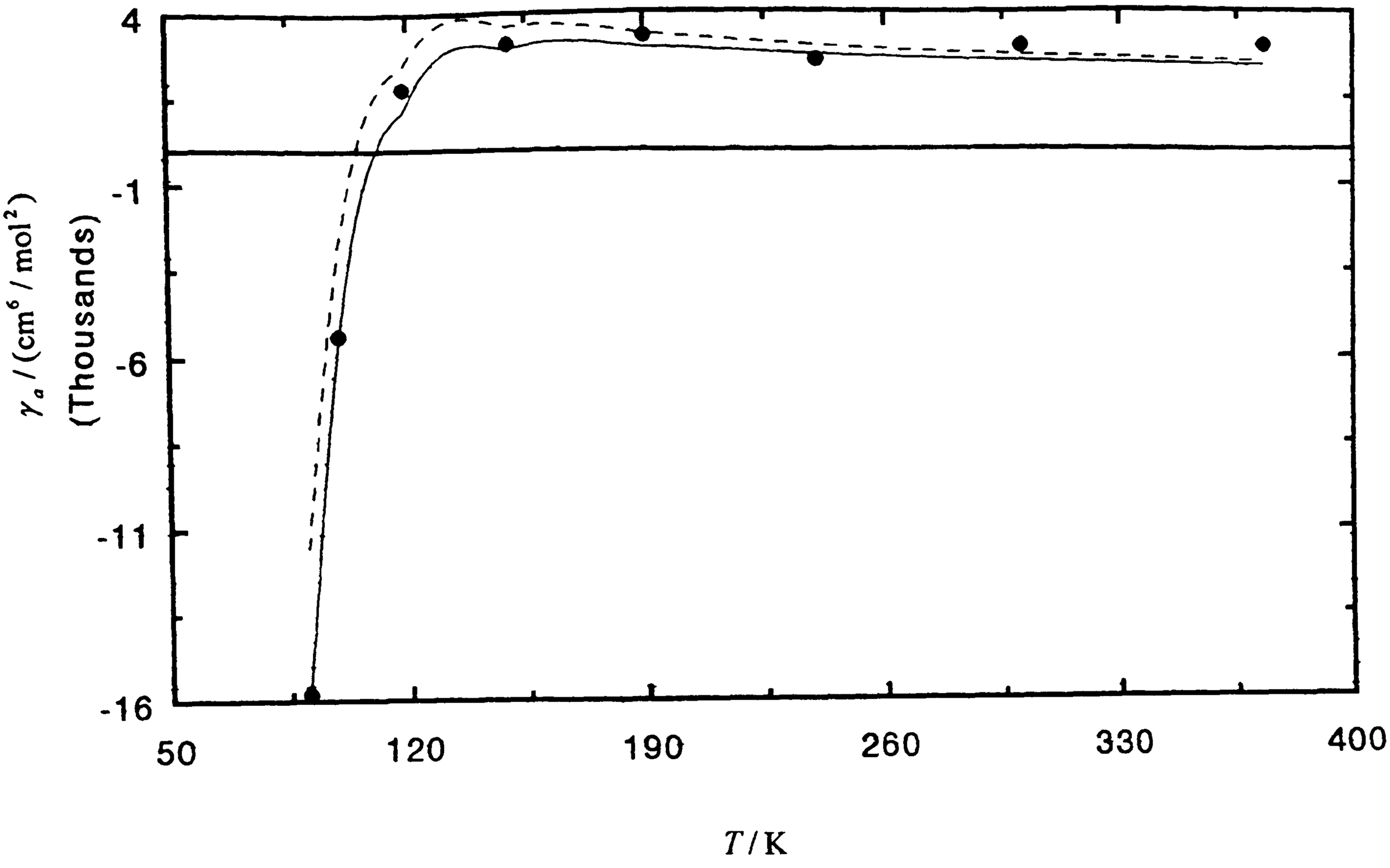

Figure 7.2. Third acoustic virial coefficients γ_a for argon calculated from HFDID1 potential [ß] together with experimental values [8]. Dashed lines for γ_a calculated using the approximation to C_6 .

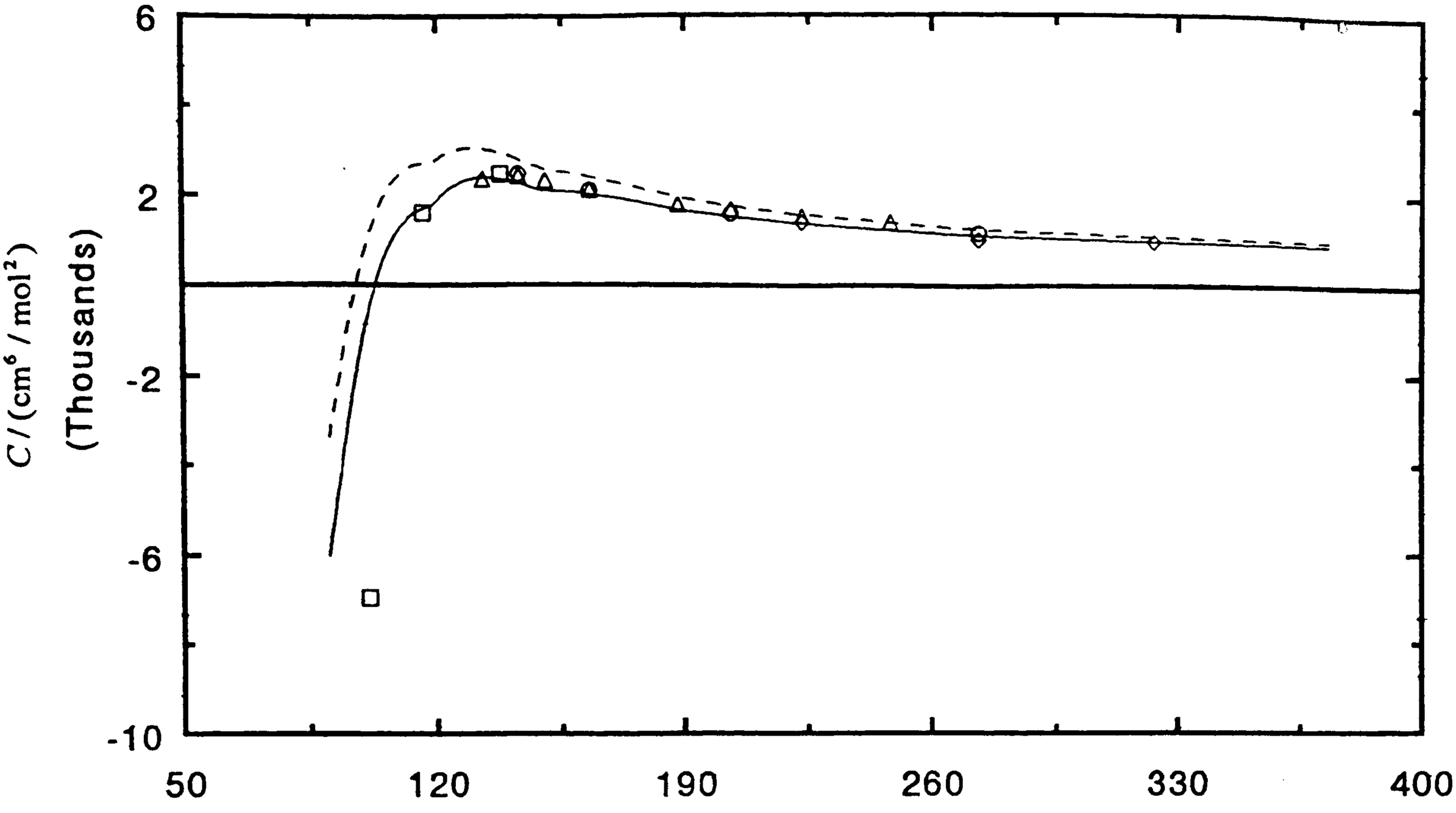

Figure 7.3. Third volumetric virial coefficients C for argon calculated from HFDID1 potential [3] together with experimental values; Δ [19], o [15], ◊ [20], □ [21]. Dashed lines for C calculated using the approximation to C_6 .

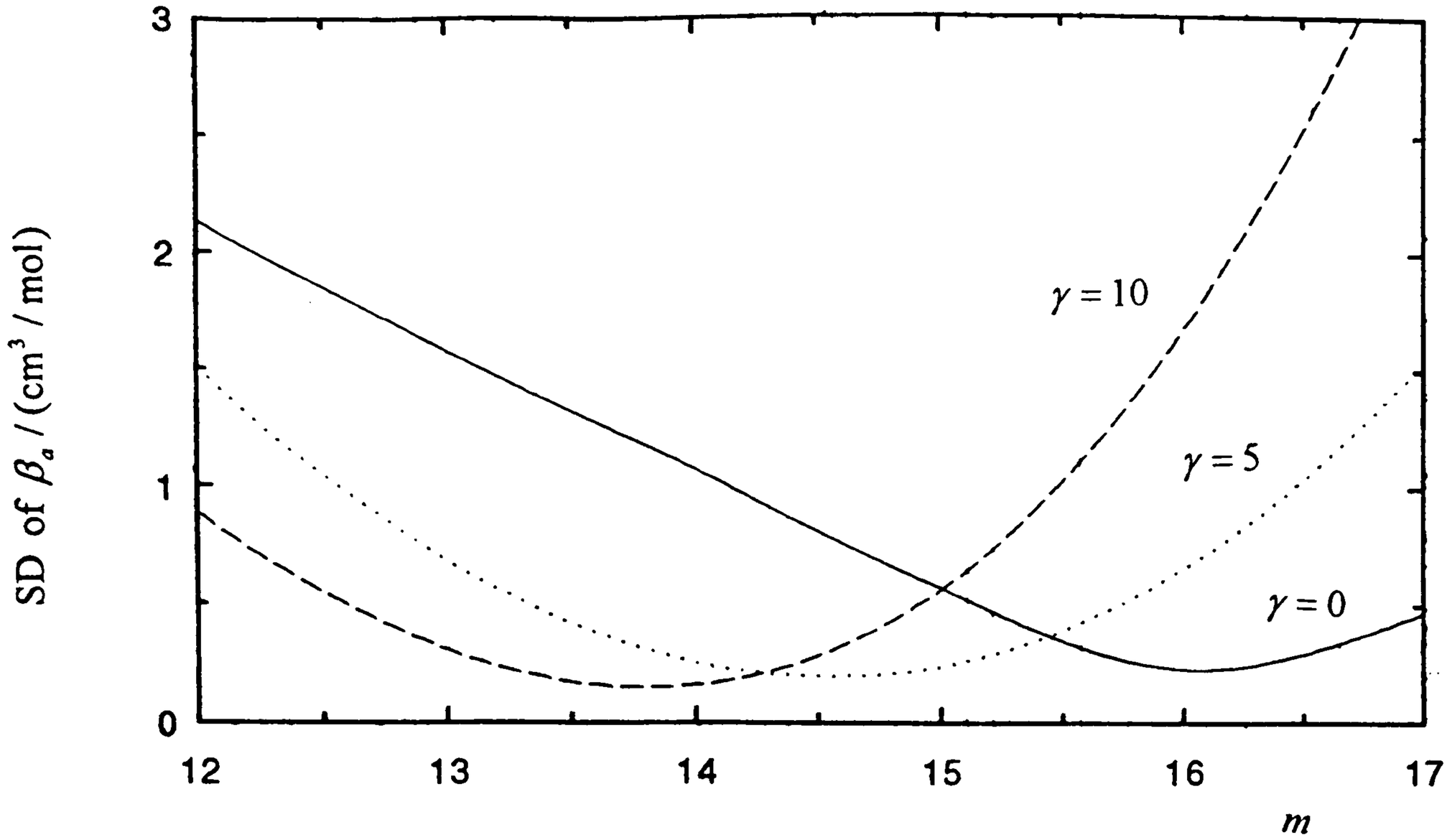

Figure 7.4. Standard deviations of the calculated β_a for argon from M-S potentials with different values of γ and m from the experimental values [8].

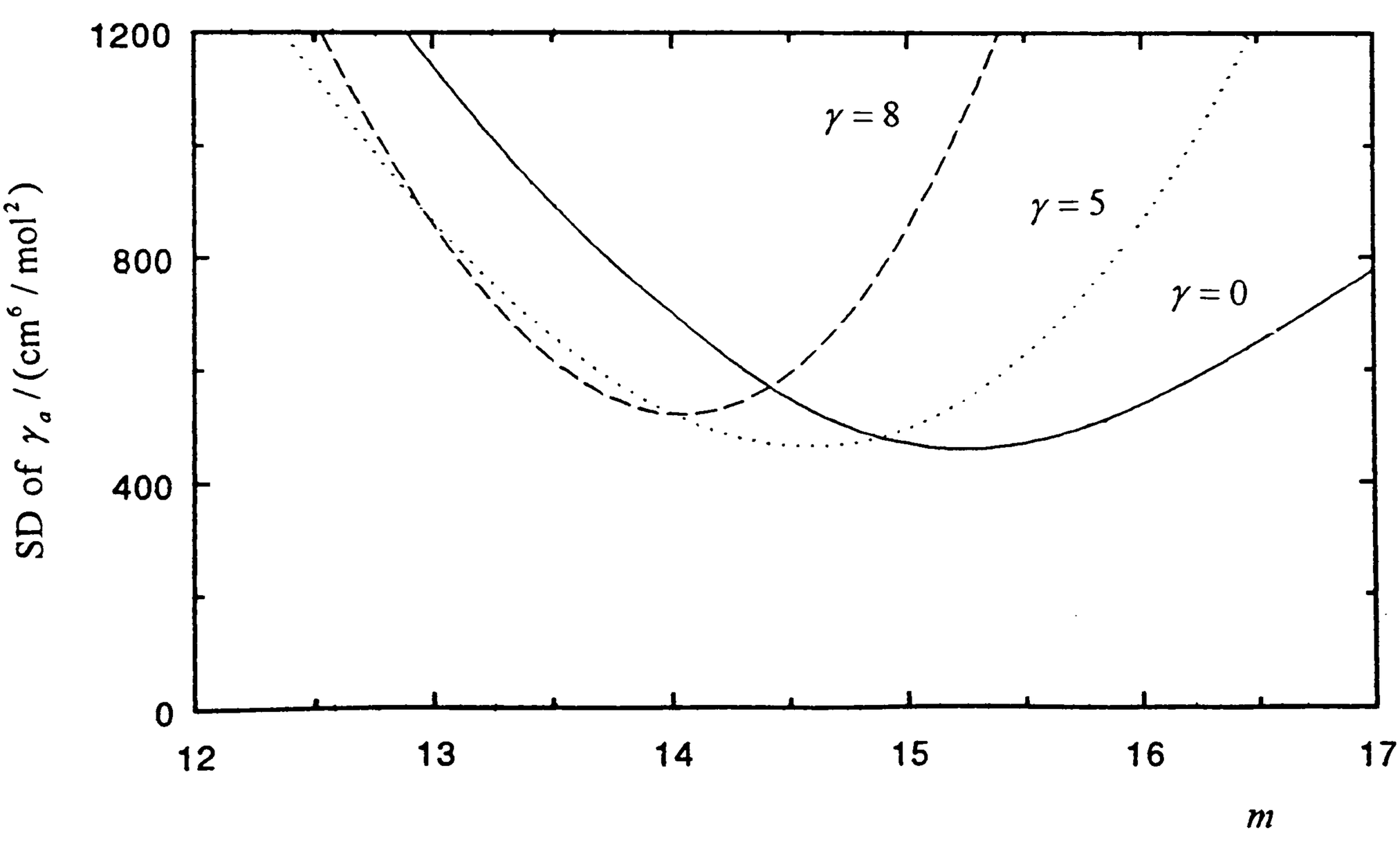

Figure 7.5. Standard deviations of the calculated γ_a for argon from M-S potentials with different values of γ and m from the experimental values [8].

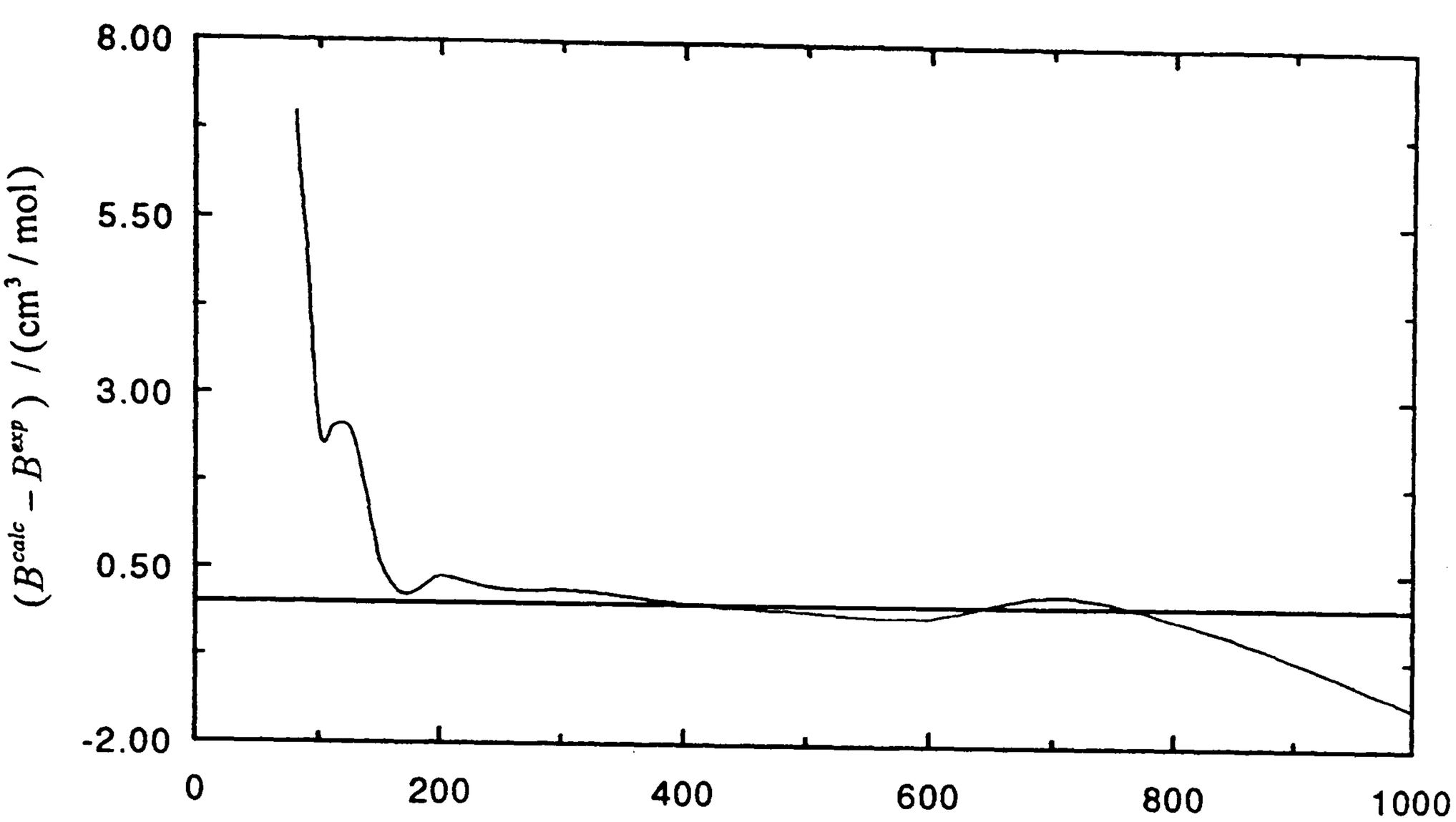

Figure 7.6. Deviations of the calculated values of B for argon from M-S (5-14.5) from the values proposed in [14].

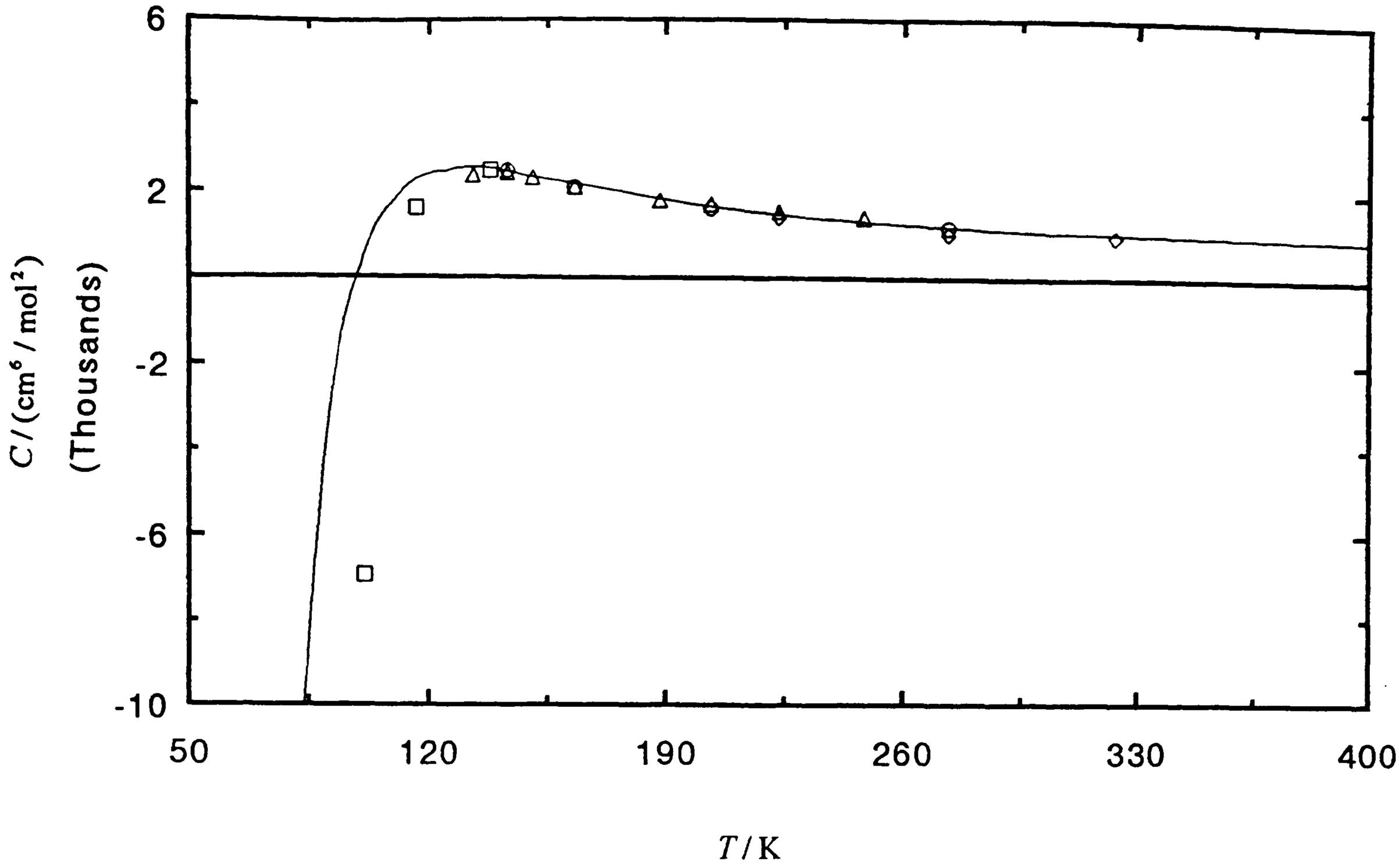

Figure 7.7. Third volumetric virial coefficients C for argon calculated from M-S (5-14.5) together with experimental values; Δ [19], o [15], ◊ [20], □ [21].

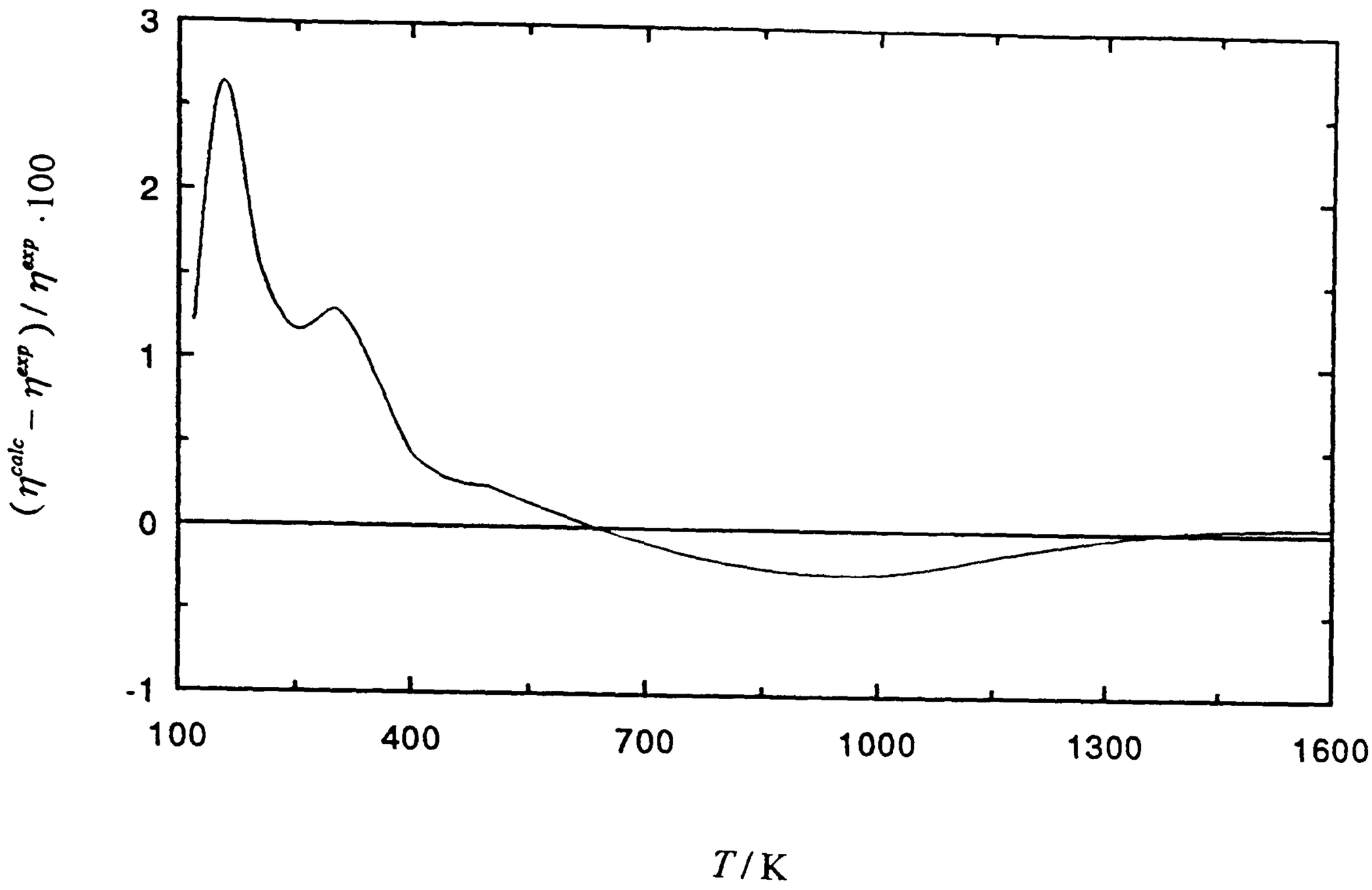

Figure 7.8. Percentage deviations of the viscosity η of argon calculated from M-S (5-14.5) from values quoted in [9].

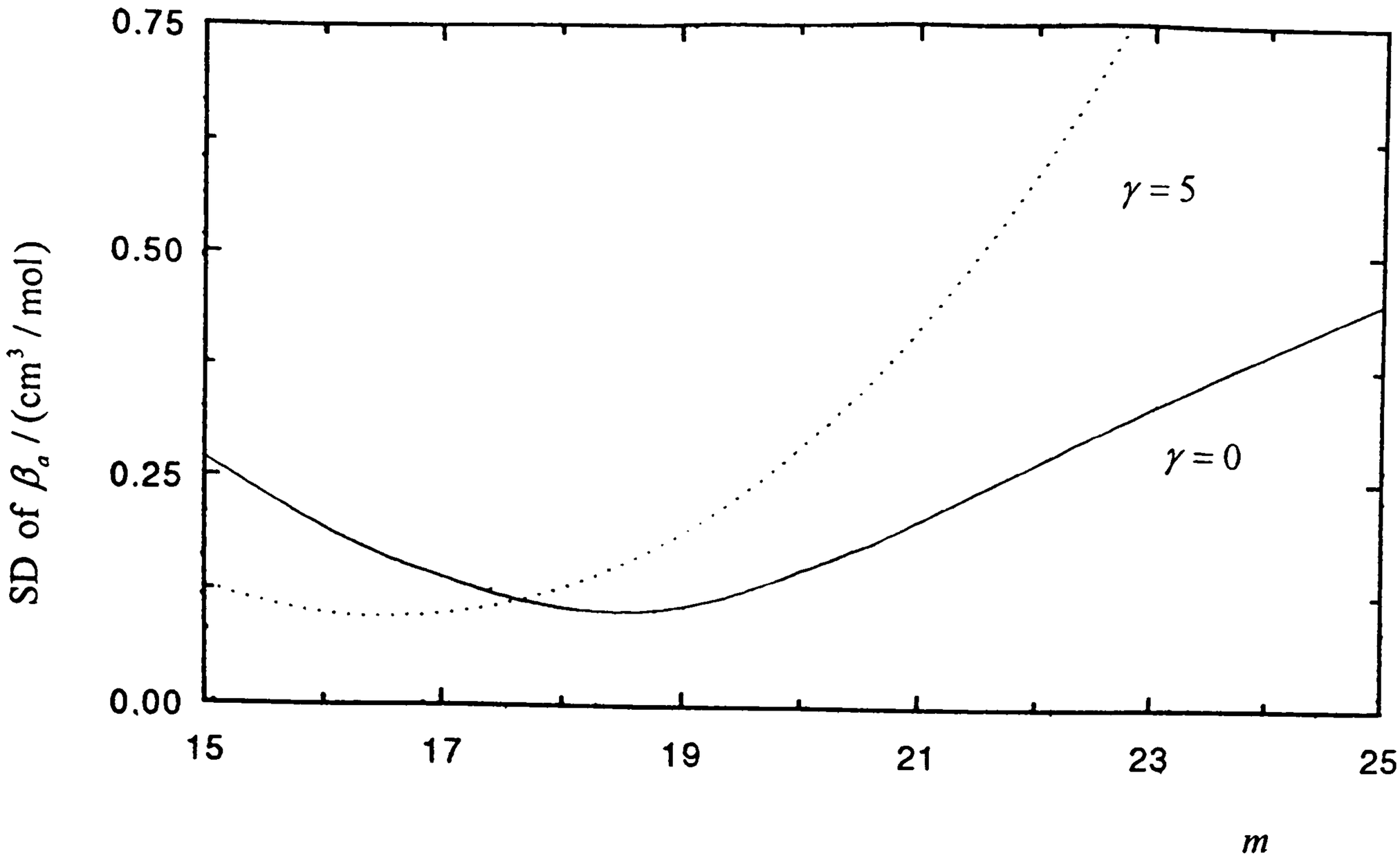

Figure 7.9. Standard deviations of the calculated β_a for methane from M-S potentials with different values of γ and m from the experimental values obtained in this work.

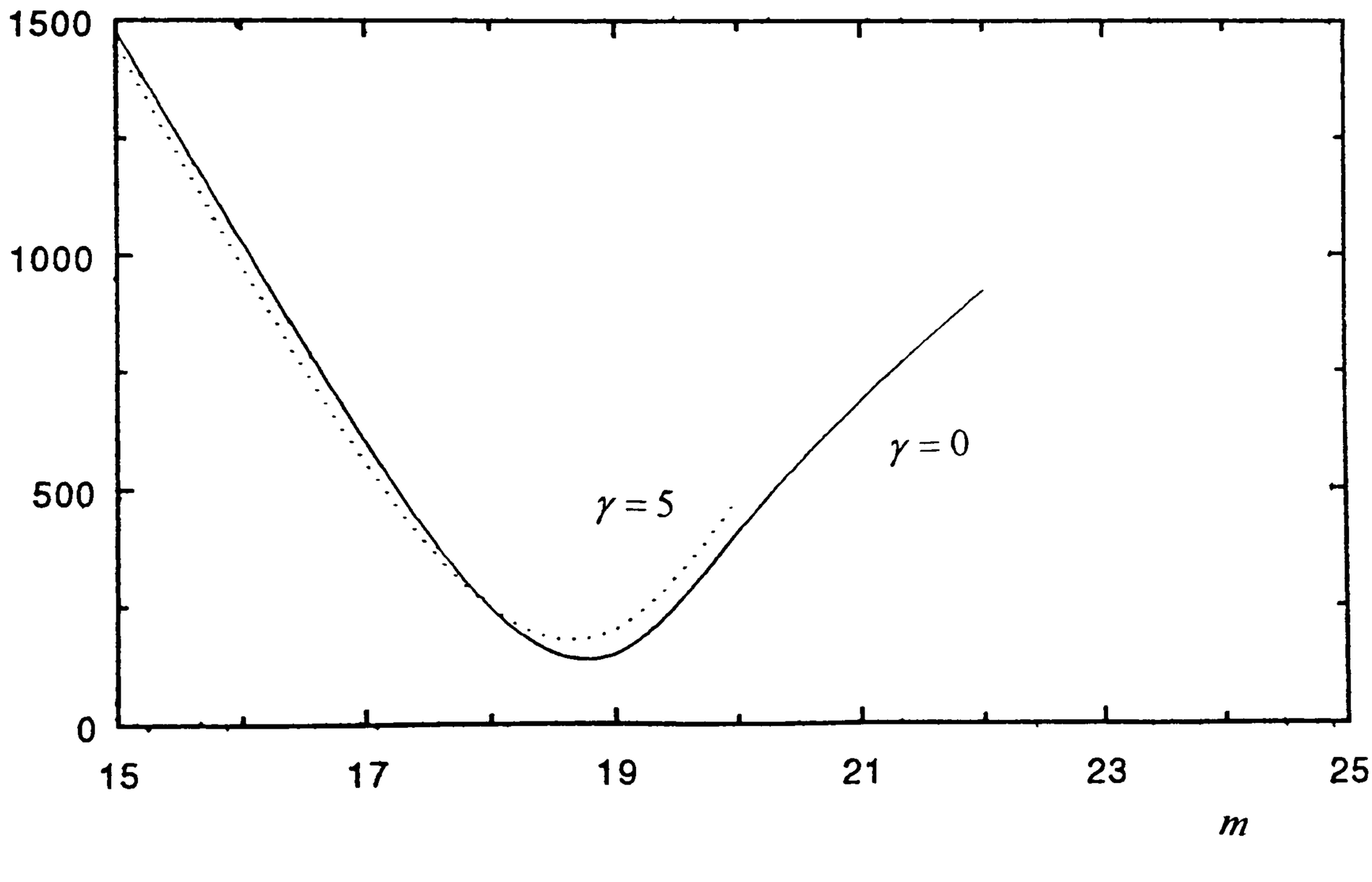

Figure 7.10. Standard deviations of the calculated γ_a for methane from M-S potentials with different values of γ and m from the experimental values obtained in this work.

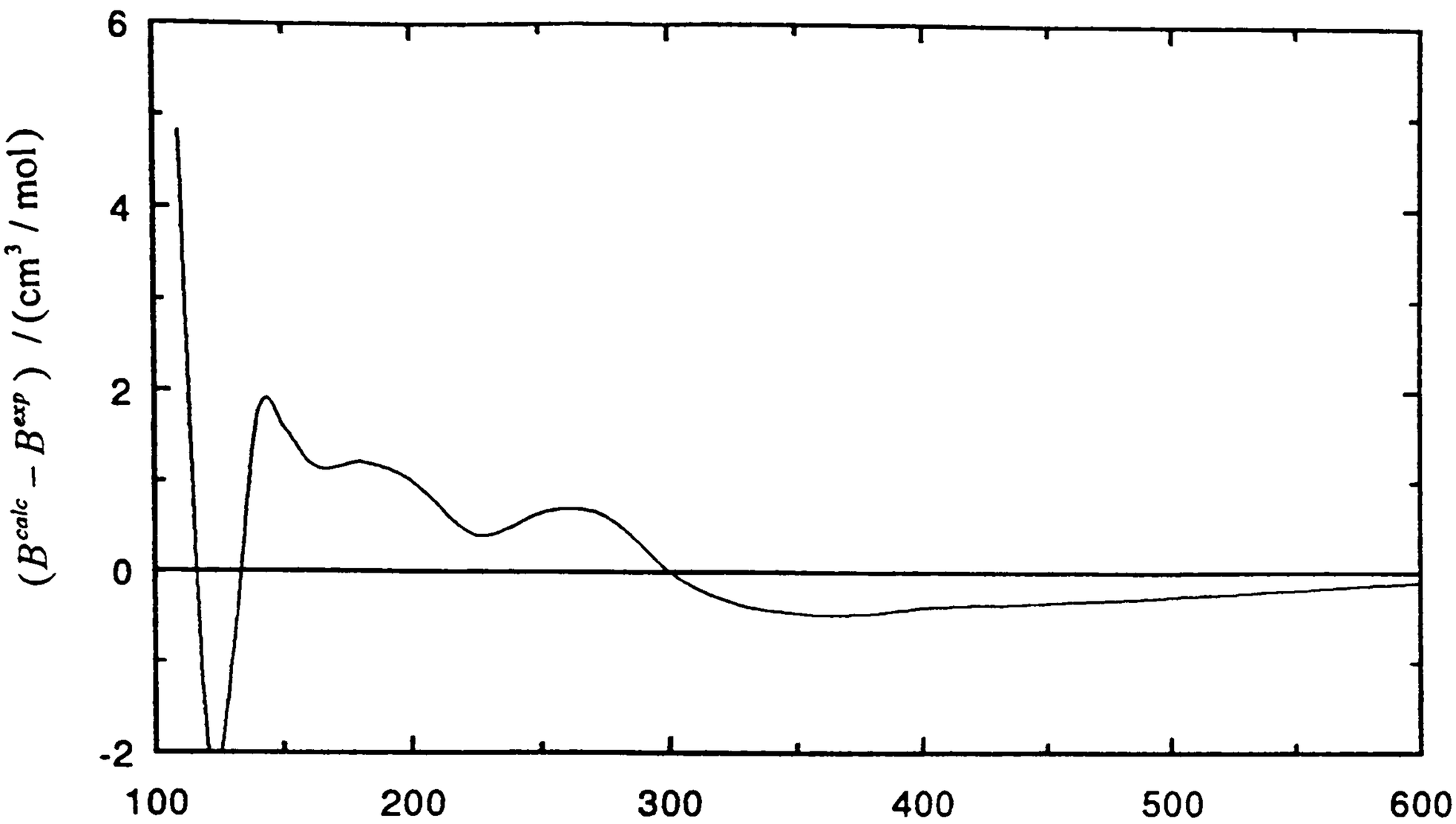

Figure 7.11. Deviations of the calculated values of B for methane from M-S (0-19) from the values proposed in [14].

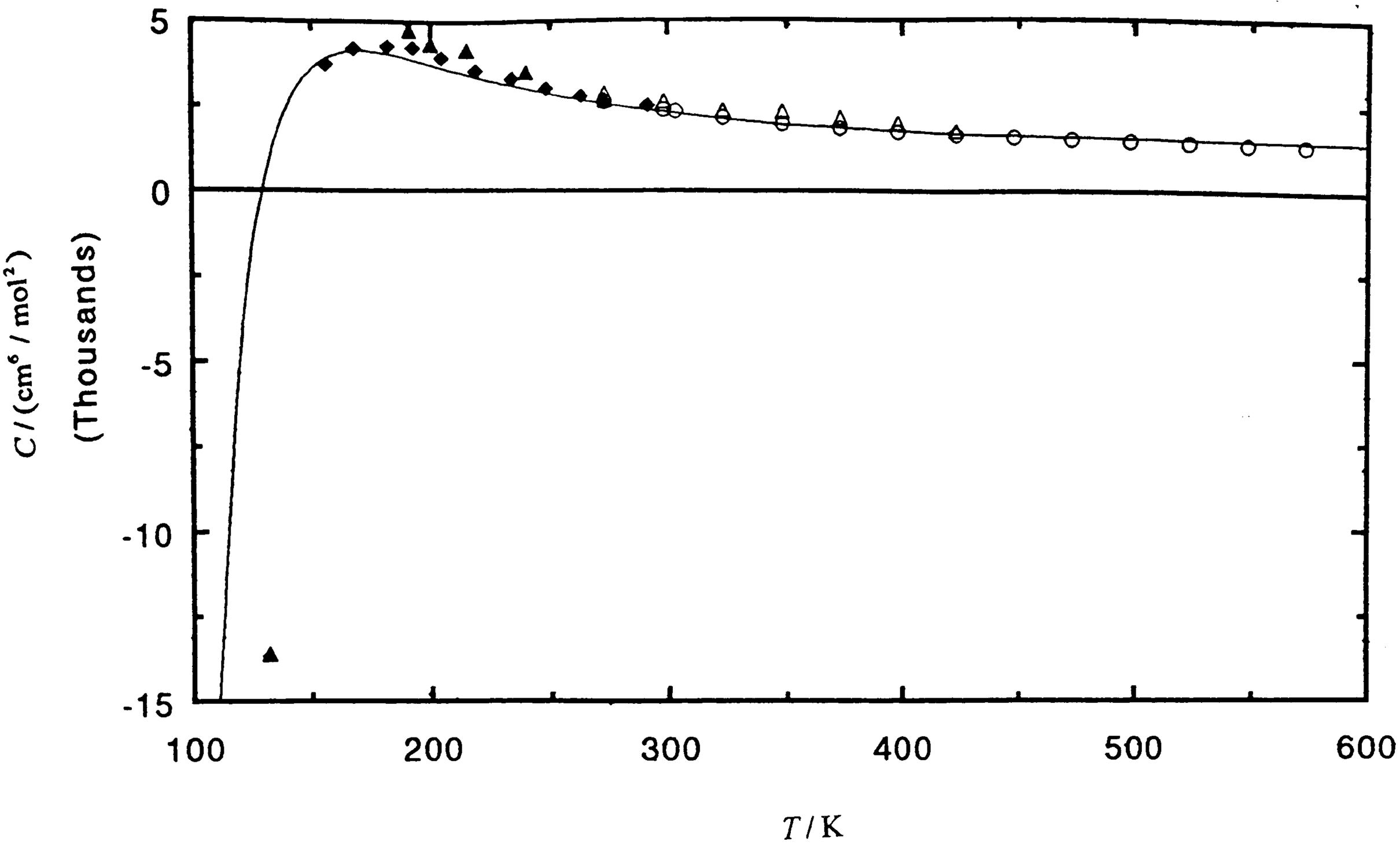

Figure 7.12. Third volumetric virial coefficients C for methane calculated from M-S (0-19) together with experimental values; Δ [22], o [23], ▲ [24], ♦ [25].

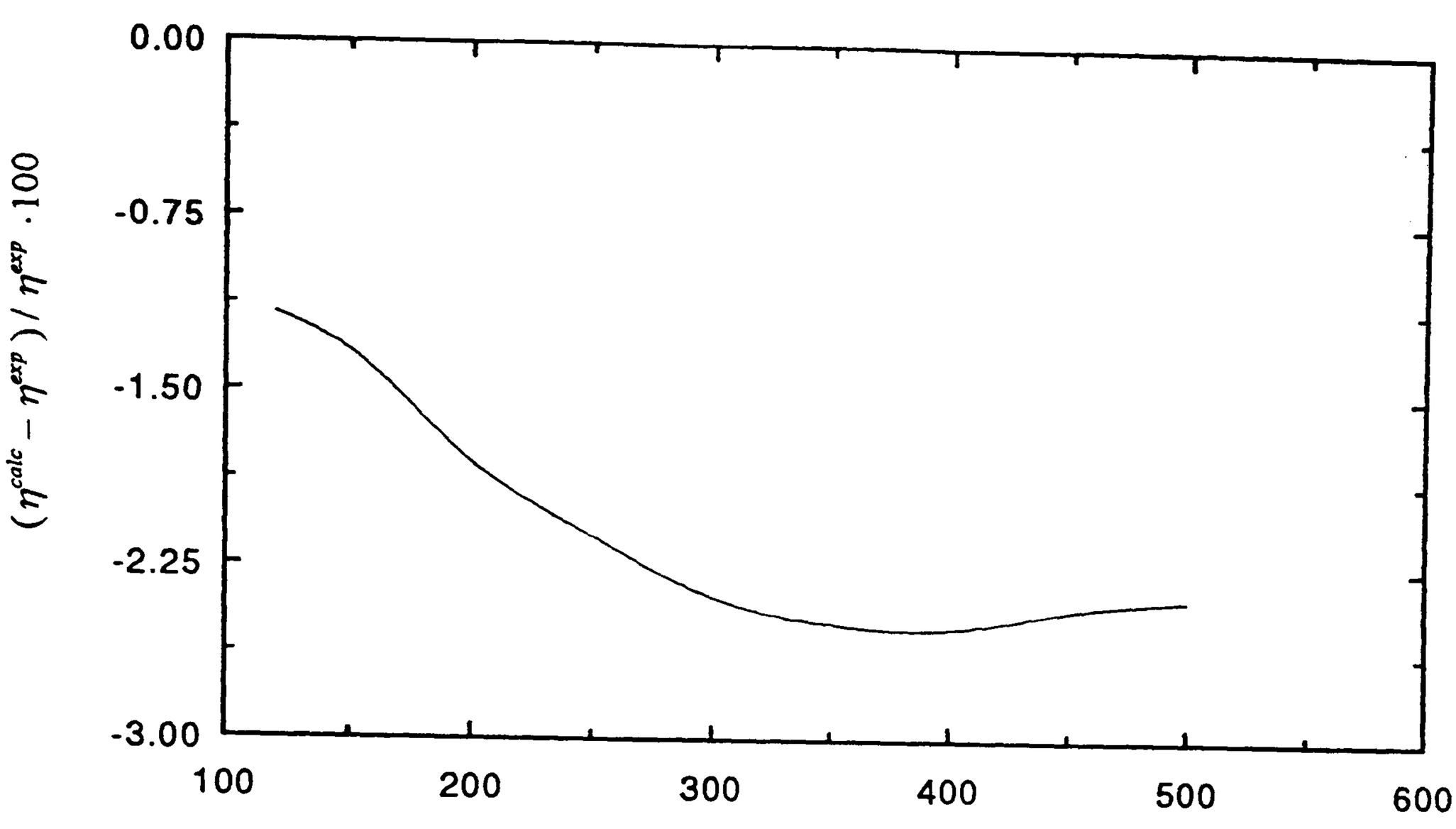

Figure 7.13. Percentage deviations of the viscosity η for methane calculated from M-S (0-19) from values quoted in [26].

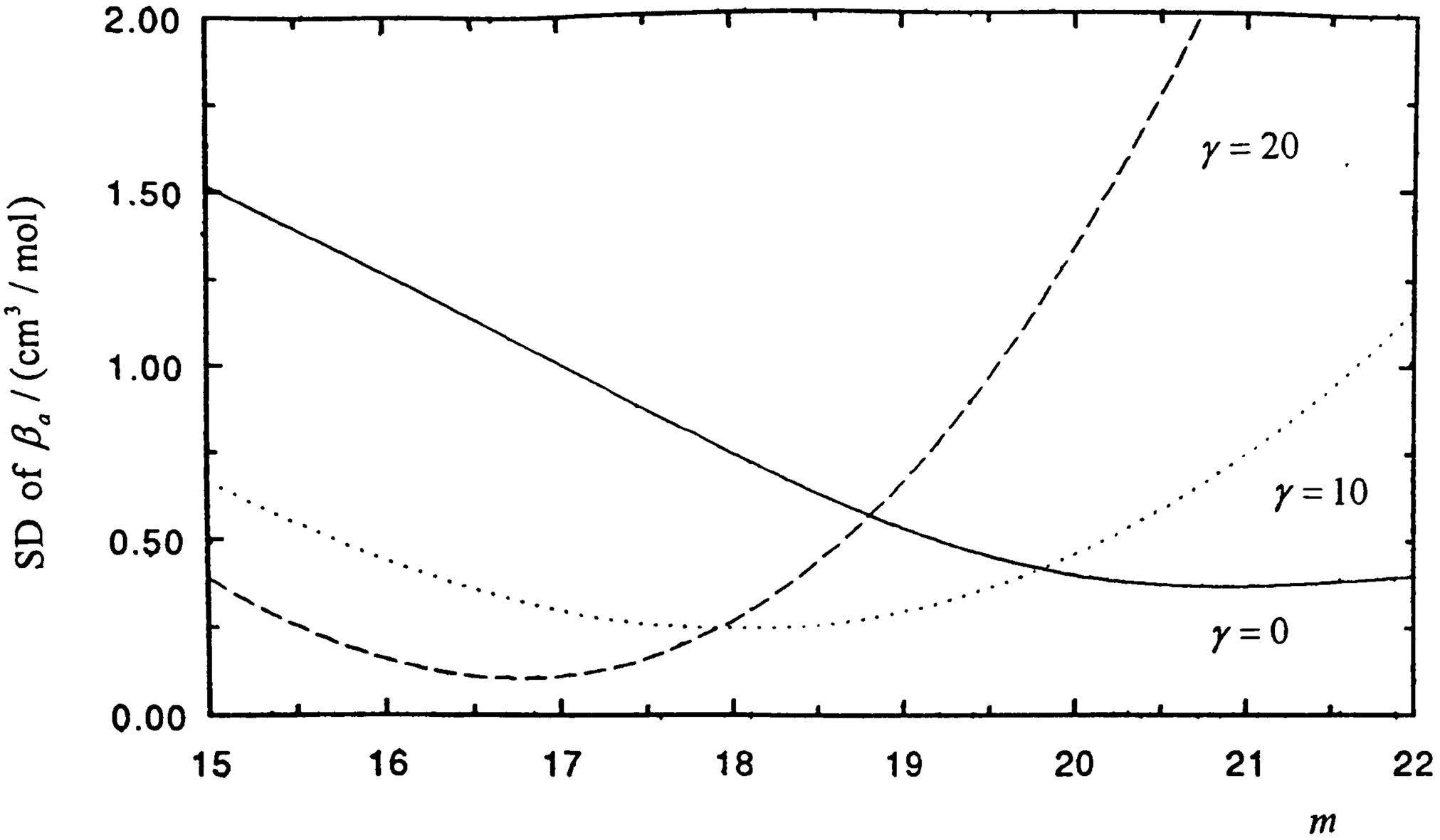

Figure 7.14. Standard deviations of the calculated β_a for nitrogen from M-S potentials with different values of γ and m from the experimental values [8].

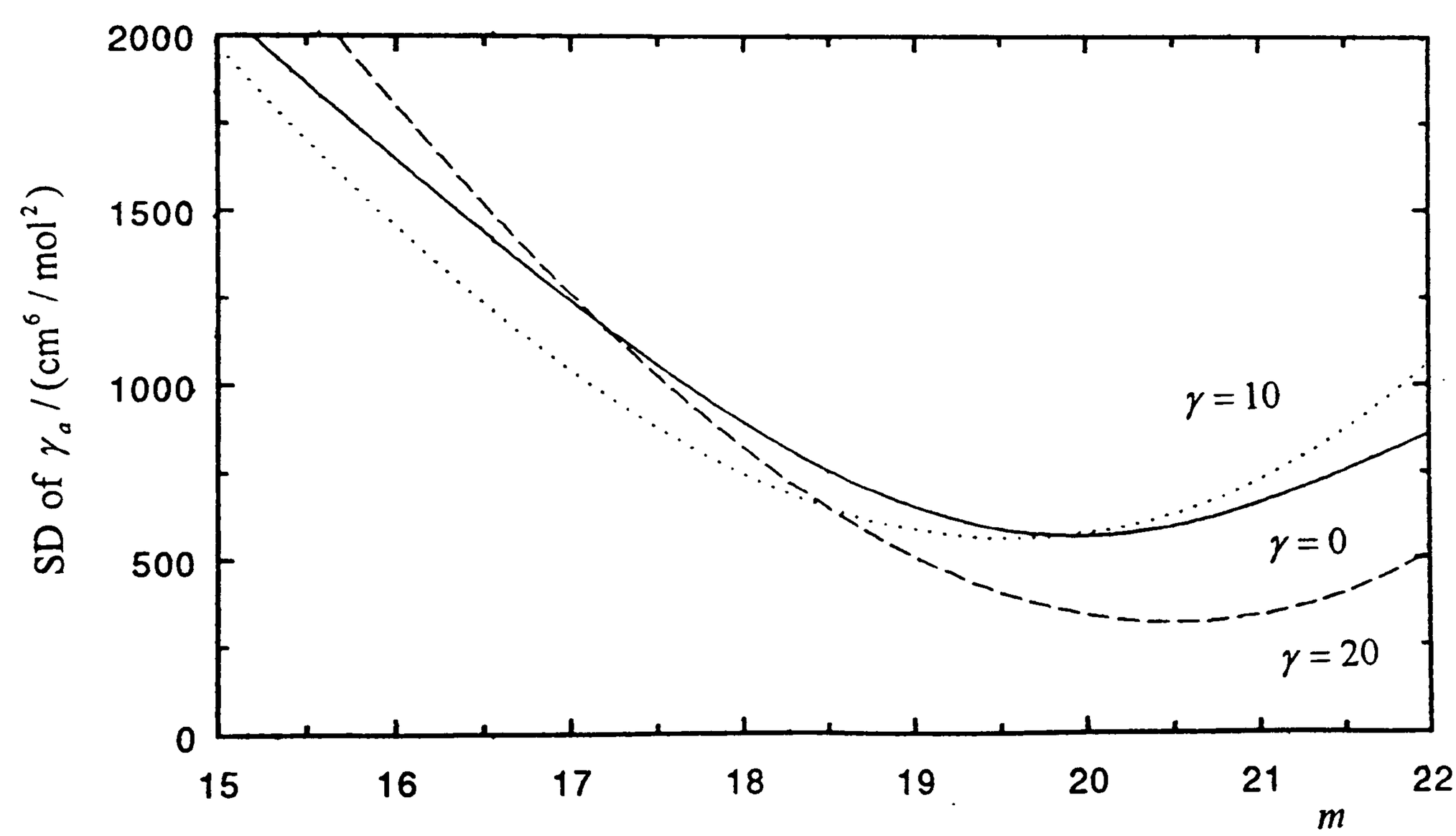

Figure 7.15. Standard deviations of the calculated γ_a for nitrogen from M-S potentials with different values of γ and m from the experimental values [8].

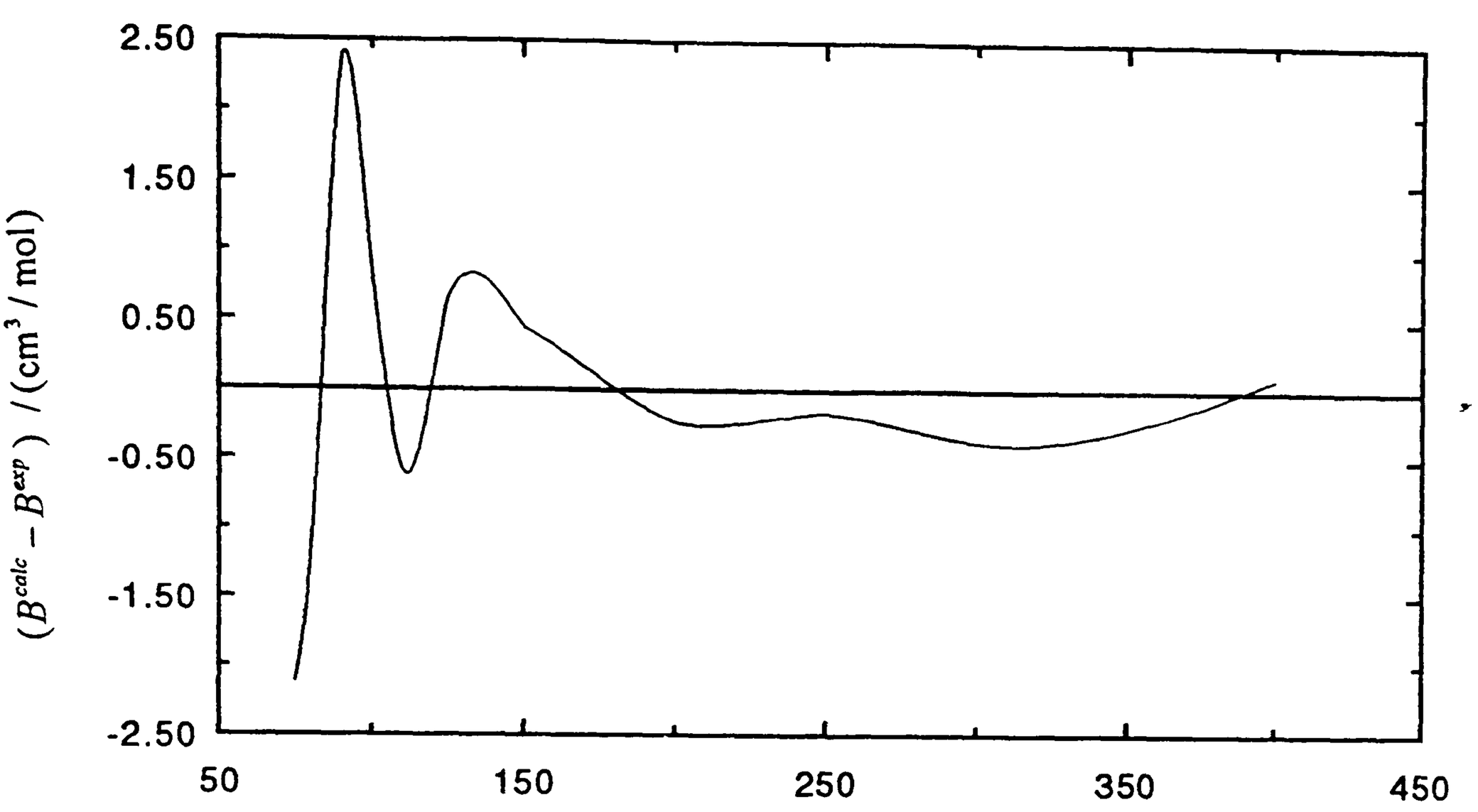

Figure 7.16. Deviations of the calculated values of B for nitrogen from M-S (10-19) from the values proposed in [14].

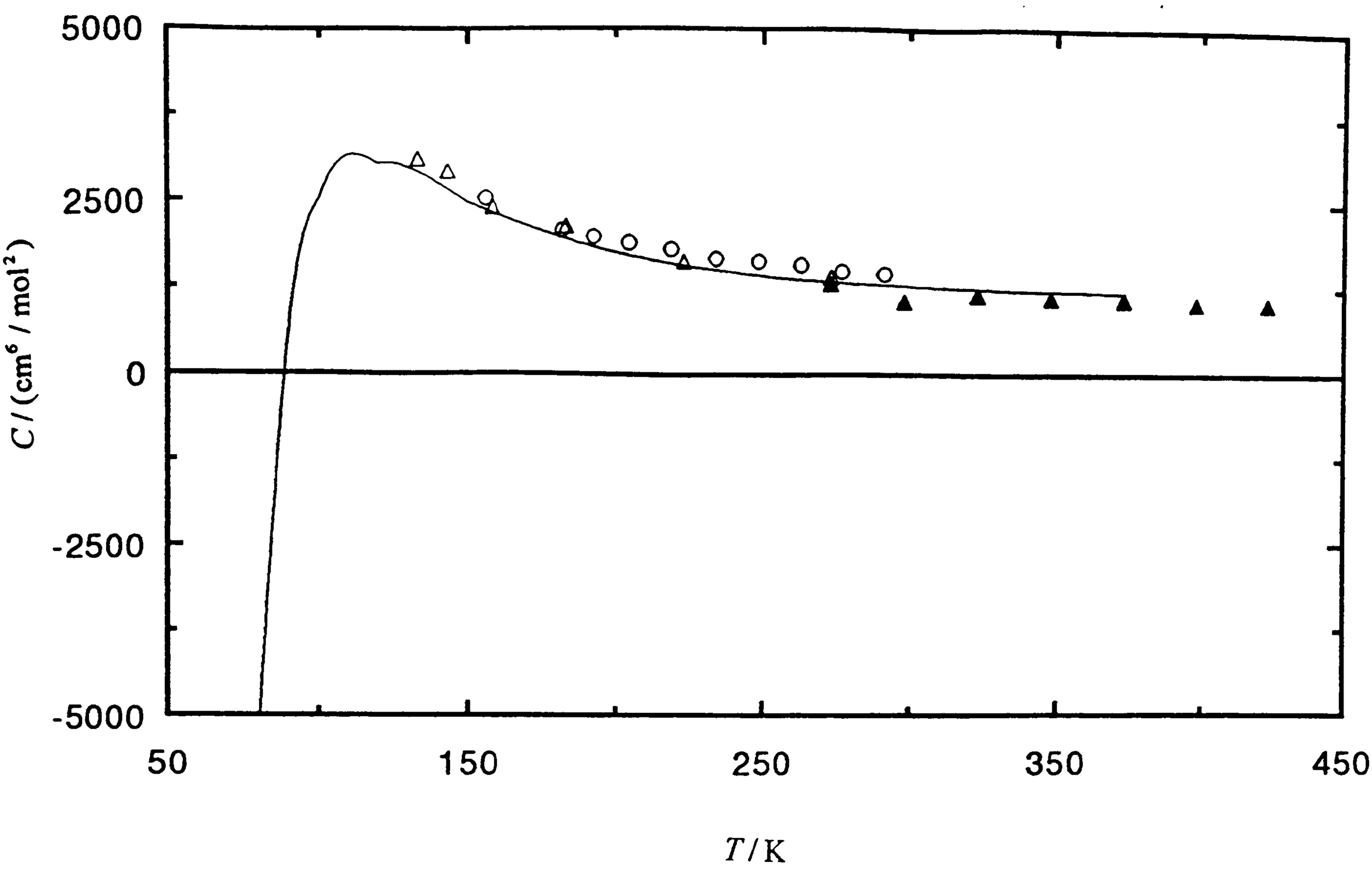

Figure 7.17. Third volumetric virial coefficients C for nitrogen calculated from M-S (10-19) together with experimental values; Δ [27], o [25], ▲ [28].

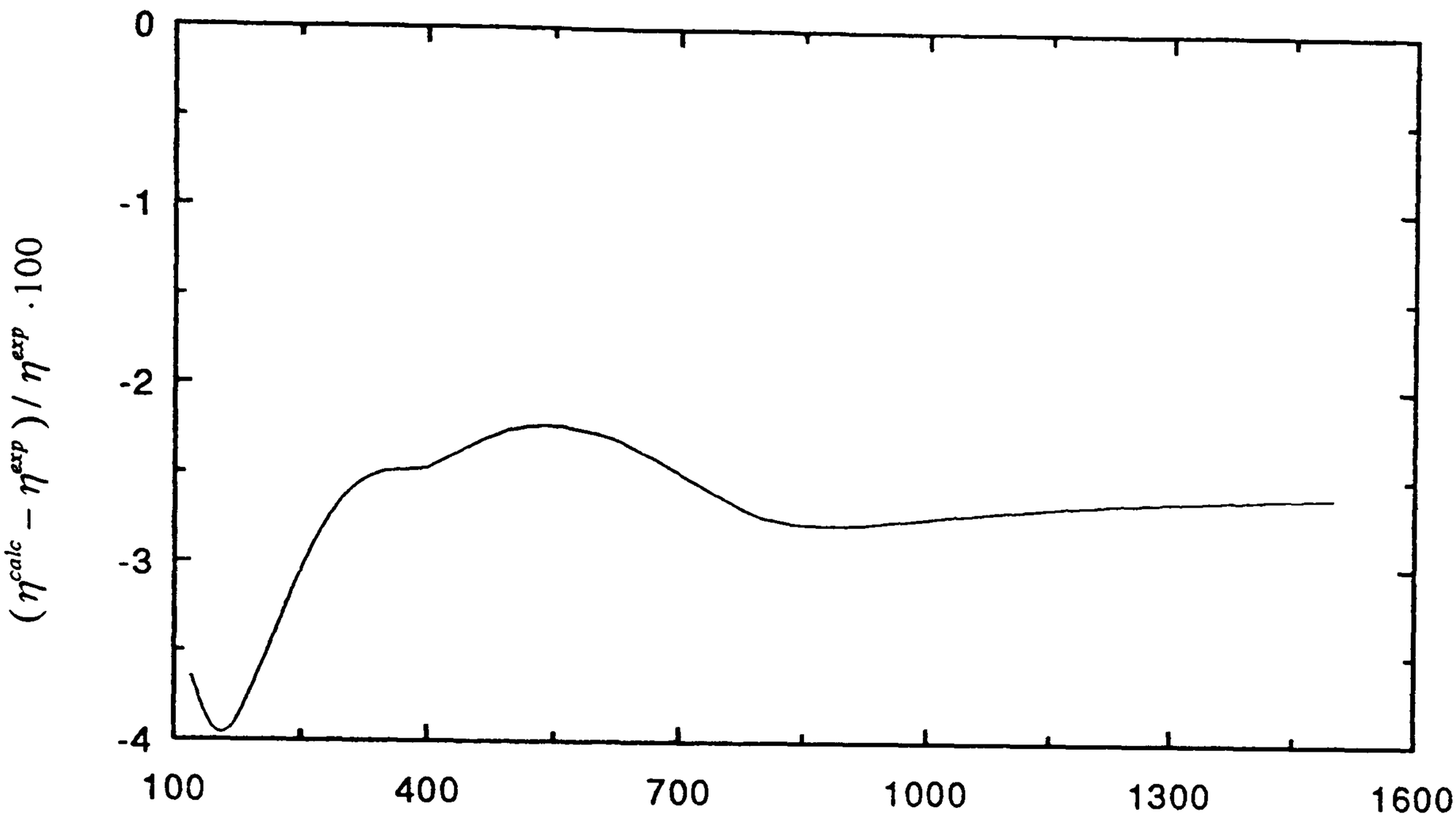

Figure 7.18. Percentage deviations of the viscosity η of nitrogen calculated from M-S (10-19) from values quoted in [9].

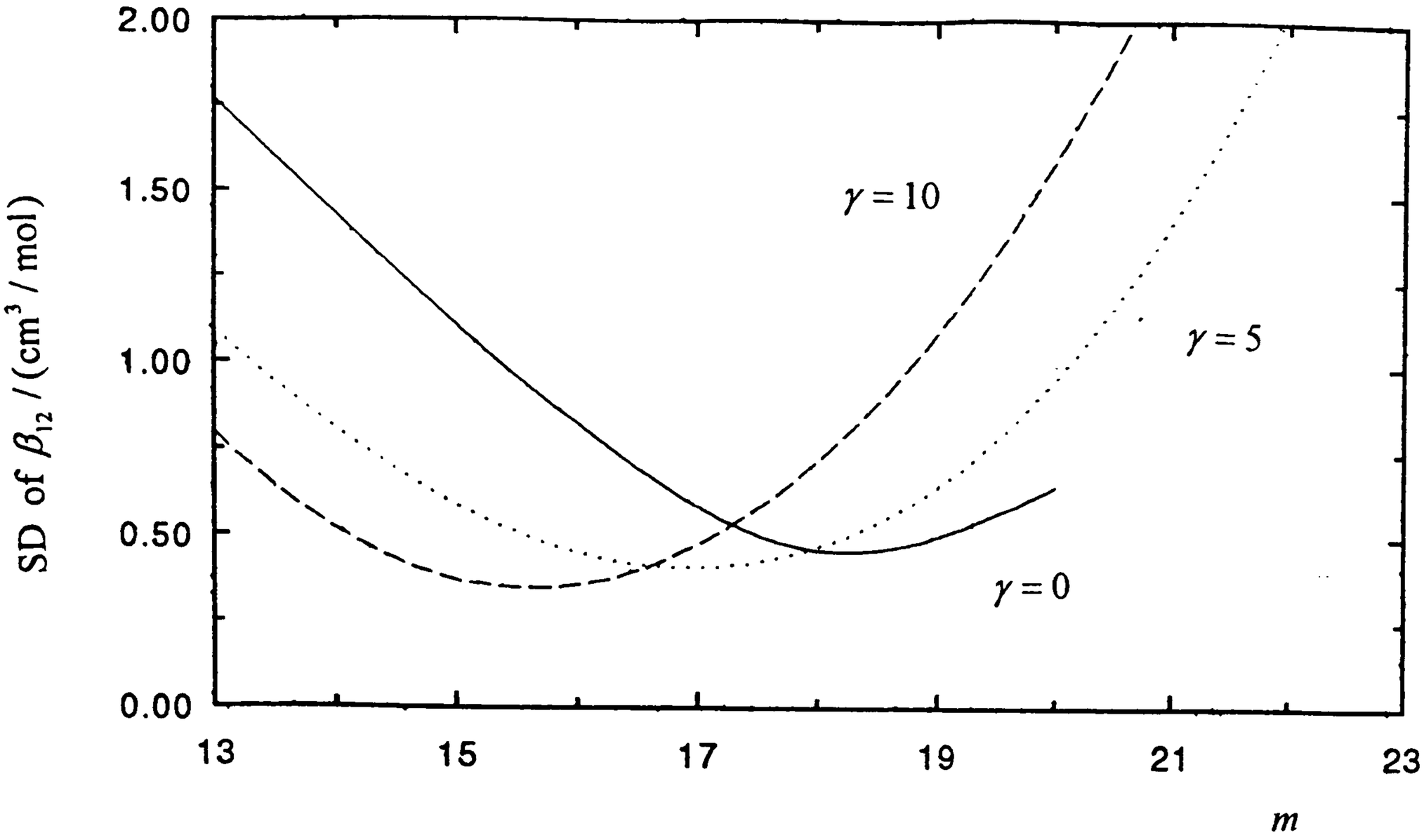

Figure 7.19. Standard deviations of the calculated β_{12} for the argon-nitrogen system from M-S potentials with different values of γ and m from the experimental values [18].

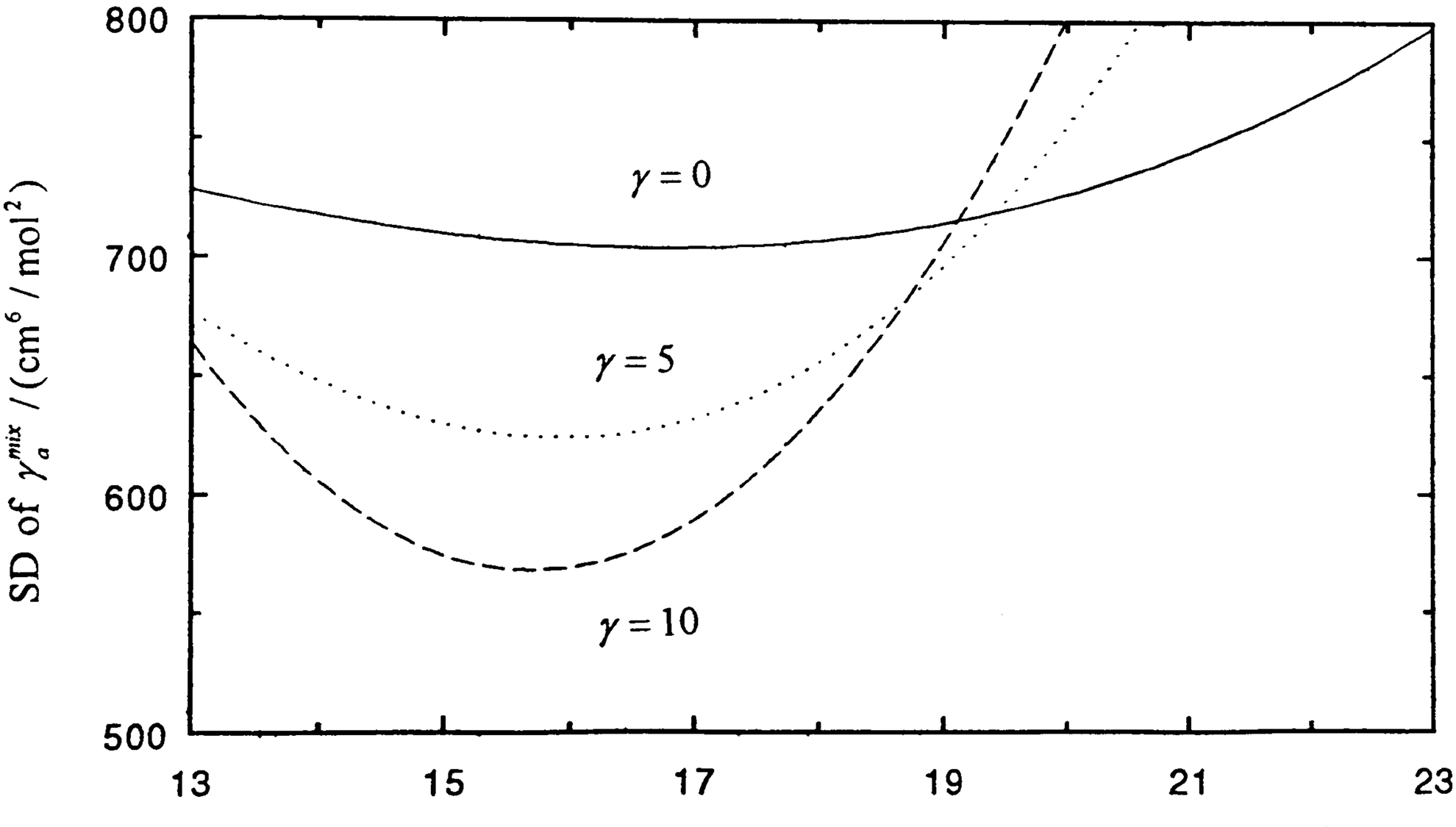

Figure 7.20. Standard deviations of the calculated γ_a for the argon-nitrogen mixture from M-S potentials with different values of γ and m from the experimental values [18].

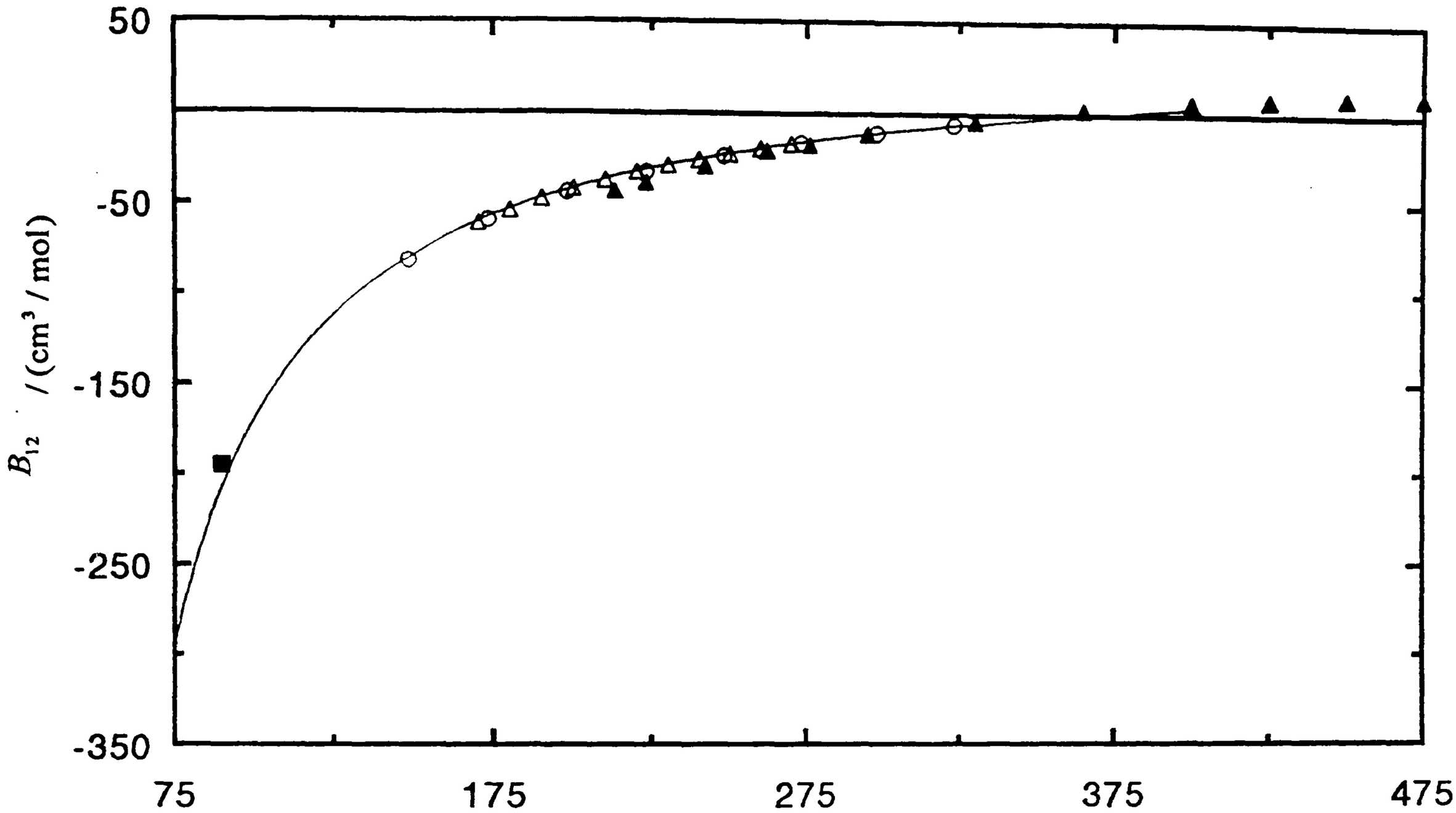

Figure 7.21. Deviations of the calculated second interaction virial coefficients B_{12} for the argon-nitrogen system from M-S (10-16) from experimental values; Δ [29], o [30], ▲ [31], ■ [32].

7.5 References

[1] G. C. Maitland and E. B. Smith, Chem. Phys. Lett. **22**, 443 (1973).

[2] C. F. Gerald and P. O. Wheatley, *Applied Numerical Analysis* (Addison-Wesley, New York, 1989).

[3] A. E. Sherwood and J. M. Prausnitz, J. Chem. Phys. **41**, 413 (1964).

[4] T. S. Storvick, T. H. Spurling and A. G. De Rocco, J. Chem. Phys. **46**, 1498 (1967).

[5] F. Leder, J. Chem. Phys. **82**, 1504 (1985).

[6] M. Rigby, personal communication.

[7] C. G. Gray and K. E. Gubbins, *Theory of Molecular Fluids*Volume 1 (Clarendon, Oxford, 1984).

[8] M. B. Ewing and J. P. M. Trusler, Physica A **184**, 415 (1992).

[9] G. C. Maitland, M. Rigby, E. B. Smith and W. A. Wakeham, *Intermolecular Forces* (Clarendon Press, Oxford, 1981), p. 567.

[10] Y. Midzuno and T. Kihara, J. Phys. Soc. Japan **11**, 1045 (1956).

[11] K. T. Tang, Phys. Rev. **177**, 108 (1969).

[12] Shobu Kaneco, J. Chem. Phys. **56**, 3417 (1972).

[13] R. A. Asiz, HFDID1 most recent potential for argon, personal communication.

[14] J. H. Dymond and E. B. Smith, *The Virial Coefficients of Pure Gases and Mixtures* (Clarendon, Oxford, 1980).

[15] R. W. Crain, Jr. and R. E. Sonntag, Adv. cryogen. Engng **11**, 379 (1966).

[16] G. P. Matthews and E. B. Smith, Mol. Phys. **32**, 1719 (1976).

[17] A. van der Avoird, P. E. S. Wormer and A. P. J. Jansen, J. Chem. Phys. **84**, 1629 (1985).

[18] M. B. Ewing and J. P. M. Trusler, Physica A **184**, 437 (1992).

[19] A Michels, J. M. Levelt and W. de Graaff, Physica,'s Grav. **24**, 659 (1958).

[20] A. L. Blancett, K. R. Hall and F. B. Canfield, Physica,'s Grav. **47**, 75 (1970).

[21] G. A. Pope, P. S. Chappelear and R. Kobayashi, J. Chem. Phys. **59**, 423 (1973).

[22] A. Michels and G. W. Nederbragt, Physica, 's Grav. **3**, 569 (1936).

[23] D. R. Douslin, R. H. Harrison, T. Moore and J. P. McCullough, J. Chem. Engng Data **9**, 358 (1964).

[24] A. E. Hoover, I. Nagata, T. W. Leland, Jr. and R. Kobayashi, J. Chem. Phys. **48**, 2633 (1968).

[26] B. A. Younglove and J. F. Ely, J. Phys. Chem. Ref. Data **16**, 577 (1987).

[25] D. R. Roe and G. Saville (unpublished results). See also D. R. Roe, Ph. D thesis, University of London (1972).

[27] F. B. Canfield, T. W. Leland and R. Kobayashi, Adv. cryogen. Engng **8**, 146 (1963).

[28] A. Michels, R. J. Lunbeck and G. J. Wolkers, Physica, 's Grav. **17**, 801 (1951).

[29] P. Zandbergen and J. J. M. Beenakker, Physica, 's Grav. **33**, 343 (1967).

[30] J. Brewer and G. W. Vaughn, J. Chem. Phys. **50**, 2960 (1969).

[31] B. Schramm and R. Gehrmann, B. Schramm and H. Schmiedel (results quoted in reference [14]).

[32] C. M. Knobler, J. J. M. Beenakker and H. F. P. Knaap, Physica, 's Grav. **25**, 909 (1959)

CHAPTER 8

CONCLUSIONS

Speed of sound measurements have been performed on gaseous methane, propane and a mixture of 85 per cent methane and 15 per cent propane. The estimated accuracy of the data obtained is 20 to 200 parts per million, depending on the purity of the samples used. The extremely high accuracy of the present speed of sound data allows them to be employed for improving existing state-of-the-art equations of state.

A method has been developed by which speed of sound data are integrated to yield the compression factor. The propagation of error of this method has been studied numerically as well as analytically for the simplified model of a perfect monatomic gas. It has been found that the method is of increasing accuracy, when the integration proceeds from lower to higher temperatures. Subsequently, the method has been successfully applied to the high accurate (20 parts per million) speed of sound data of methane. This also opens the possibility for the implementation of the method to other substances.

The speed of sound data were fitted into a virial series in the density yielding second and third acoustic virial coefficients and the perfect-gas heat capacity. The perfect gas heat capacities obtained have an accuracy which is comparable with that of data obtained from spectroscopic measurements. Second and third acoustic virial coefficients of these substances are reported for first time.

Based on the functional relationship of the second and third acoustic virial coefficients to the intermolecular pair-potential, a new methodology has been developed which allows approximate potential determinations. According to this methodology second and third acoustic virial coefficients were fitted simultaneously to a simple but flexible spherical potential model. The non-pairwise additive part of the three-body

potential was approximated by the Axilrod-Teller triple-dipole term, the adequacy of which has been tested for argon. The intermolecular pair potentials obtained for the spherical substances of argon and methane were found to be very good approximations of the true potential, as the calculations of the second and third volumetric virial coefficients and, independently, of the viscosity confirmed.

In order to check the possibility of a successful adaptation of the method to non-spherical substances, it has been applied to the moderately anisotropic nitrogen. In this case, the calculation of the second and third virial coefficients was proven equally successful with that for spherical substances. This fact is a strong indication that a similar methodology which in addition takes into account the orientation dependence of the substances may be established to provide good approximations to the true potential for non-spherical substances.

Application of the method to an argon-nitrogen system yields second and third interaction volumetric virial coefficients. The accuracy of the second interaction volumetric virial coefficients obtained is estimated to be better than the accuracy of values previously reported. Third interaction volumetric virial coefficients are reported for first time over a wide range of temperatures. Such derivations, without the need of explicit experimental measurements, are extremely important for the development of equations of state for gaseous mixtures.